Self-assembly of ssDNA-amphiphiles into micelles, nanotapes and nanotubes

A Dissertation
SUBMITTED TO THE FACULTY OF
UNIVERSITY OF MINNESOTA
BY

Timothy R. Pearce

IN PARTIAL FULFILLMENT OF THE REQUIREMENTS
FOR THE DEGREE OF
DOCTOR OF PHILOSOPHY

Adviser: Efrosini Kokkoli

December 2014

Acknowledgements

My time at the University of Minnesota has been tremendously rewarding because of countless fun, caring, friendly, and helpful people, many of who will go unacknowledged. Please forgive me.

I am deeply indebted to my advisor, Efie, for her constant support, motivation, and inspiration throughout my PhD. Thank you for allowing me to pursue many of my personal passions and crazy ideas but keeping me from getting too far off course, teaching me how to tell a good story, and pushing me to succeed. I would like to give special thanks to Dr. Chun Wang, Dr. Wei Shen, and Dr. Ron Siegel for their helpful advice regarding my thesis research and professional education through many informal conversations and for serving on my thesis committee. Additionally, I would like to thank Dr. Tim Walseth, Dr. Scott McIvor, Dr. Srinand Sreevatsan, and Dr. Ben Hackel, who graciously opened their labs and office doors to support the pursuit of various projects. Thank you for your willingness to help and advise.

A huge thanks is given to all of the Kokkoli group members I have had the pleasure of working alongside and learning from over the past six years. In particular, I want to thank my officemates of 218 Amundson Hall, Nicole, Maroof, Matt, Brett, Rachel, Carolyn, Frankie, and Mike. The time we spent together in the office sharing stories (and discussing science!) will be remembered fondly. I would be remiss if I didn't acknowledge Brett Waybrant for his unwavering mentorship and friendship during the first five years of my PhD. Without question, my PhD experience would have be remarkably less successful and fulfilling if not for Brett's friendship and willingness to

teach and collaborate. I also owe thanks to Wenjie Fei for her help around the lab during the majority of my PhD.

I had the good fortune of utilizing a number of University and National facilities over the course of my PhD. The SAXS experiments were performed at Argonne Nation Lab, which is supported by E.I. DuPont de Nemours & Co., The Dow Chemical Company, Northwestern University, and the U.S. Department of Energy. Cryo-TEM imaging was carried out in the Characterization Facility at the University of Minnesota, which receives partial support from NSF through the MRSEC program. The CD experiments were performed at the Biophysical Spectroscopy Center in the University of Minnesota Department of Biochemistry, Molecular Biology, and Biophysics. All of the people who supported my research in these facilities were outstanding and thanks to you all. In particular, I owe a huge thank you to Dr. Bob Hafner and Dr. Wei Zhang in the University of Minnesota Characterization Facility for their help, both technically and scientifically, with the cryo-TEM experiments.

And finally, I'd like to acknowledge my wonderful and loving wife Jamie, who persevered alongside me throughout the entirety of my PhD. Thank you for your love and support.

Abstract

The field of DNA nanotechnology utilizes DNA as a construction material to create functional supramolecular and multi-dimensional structures like two-dimensional periodic lattices and three-dimensional polyhedrons with order on the nanometer scale for many nanotechnology applications including molecular templating, nanosensors, and drug delivery. Single-stranded DNA (ssDNA) is often used to create these nanostructures as the DNA bases provide an intrinsic molecular code that can be exploited to allow for the programmed assembly of structures based upon Watson-Crick base-pairing. However, engineering these complex structures from biopolymers alone requires careful design to ensure that the intrinsic forces responsible for organizing the materials can produce the desired structures. Additional control over supramolecular assembly can be achieved by chemically modifying the ssDNA with hydrophobic moieties to create amphiphilic molecules, which adds the hydrophobic interaction to the list of contributing forces that drive the self-assembly process. We first explored the self-assembly behavior of a set of ssDNA aptamer-amphiphiles composed of the same hydrophobic tail and hydrophilic ssDNA aptamer headgroup but with different spacer molecules linking these groups together. Through the use of cryo-transmission electron microscopy (cryo-TEM), small angle x-ray scattering (SAXS), and circular dichroism (CD) we show that the aptamer-amphiphiles can assemble into a variety of structures depending on the spacer used. We demonstrated, for the first time, the creation of self-assembled aptamer-amphiphile nanotape structures and show that the choice of the spacer used in the design of aptamer-amphiphiles can influence their supramolecular self-assembly as well as the secondary structure of the aptamer headgroup. We next explored the role of the ssDNA headgroup on the amphiphile self-assembly behavior by designing amphiphiles with headgroups of multiple lengths and nucleotides sequences. Amphiphiles of each

headgroup length that contained hydrophobic spacers were found to assemble into twisted nanotapes, helical nanotapes and nanotubes as the nanotapes grew in width. In few instances, guanine-rich headgroups were capable of forming nanotape and nanotube structures in the absence of the hydrophobic spacer. Together, these studies demonstrate the ability of ssDNA-amphiphiles to form complex nanostructures that may be useful in a variety of DNA nanotechnology applications.

Contents

List of Tables

List of Figures

1 Introduction

The fabrication of materials and structures with dimensions on the nanometer scale has been the focus of intense research over the past 40 years, with over $10 billion dollars spent each year on research and development of these materials for applications in energy, electronics, and medicine.[1,2] Nanofabrication can be achieved through two complimentary approaches: top-down processes and bottom-up processes.[3,4] In top-down processes, external inputs are applied to a material to remove specific sections leaving behind the desired structures. Common methods of top-down fabrication including lithography, etching, and milling can produce structures with features 10's of nanometers in size and are responsible for the tremendous achievements in the electronics industry. In contrast, bottom-up approaches attempt to build up the desired structures piece-by-piece.[5] This approach offers an opportunity to further reduce the size of the structures and produce substantially more complex structures. A technologically advanced but inefficient way to perform manipulations of individual molecules is though the use of scanning probe microscopes capable of physically pushing and pulling molecules into specific positions one-by-one.[6] An alternate approach to controlling the assembly of individual molecules relies on the self-organization of molecules into the desired positions driven by the intrinsic chemical properties of the molecules. The spontaneous but controlled generation of well-defined, supramolecular nanostructures through self-organization offers a powerful alternative to expensive, inefficient top-down nanofabrication techniques and nanomanipulation but remains a challenge to utilize.[7]

This thesis discusses an approach for creating a variety of different nanostructures

through bottom-up molecular assembly of ssDNA-amphiphiles. While ssDNA-amphiphiles have only recently been created, many other types of amphiphiles have been extensively studied over the past half-century to understand their ability to spontaneously assemble into numerous structures and used for applications in many fields. This chapter gives an introduction to self-assembly of amphiphilic molecules into nanostructures and provides context for the remaining chapters of the thesis.

1.1 Overview of amphiphiles

1.1.1 Anatomy of an amphiphile

Amphiphiles are molecules that contain two distinct regions: a region that likes to interact with solvent (solvophilic) and a region that does not (solvophobic). When the solvent is water the solvent-loving portion of the molecule is referred to as hydrophilic and the solvent-hating portion is called hydrophobic (Figure 1.1).

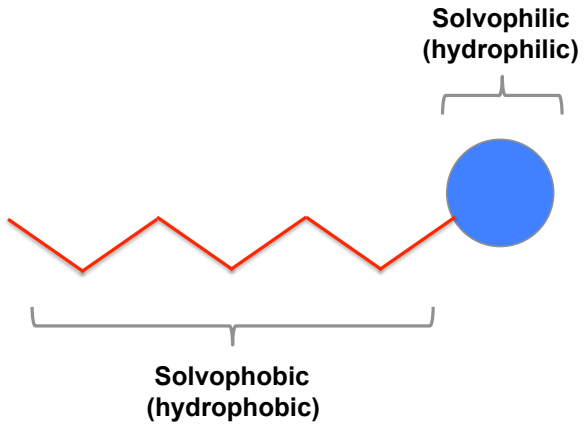

Figure 1.1: Schematic of a simple amphiphile. Amphiphilic molecules contain both solvent-loving (solvophilic/hydrophilic) and solvent-hating (solvophobic/hydrophobic) regions.

The dual nature of these molecules provides them with the unique ability to

spontaneously aggregate into macromolecular structures when placed in water, a process driven by the molecules' desire to reduce the number of interactions between the hydrophobic portions of the molecules and the water. A commonly encountered class of amphiphilic molecules is surfactants – a word derived from the phrase *surface-active agents* – due to their tendency to reside at the interface of two fluids.[8]

1.1.2 Amphiphiles in our lives

1.1.2.1 Biological

Amphiphilic molecules are ubiquitous throughout our natural world, acting as the fundamental building material from which every cell in every plant and animal is created.[9] Phospholipids, formed by two linear hydrocarbon chains tethered to a polar phosphate containing headgroup, spontaneously arrange themselves into bilayer membrane vesicles that serve as the walls of our cells. However, these lipid vesicles alone cannot create a functioning cell. They require a number of other amphiphilic molecules to set up residence within this lipid membrane.[10] These molecules include amphiphilic proteins, which shuttle nutrients and waste into and out of the cell, glycoproteins, which allow the cell to interact with surround cells, and glycolipids, which allow cells to communicate with each other. Proteins and peptides are especially adept at molecular self-assembly, a result of the various hydrophobic, hydrophilic, charged and neutral amino acids from which they are formed.

1.1.2.2 Industrial

The first use of amphiphiles by man for industrial applications occurred around 2,800 BCE in ancient Babylon, as documented by a cave painting that showed a combination of animal fat and wood ashes taken from a cooking fire formed a soap-like substance

that could be used as a cleaning agent.[11] Today, amphiphiles such as surfactants form a multibillion-dollar industry, with applications in wide-ranging industries like personal care, crop protection, energy production, construction, and textiles.[12] While a number of natural amphiphiles are still used for industrial applications, most of the commonly used surfactants are man-made. These molecules are designed to manipulate the properties of surfaces and interfaces to aid a number of industrial processes including cleaning, emulsification, foaming, and lubricity.[12] In comparison to biologic amphiphiles the molecular structures of industrial amphiphiles are often simple, most often composed of single hydrocarbon (alkyl) tails and a small polar or ionic hydrophilic headgroup.

1.1.3 Forces governing amphiphile assembly

Bottom-up assembly of amphiphiles into macromolecular structures is governed by various interactions between the individual molecules. In addition to the hydrophobic interactions between the tails of the amphiphiles, the interactions between the headgroups of the amphiphiles can be repulsive or attractive in nature, and the summation of the forces produced by these interactions governs the size and shape of the assembled structure. Tuning the strength and directionality of the intermolecular interactions is therefore paramount to manipulating and ultimately controlling macromolecular self-assembled systems.[13] Understanding these forces is critical if molecular assembly is to achieve the level of complexity desired by scientists and engineers for applications in many fields including energy, electronics, and medicine. The following paragraph briefly describes the major forces that influence the assembly of amphiphilic molecules.

Hydrophobic interactions are the primary driver of amphiphile assembly, with the

hydrophobic portions of the amphiphiles aggregating together to reduce their interactions with the surrounding water molecules. This attractive force plays a critical role in determining the shape of macromolecular organizations, including biological structures.[9,14] Van der Waals forces are another source of attraction between amphiphiles, originating from the spontaneous and continuous movement of electrons within atoms or molecules, which leads to dipole- and induced-dipole interactions.[8,15] Van der Waals interactions are almost always attractive and can be quite strong, especially when considering interactions between particles containing a large number of atoms or particles.[2,16] Electrostatic forces, most often produced in the headgroups of amphiphiles, can have significant influence over the amphiphile assembly process. Typically, electrostatic forces are repulsive as the headgroups of the individual amphiphiles share the same charge, either positive or negative. Electrostatic interactions between particles suspended in a solution can be modified, or "tuned", by manipulating the effective electrostatic surface charge of the molecules, a feat that can be accomplished by changing the amount or type of electrolyte added to the solution, the pH of the solution, or the solvent.[17–19] These factors offer simple approaches to control the attractive and repulsive forces between particles that can help guide their assembly into multi-molecular structures.[7] Finally, hydrogen bonding between amphiphiles can act as an attractive force both within and between amphiphiles, and can dramatically alter their assembly behavior by changing an individual amphiphile's shape or by allowing amphiphiles to interact with one another.[20]

1.1.4 Understanding amphiphile assembly through packing considerations

Theoretical and experimental study of amphiphile self-assembly began in earnest during

the 1970's, pioneered by Tanford and Israelachvili, with the goal of understanding the fundamental aspects that govern the self-assembly process.[9,10,21] Tanford developed a quantitative expression for the standard free energy change produced by aggregation of amphiphiles based on two competing forces: (1) an attractive force caused by the hydrophobic attraction of the hydrocarbon chain units at the hydrocarbon-water interface and (2) a repulsive force between neighboring headgroups caused by hydrophilic, steric, and ionic repulsion.[8,9] Using this concept Tanford was able to describe why amphiphiles form self-assembled aggregates, why they grow and adopt specific morphologies, and why they are finite in size. Around the same time Israelachvili described the concept of a molecular packing parameter, that when coupled with general thermodynamic principles can help explain the shape and size of self-assembled aggregates at an equilibrium state.[19,21] These two frameworks for understanding self-assembly have found widespread acceptance in the scientific communities and have been heavily relied upon to explain experimental results.[22]

The molecular packing parameter utilizes three geometric parameters of an amphiphile to predict the shape of an aggregate formed by the self-assembly of the amphiphile: (1) the headgroup area per amphiphile occupied at the surface of the aggregate a_o, called the optimal headgroup area, (2) the volume of the hydrophobic tail *v*, and (3) the length of the hydrocarbon tail l_c (Figure 1.2). Using these three elements, a dimensionless packing parameter (*P*) can be defined as $v/(a_o\ l_c)$. The molecular packing parameter *P* falls between 0 and 1/3 for spherical micelles, between 1/3 and 1/2 for cylindrical micelles, and between 1/2 and 1 for bilayer structures. Thus, the packing parameter can be used as an indicator of the shape of self-assembled structures formed by amphiphiles

in solution.

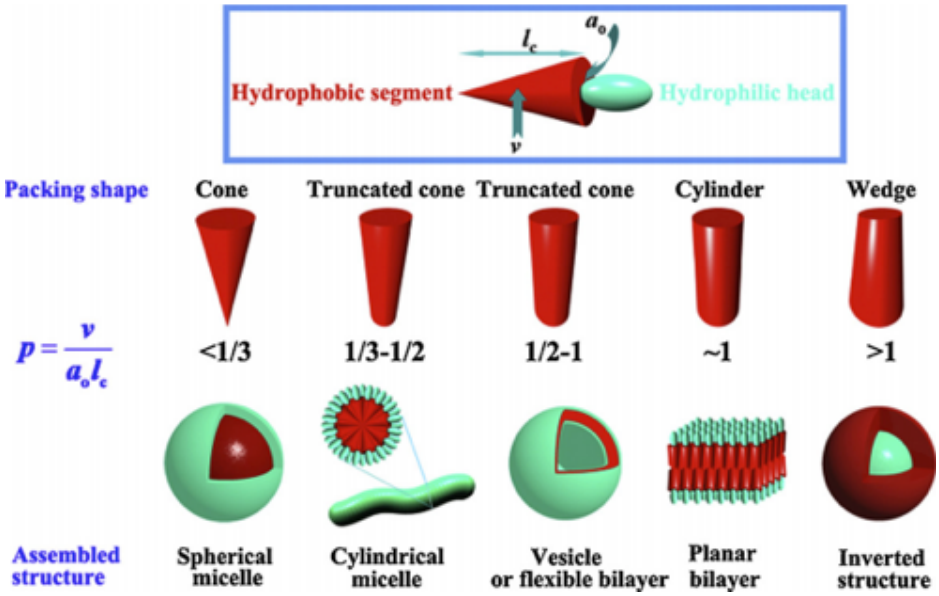

Figure 1.2: A graphical representation of the relationship between the packing parameter and the shape of the self-assembled structure. Reprinted with permission from Zhang *et al*.[23]

Many of the early experiments used to develop and verify that the molecular packing parameter could be used to predict the shapes of aggregates were performed with common single-tailed industrial surfactants like sodium dodecyl sulfate as well biological double-tailed phospholipids.[19,22] This early work also demonstrated that in many common surfactants the ratio of the volume of the hydrophobic tail to the tail length (v/l_c) was independent of tail length. Therefore, for a given hydrophobic tail area, the area occupied by the headgroup of the amphiphile was the critical parameter in determining the packing parameter. The initial approach used by Israelachvili to estimate the headgroup area per molecule of an amphiphile relied on Tanford's model of the free energy change resulting from aggregation. Israelachvili posited that at equilibrium, the

headgroup area of the amphiphile is directly proportional to the headgroup interaction parameter α and inversely proportional to the interfacial free energy parameter σ as shown in the following equation.

$$a_o = \left(\frac{\alpha}{\sigma}\right)^{1/2}$$

This relationship reveals that when the headgroup interaction parameter α is large, a_o will be large, and the packing parameter small, and vice versa. This relationship has proven to be useful in explaining assembly behavior of a variety of amphiphiles.[19,22,24] For example, the self-assembled structures of surfactants made from hydrophobic poly(propylene glycol) tails and hydrophilic poly(ethylene glycol) (PEG) headgroups were found to transition from bilayers to spherical micelles as the length of the PEG headgroup was increased from 6 to 13 PEG monomers.[25] This observation can be understood by packing parameter arguments as detailed earlier. Specifically, the increasing number of hydrophilic PEG monomers in headgroups of the amphiphiles caused an increase in the amphiphiles' headgroup areas a_o. An increase in headgroup area of an amphiphile without a change to the hydrophobic portion of the amphiphile produced a smaller packing parameter, which predicts the transition from a bilayer to spherical micelle morphology that was observed. Similarly, amphiphiles containing negatively charged polyacrylic acid headgroups transitioned from spherical micelles to cylindrical micelles and vesicles when sodium chloride was added to the solution to screen the charges of the polyacrylic acid headgroups. The reduction in the electrostatic repulsion of the headgroups following the addition of salt reduced the amphiphiles' effective headgroup area, which produced a larger packing parameter that is predictive of a transition from spherical to cylindrical micelle and vesicle morphologies.[26]

The reliance on geometric relationships in defining the packing parameter and the implicit reference to, but incorrect understanding of, headgroup area as headgroup "size" has led some to misuse the packing parameter.[22] Most often the headgroup area is erroneously defined as the physical area or volume occupied by the headgroup, which ignores the thermodynamic considerations that form the true basis for the packing parameter. This does not mean that the physical size of the headgroup is unrelated to the headgroup area but rather that the headgroup area must be estimated with consideration given to other factors as well, including temperature, salts, interactions between headgroups, and amphiphile tail packing.[27] In many cases headgroup area cannot easily be determined and thus remains a parameter that must be determined based on experimental results that probe aggregate shape, size, and molecular organization.[22] This is especially true for complex amphiphiles with large ionic headgroups when the conformation of the headgroup plays an additional role in defining the size of the self-assembled structure.[28]

1.2 Peptide-amphiphiles

The complexity that exists throughout our natural world clearly demonstrates the powerful ability of molecular self-assembly. Harnessing this power to create novel biomaterials has been a long-sought goal of scientists and engineers and has inspired the creation of a number of classes of amphiphilic molecules that contain biologic components that help influence the assembly process. One class of molecules is peptide-amphiphiles, which were first created in the 1980's and have since been the subject of substantial research, including by the Kokkoli group.[29–34] The knowledge gained from the peptide-amphiphile literature and our lab's prior experiences with these

molecules played a substantial role in shaping the direction of this thesis and will be briefly reviewed, with special attention paid to the design of the amphiphile and its effect on self-assembly.

1.2.1 Peptide-amphiphile construction

Peptide-amphiphiles are formed by covalently linking a peptide headgroup with a hydrophobic tail (Figure 1.3). The peptide headgroup is typically 5-20 amino acids in length and is overall hydrophilic, although it can include both hydrophilic and hydrophobic amino acids.[35] The hydrophobic tail is commonly formed by a mono- or dialkyl hydrocarbon chain, but hydrophobic polymers have also been used.[36,37] A spacer is often included between the peptide headgroup and the hydrophobic tail of the amphiphiles to control the shape of the peptide-amphiphile assemblies, as well as to improve the bioactivity of the peptide headgroups by maintaining their secondary structure and increasing the peptide's accessibility to its molecular target.[29]

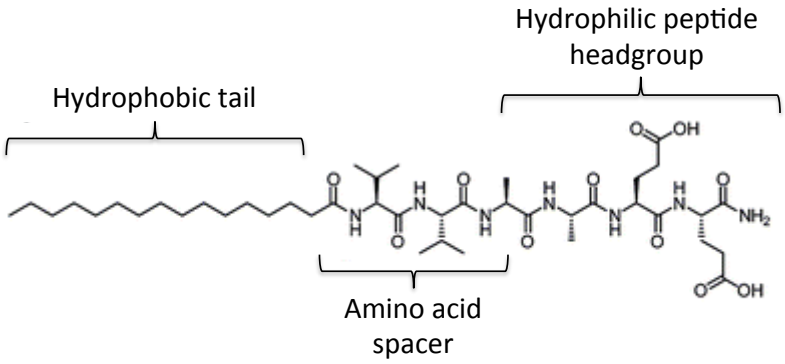

Figure 1.3: Peptide-amphiphiles are formed by covalently linking a hydrophobic tail to a hydrophilic peptide headgroup. In some cases, an amino acid spacer sequence is included in the design of the amphiphile to modulate the amphiphile self-assembly.

When these molecules are placed in an aqueous solution they assemble into a variety of three dimensional structures that are held together by non-covalent amphiphile-

amphiphile as well as amphiphile-solvent interactions.[32,38] Significant effort has been spent to understand the fundamental forces that drive peptide-amphiphile assembly, which now allows researchers the ability to rationally design peptide-amphiphiles that assemble into the desired supramolecular morphology based solely on the molecular composition of the individual amphiphiles.[38,35] In particular, peptide-amphiphiles offer three molecular components that can be used to control their self-assembly: the hydrophobic tail, the spacer, and the hydrophilic headgroup. A brief summary of how these factors can be used to influence the self-assembly of peptide-amphiphiles is reviewed in the following section.

1.2.2 Manipulating peptide-amphiphile self-assembly

Controlling the morphology of the self-assembled structures has been achieved by changing the length,[39–41] arrangement,[42] and amino acid composition[43,44] of the peptide portion of the amphiphile. The underlying mechanisms that produce morphological changes in the macromolecular organization are rooted in the intra- and inter-peptide interactions of the headgroups caused in large part by steric and electrostatic forces and hydrogen bonding.[45,46] In many cases, the macromolecular structural changes that occur following peptide headgroup manipulation can be understood via packing parameter arguments. For example, peptide-amphiphiles with relatively lengthy headgroups that initially formed spherical micelles were observed to rearrange into cylindrical micelles when the peptide headgroups were shortened (Figure 1.4).[40,41]

The self-assembly of peptide-amphiphiles is also sensitive to the type of hydrophobic tails used to create the amphiphiles. Commonly used alkyl tails are between 12 and 20

carbons in length and contain either a single chain (Figure 1.3) or two chains as found in most phospholipids, although aromatic lipids,[47] dendrimers,[48] and polymers[36,37] have all been used.

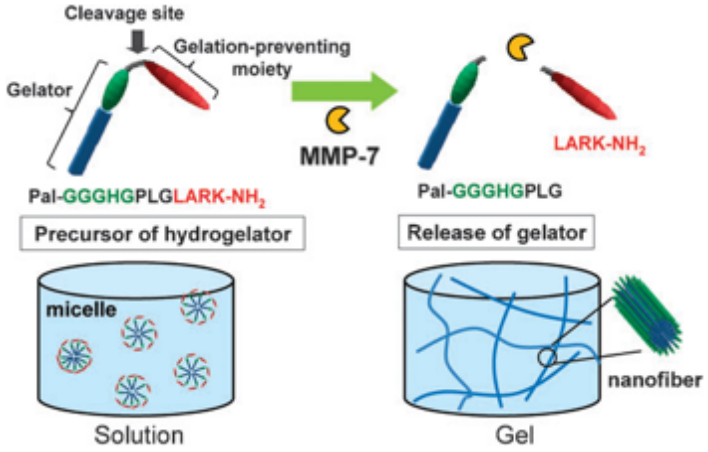

Figure 1.4: Enzymatic cleavage of a peptide-amphiphile headgroup produces a transformation from spherical to cylindrical micelles as the peptide headgroup is reduced in size. Reprinted with permission from Koda *et al*.[40]

Gore *et al*., performed a series of elegant experiments that demonstrates the effect the hydrophobic tail can play on the self-assembly of peptide-amphiphiles.[42] In these experiments the self-assembly behavior of amphiphiles containing the same peptide headgroup but tails of various length (12-20 carbons) and alkyl chain number (1 or 2) were observed with electron microscopy and neutron scattering. Single-tailed amphiphiles of all lengths assembled into spherical micelles, as did double-tailed amphiphiles with 12 and 14 carbons. However, increasing the length of the double tail to 16, 18 and 20 carbons induced a change in the self-assembly behavior of the amphiphiles from spherical micelles with high membrane curvature to bilayer aggregates with lower membrane curvature. The observed change in morphology could not be explained through packing parameter arguments, as the packing parameter was

independent of tail length and identical for all of the double-tailed amphiphiles. The authors hypothesized that the change in aggregation shape was instead caused by differences in the molecular packing of the hydrophobic tails of different lengths. In spherical aggregates the hydrophobic tails must bend to occupy the large amount of volume close to the hydrophobic-hydrophilic interface. In bilayer aggregates the hydrophobic tails could extend straight into the bilayer due to a uniform distribution of volume throughout the bilayer. Thus, amphiphiles with longer chain lengths are expected to pack more favorably in low-curvature bilayer aggregates while shorter chain lengths are expected to pack more favorably in high-curvature spherical aggregates as observed. Similarly, a cell-penetrating TAT peptide headgroup (GRKKRRQRRRPPQ) was conjugated to one, two or four 18-carbon lipid tails to explore the effect of tail number on self-assembly.[49] Amphiphiles containing only a single tail did not appear to self-assemble while amphiphiles with two and four tails began assembling at 209 micromolar (μM) and 21 μM, and formed spherical micelle and cylindrical micelles, respectively. These results showed that the relative hydrophobicity and hydrophobicity of an amphiphile can influence both the shape of the self-assembled structures as well as the concentration at which aggregation begins to occur.

Spacer molecules used to link the hydrophobic tails and hydrophilic peptide headgroups can also influence the morphology of peptide-amphiphile macromolecular structure. Spacer molecules are often created by a short string of amino acids that can be hydrophobic, hydrophilic, charged, or have a propensity to form intermolecular hydrogen bonding (Figure 1.3), although a number of spacer molecules including PEG[50,51] and alkyl hydrocarbons[49] have also been used. The attractive hydrogen bonding between

amino acids can give rise to β-sheet structures and allows for close packing of the peptide headgroups. When the headgroups adopt this compact secondary structure rather than a random coil structure the effective size of the headgroups is reduced, resulting in self-assembled aggregates with less interfacial curvature.[32,52] For example, peptide-amphiphile designs that employed a β-sheet forming amino acid spacer sequence between the main peptide headgroup and hydrophobic tail were found to form cylindrical micelles (less curvature) while spherical micelles (more curvature) were formed when amino acids not capable of forming β-sheet interactions were used.[44] Conversely, the inclusion of a hydrophilic polyethylene glycol spacer is capable of inhibiting the formation of tightly packed peptide headgroups, causing only highly curved macromolecular organizations like spherical micelles to exist.[50]

1.2.3 Nanotapes, nanotubes, and membrane curvature

Peptide-amphiphiles have been observed to form nanotapes[45,53–55] and nanotubes[39,56,57] along with the more standard structures like spherical and cylindrical micelles,[39] oblate ellipsoids,[42] and vesicles.[58] Nanotapes and nanotubes are often formed by bilayers of amphiphiles, with the tails oriented towards one another forming a hydrophobic core surrounded by the hydrophilic peptide headgroups on either side, although monolayers of molecules can also form ribbon-like structures and nanotubes. Nanotape and nanotube structures have also been observed to form from solutions of lipids[59–62] and amphiphilic peptides.[63,64] Ziserman *et al*. used cryo-transmission electron microscopy (cryo-TEM) imaging to study the assembly changes that occurred over time within a solution of amphiphiles containing two 12-carbon chains and two lysines as their headgroups over time.[56] Minutes after dissolving the amphiphiles, cryo-TEM images

showed the existence of thin fibers/ribbons formed by monolayers of molecules. After 24 hours, the ribbons had laterally aggregated into wider structures and began to twist. By one week, the twisted ribbons had further widened and adopted a helical morphology and after four months nanotubes were observed (Figure 1.5).

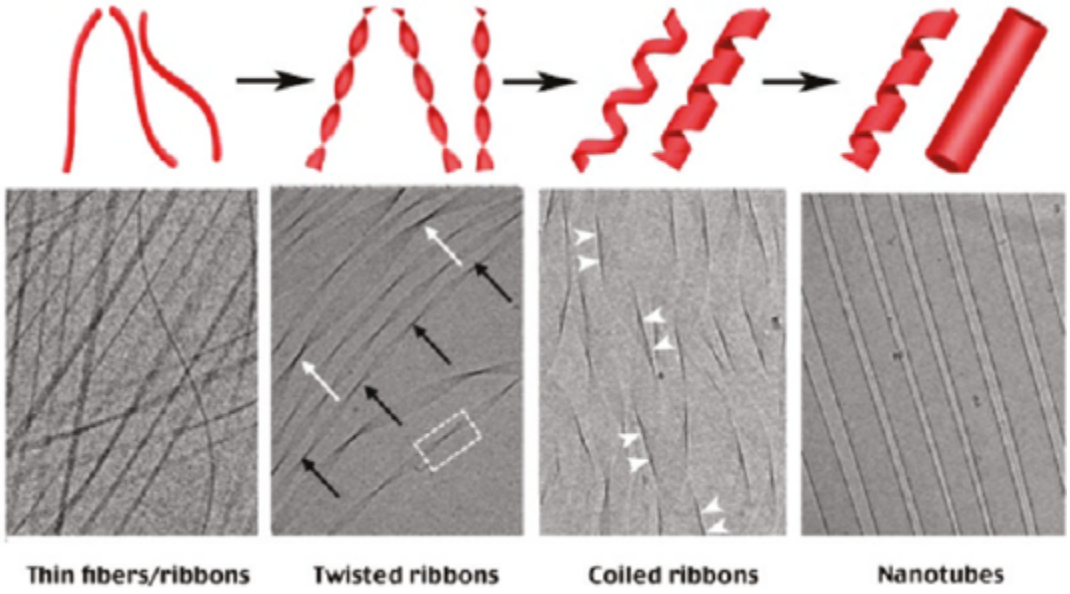

Figure 1.5: A pathway to nanotube formation. Over time, thin fibers grow into twisted nanotapes (ribbons), helical (coiled) nanotapes and nanotubes. Reprinted with permission from Ziserman *et al*.[56]

Two additional studies using peptide headgroups inspired by the study of amyloid β protein fibrillization also observed similar transitions between twisted and helical bilayer nanotapes and bilayer nanotubes[65] and between twisted bilayer nanotapes and helical bilayer nanotapes.[55] In the first study single 16-carbon hydrophobic tails were conjugated to a peptide headgroup that contained the KLVFF amino acid sequence found in the amyloid β protein, with two addition lysine (K) residues added to promote amphiphile solubility. The presence of the phenylalanines (F) in the headgroup allowed

for aromatic π-π stacking interactions between the headgroups, an interaction which was hypothesized to be important for the transition of twisted nanotapes to helical nanotapes and helical nanotapes to nanotubes.[65] The second study utilized the same 16-carbon single tail and a peptide headgroup that contained three phenylalanines followed by three lysines.[55] Again, the presence of the phenylalanines in the headgroup was thought to contribute to the transformation of twisted nanotapes to helical nanotapes, as the aromatic π-π stacking interactions between the headgroups were found to increase at the same time that the transition from twisted to helical morphology occurred. The authors of each study concluded that a combination of hydrophobic forces and hydrogen bonding between the peptide headgroups was critical to achieving the bilayer nanotape morphology and that aromatic π-π stacking interactions in the peptide headgroup may have played a role in the twisted to helical nanotape transitions.[55,65] However, the specific mechanisms that produced these structures and their transitions were not elucidated.

There are two theories to explain the transformation of helical nanotapes into nanotubes: a closing pitch mechanism and a growing width mechanism (Figure 1.6). In the closing pitch mechanism, the width of a helical nanotape remains constant while the pitch length, defined as the distance spanned by one complete helix turn, shortens until the edges of the nanotape interact with one another. Alternately, in the growing width mechanism, the width of the helical nanotape increases as material is added to the helical structure while the pitch length remains constant. This growing width continues until the edges of the helical nanotape touch one another. In each case, the edges of the helix can either rearrange and seal into a smooth nanotube or they can remain

unsealed, which creates a nanotube that maintains its helical stripes. Interestingly, experiments have found that some amphiphiles form nanotubes through the shortening pitch mechanism,[66] some through the growing width mechanisms,[67] and some through a combination of the two,[56] showing that there is not a single mechanism responsible for nanotube formation.

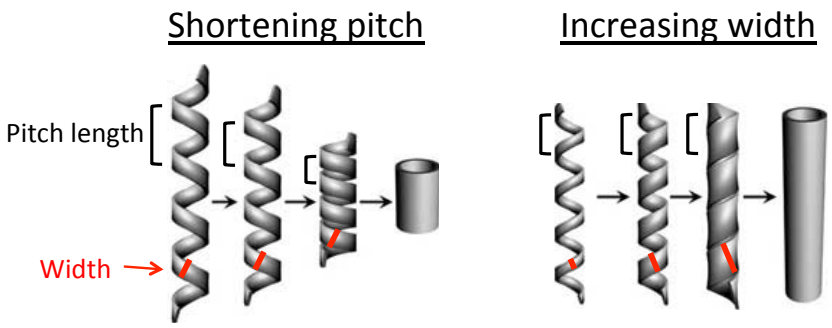

Figure 1.6: Two mechanisms of nanotube formation. Left: shortening pitch length with constant width. Right: increasing width with constant pitch length. In both cases the edges of the helical nanotape interact with one another and seal into a nanotube. Adapted with permission from Jung *et al.*[66]

1.3 Nucleic acid-amphiphiles

Another class of biologically based amphiphiles can be constructed by replacing the short amino acid chains of peptide-amphiphiles with short segments of nucleic acids to create nucleic acid-amphiphiles. While peptides have long been appreciated for their role in many cellular processes and thus an obvious material to utilize for bioengineering applications, the role of short nucleic acid sequences like siRNA[68], antisense DNA[69], and aptamers[70] have only more recently been discovered and used. Their use in place of peptides as hydrophilic headgroups of amphiphiles offers a new class of amphiphile that can be used for molecular diagnostics, drugs, and as targeting molecules for nanoparticle drug delivery. In addition to their biological relevance, short pieces of DNA

can be used for a wide range of synthetic biology and chemistry applications such as DNA-templated synthesis[71,72], catalysis[73], molecular detection[70], and DNA computing[74], many of which utilize Watson-Crick base-pairing as a programming language to provide instructions for the molecular organization of nucleic acids.

Precisely controlling the assembly of short pieces of ssDNA into larger structures is paramount for the advancement of these applications, and a bottom-up assembly process that is afforded by creating nucleic acid-amphiphiles is an attractive technique that could help achieve this control. In comparison to other types of amphiphilic molecules like lipids, amphiphilic peptides, and peptide-amphiphiles, there has been substantially less research about DNA-amphiphile assembly. This may be due to the majority of DNA-amphiphiles assembling into spherical and cylindrical micelles, leading to a perceived difficulty in designing DNA-amphiphiles that could assemble into more intricate structures like nanotapes and nanotubes. The following sections of this chapter provide a summary of the research conducted with DNA-amphiphiles, with an emphasis placed on research that illuminates how the assembly of these amphiphiles can be directed or controlled. The nucleic acid segments of these amphiphiles are typically composed of single-stranded nucleic acids but in some instances double-stranded segments are used. For the remainder of this thesis, when double-stranded segments of DNA or RNA are used they will be referred to as dsDNA and dsRNA to differentiate them from ssDNA and ssRNA.

1.3.1 Lipid-based nucleic acid-amphiphiles

Lipid-based nucleic acid-amphiphiles are structurally similar to peptide-amphiphiles,

formed by ssDNA or ssRNA oligonucleotide headgroups attached to lipids and lipid-like tials.[75–78] Single- and double-tailed lipids and cholesterol account for the majority of the hydrophobic tails utilized for amphiphile synthesis[79–81] and the nucleic acid headgroups typically contain 15 or more nucleotides and are selected based on the desired application (e.g. gene knock-down,[82] cell targeting,[78] molecular tethers[83]). Despite the relatively large sizes of the nucleic acid segments in comparison to the hydrophobic tails, the amphiphiles can self-assemble when dissolved with aqueous solutions. Interestingly, the critical aggregation concentration is often quite low, occurring at nanomolar (nM) concentrations.[78,84,85] The ability for the amphiphiles to assemble at these low concentrations is surprising given 1,2-dimyristoyl-sn-glycero-3-phosphoglycerol (DMPG), a common double-tailed lipid, assembles at μM concentrations and that the nucleic acid-amphiphiles have substantially larger polyanionic headgroups and similar hydrophobic tails. Partial base pairing or other secondary structure formation between the nucleotide headgroups of the amphiphiles may help overcome the steric and electrostatic repulsion in the headgroups, thus permitting the amphiphiles to self-assemble at lower concentrations than expected.[79] Lipid-based nucleic acid-amphiphiles most commonly assembly into spherical micelles[75–78,84–87] and a few have been found to form vesicles,[88,89] but none have been observed to form the nanotape and nanotube morphologies produced by peptide-amphiphiles.

1.3.2 Polymer-based nucleic acid-amphiphiles

Nucleic acid-amphiphiles can be created by conjugating any type of DNA or RNA sequence to hydrophobic polymers or block copolymers. To date, a variety of polymers have been utilized including poly(lactic-co-glycolic) acid [90], poly(propylene oxide)[91,92],

polystyrene,[89] polybutadiene,[93] and polycaprolactone.[94] A wide range of ssDNA headgroups have also been used, with the selection of the headgroup based on the desired functionality of the polymeric ssDNA-amphiphile (e.g. chemical reactions[95], drug delivery vehicles that can be modified to include targeting molecules[91], molecular patterning[94]). When dissolved in water, most of these polymeric materials assemble into spherical micelles.[90–92] However, the relative sizes of the hydrophobic polymer and hydrophilic ssDNA doesn't reliably predict what morphology the self-assembled structures will adopt. For example, a combinatorial study of ssDNA-amphiphiles was performed utilizing a set of amphiphiles created with ssDNA headgroups 5, 10 and 25 nucleotides long and hydrophobic polystyrene polymers with molecular weights (MW) of 4100, 7200, and 9500.[89] Every combination of ssDNA headgroup length and polymer molecular weight produced spherical micelles, despite the hydrophobic polymer being more than 10 times larger than the hydrophilic headgroup. Alternately, ssDNA-amphiphiles constructed with a polybutadiene polymer (MW: 2000) and a cytidine ssDNA headgroup (MW: ~3400) assembled into a bilayer vesicle.[93] The origin of this discrepancy between hydrophobic/hydrophilic size and the morphology of the self-assembly may lie in the difference in hydrophobic polymer packing within the core of the structures, but has not yet been definitively proven.

1.3.3 Manipulating nucleic acid-amphiphile self-assembly

Unlike the peptide-amphiphile literature, there are only a few reports describing the effects of physical parameters like temperature, solution pH and ionic strength on nucleic acid-amphiphiles assembly. However, the nucleic acid headgroup used to create the amphiphiles has been successfully used to manipulate the self-assembled structure of

the DNA-amphiphiles. This ability relies on the capability of the adenine (A), thymine (T), cytosine (C) and guanine (G) nucleobases of DNA to interact non-covalently with one another via Watson-Crick base pairing as well as non-standard Hoogsteen interactions.[96] These interactions provide an opportunity to add, subtract, or rearrange portions of the headgroup to change its size and shape, thus impacting the assembly behavior of the amphiphile.

A common approach for adding nucleotides to the ssDNA headgroups of amphiphiles is through the addition of complimentary sequences that can hydrogen bond with the ssDNA of the amphiphile to form canonical Watson-Crick duplexes. For example, ssDNA-amphiphiles that initially self-assembled into bilayer vesicles rearranged into spherical micelles following the addition of complimentary ssDNA to the vesicle sample.[85] Similarly, addition of complimentary ssDNA to cylindrical micelles induced a transition to spherical micelles while a reduction in the size of the dsDNA headgroups caused by phosphodiesterase enzymatic degradation of the dsDNA produced a transition from spherical to cylindrical micelles (Figure 1.7).[97] All of these transitions can be understood through simple packing parameter arguments. When the size of the ssDNA headgroup is increased, self-assembly into spherical micelles with higher curvature is expected, as more area per molecule at the hydrophilic – hydrophobic interface is required. When the size of the headgroup is reduced, each headgroup takes up less interfacial area and can allow structures with less membrane curvature to form.

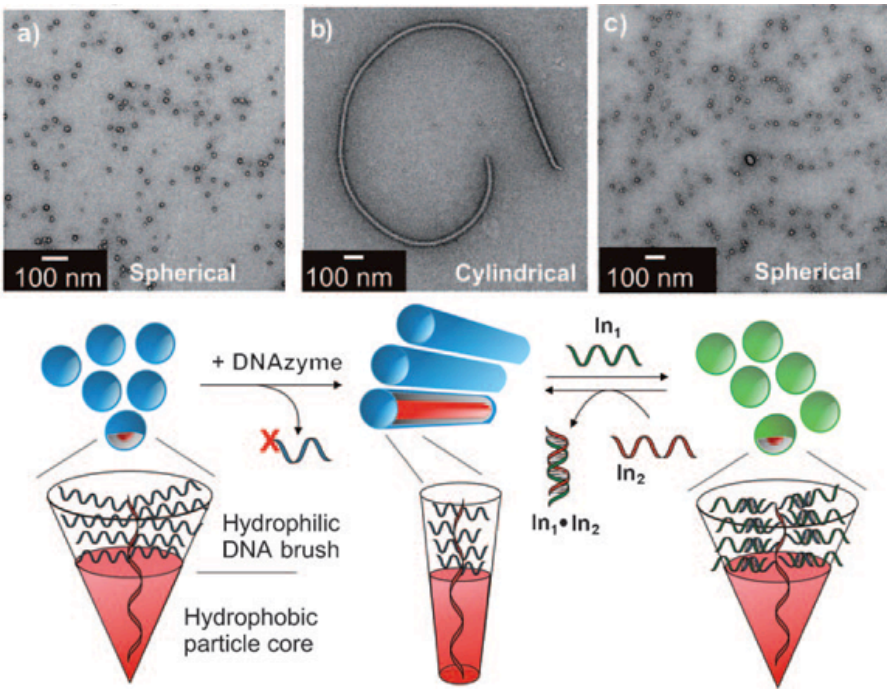

Figure 1.7: Assembly of DNA-amphiphiles into spherical and cylindrical micelles. TEM images of a) 25 nm spherical micelles assembled from initial ssDNA-amphiphiles; b) cylindrical micelles formed following enzyme addition to spherical micelles; c) spherical micelles formed after addition of complimentary ssDNA to a cylindrical micelle sample. Reprinted with permission from Chien *et al*.[97]

Non-canonical base-base interactions can also be exploited to influence the self-assembly behavior of ssDNA-amphiphiles. Like Watson-Crick base pairing, these non-canonical interactions are largely a function of hydrogen bonding between nucleobases but produce different secondary structures including i-motifs[98] and G-quadruplexes.[99] I-motifs are composed of two parallel-stranded DNA duplexes held together in an antiparallel orientation by intercalated protonated cytosine – cytosine base pairing interactions while G-quadruplexes are formed by stacks of G-quartets each composed of four guanine nucleotides held in a planar geometry by Hoogsteen bonds (Figure 1.8).

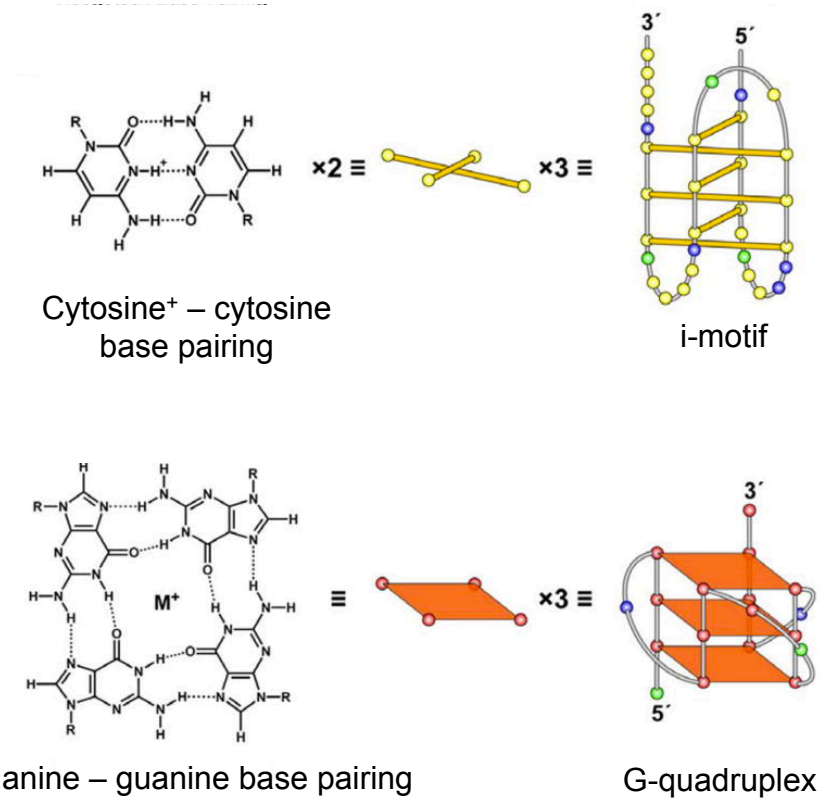

Figure 1.8: Cytosine$^+$ – cytosine and guanine – guanine base pairing can give rise to i-motif and G-quadruplex secondary structures in ssDNA sequences. Reprinted with permission from Kendrick and Hurley.[100]

Zhao *et al*. designed ssDNA-amphiphiles with ssDNA headgroups that could transiently form cytosine$^+$ – cytosine interactions and organize into intermolecular i-motif structures.[101] This transient i-motif was a function of the pH of the solution used to dissolve the amphiphiles. At low pH (< 5) the compact i-motif readily formed, while at high pH (> 8) the ssDNA headgroup formed diffuse random coil structures. At high pH when the ssDNA headgroups adopted random coil secondary structure, the amphiphiles self-assembled into spherical micelles 20 nm in diameter. When the pH was lowered the amphiphiles instead assembled into cylindrical micelles 15 nm in diameter and tens of microns in length. G-quadruplex interactions were utilized by Liu *et al*. to create highly

stable spherical micelles capable of resisting disassembly by serum proteins.[102] This was accomplished by adding a guanine-rich segment of ssDNA between the lipid-like hydrophobic tail and an immune stimulating oligonucleotide headgroup. Once assembled into spherical micelles based on hydrophobic forces provided by the lipid-like tail, the guanine-rich segments of the amphiphiles were in close proximity to one another and in position base pair with neighboring guanine-rich segments, producing the G-quartet structures that could then stack to form G-quadruplexes. The existence of these strong G-quadruplex interactions gave rise to micelles that did not readily dissociate into monomers when exposed to serum proteins while micelles lacking the guanine-rich sequences quickly disassembled into monomers.

2 The role of spacers on the self-assembly of DNA aptamer-amphiphiles into micelle and nanotapes*

*Adapted with permission from Pearce *et al*. Copyright 2014 The Royal Society of Chemistry.

2.1 Synopsis

The self-assembly of single-stranded DNA (ssDNA) aptamer-amphiphiles was influenced by the choice of spacer used to link the hydrophobic tail and aptamer headgroup. Aptamer-amphiphiles without spacers or with hydrophilic spacers formed globular micelles while amphiphiles with hydrophobic spacers formed bilayer nanotapes, which are the first such structures formed by DNA-amphiphiles.

2.2 Introduction

Biopolymers formed from nucleic and amino acid building blocks can be used to create functional supramolecular and multi-dimensional structures that rely on extensive intermolecular interactions to produce biocompatible materials with order on the nanometer scale for applications in electronics, biosensing, and tissue engineering.[2,13,103] ssDNA in particular has been extensively used to create these materials as the DNA bases provide an intrinsic molecular code that can be exploited to allow for programmed assembly of structures based upon Watson-Crick base-pairing. However, creating materials and devices from biopolymers alone requires careful design to ensure that the intrinsic forces responsible for organizing them – like electrostatic interactions, van der Waals forces, hydrophobic forces, and hydrogen bonding – are sufficient to produce the

desired features.[2,13,103]

Additional control over macromolecular assembly can be achieved by chemically modifying the biopolymers with hydrophobic moieties to create amphiphilic molecules. This modification uses hydrophobic forces to direct the self-assembly process.[32] This strategy has been widely utilized to form peptide-amphiphiles consisting, typically, of hydrocarbon chains conjugated to hydrophilic peptide headgroups.[104] But despite widespread research utilizing ssDNA for bionanotechnology applications, ssDNA-amphiphiles have not been studied as thoroughly as peptide-amphiphiles. A perceived difficulty in constructing architecturally diverse structures from these molecules brought about by their tendency to form spherical micelles regardless of the type of hydrophobic block (polymeric, hydrocarbon/lipid) or DNA headgroup[86,90,105] may explain the relative lack of attention given to DNA-amphiphiles. Recently, however, polymer-based ssDNA-amphiphiles were found to transition between spherical and cylindrical micelles in response to changes in the bulkiness of the amphiphiles' DNA headgroups.[97,101] This suggests that rational design of the amphiphile components may provide the ability to control the organization of short pieces of ssDNA into larger structures using a bottom-up assembly process.

2.3 Materials and Methods

2.3.1 Materials

Toluene, chloroform, acetone, methanol, and triethylamine were purchased from Fischer Chemical (Hanover Park, IL). Ammonium acetate, Nile red, sodium acetate, dimethylformamide, dichloromethane, aminododecanoic acid, succinic anhydride,

dicyclohexylcarbodiimide, *N*-Hydroxysuccinimide, L-glutamic acid, p-toluene sulfonic acid monohydrate, hexadecanol, ethyl acetate, ethanol, and acetonitrile were purchased from Sigma-Aldrich (St Louis, MO). α-carboxy γ-amino heterobifunctional PEG_4 and PEG_8 spacers were purchased from Thermo Scientific (Rockford, IL), the aptamer from Integrated DNA Technologies (Coralville, IA), cetyl trimethylammonium bromide from Acros Organics (Morris Plains, NJ), hexafluroisopropanol (HFIP) from Oakwood Products Inc. (West Columbia, SC), lacey Formvar/carbon, 200 mesh, copper grids from Ted Pella Inc. (Redding, CA), and 1.5 mm diameter quart capillaries from Charles Supper Company (Natick, MA).

2.3.2 Aptamer-amphiphile synthesis

Hydrophobic dialkyl tails previously created by our group[30] were modified with *N*-Hydroxysuccinimide (NHS) to make them amine reactive. To create the NHS activated tails, $(C_{16})_2$-Glu-C_2 tails were dissolved in ethyl acetate followed by the addition of 2x molar excess of both NHS and dicyclohexylcarbodiimide (DCC). The solution stirred at 40 °C for 2 h. The solution was filtered to remove the dicyclohexylurea byproduct and placed at -20 °C to precipitate the activated tails. The precipitate was collected and dried in a vacuum oven. Hydrophilic PEG_4 and PEG_8 spacers were added to $(C_{16})_2$-Glu-C_2-NHS tails by reacting the activated tails with the heterobifunctional PEG_4 or PEG_8 in dichloromethane at room temperature for 2 h. Unreacted PEG spacers were removed by washing the product with 1 mL aliquots of purified water. C_{12} spacers and $(C_{16})_2$-Glu-C_2-NHS tails were dissolved in 60 °C methanol, reacted for 2 h, and dried $(C_{16})_2$-Glu-C_2-C_{12} tails were redissolved with dichloromethane and filtered to remove unreacted C_{12} spacers. $(C_{16})_2$-Glu-C_2-PEG_x or $(C_{16})_2$-Glu-C_2-C_{12} tails were activated with NHS as

described above. To create $(C_{16})_2$-Glu-C_2-C_{24} tails, C_{12} spacer was added to NHS-activated $(C_{16})_2$-Glu-C_2-C_{12} tails, followed by re-activation of the terminal carboxyl group with NHS. Synthesis schemes for the aptamer-amphiphiles are shown in Figure 2.1

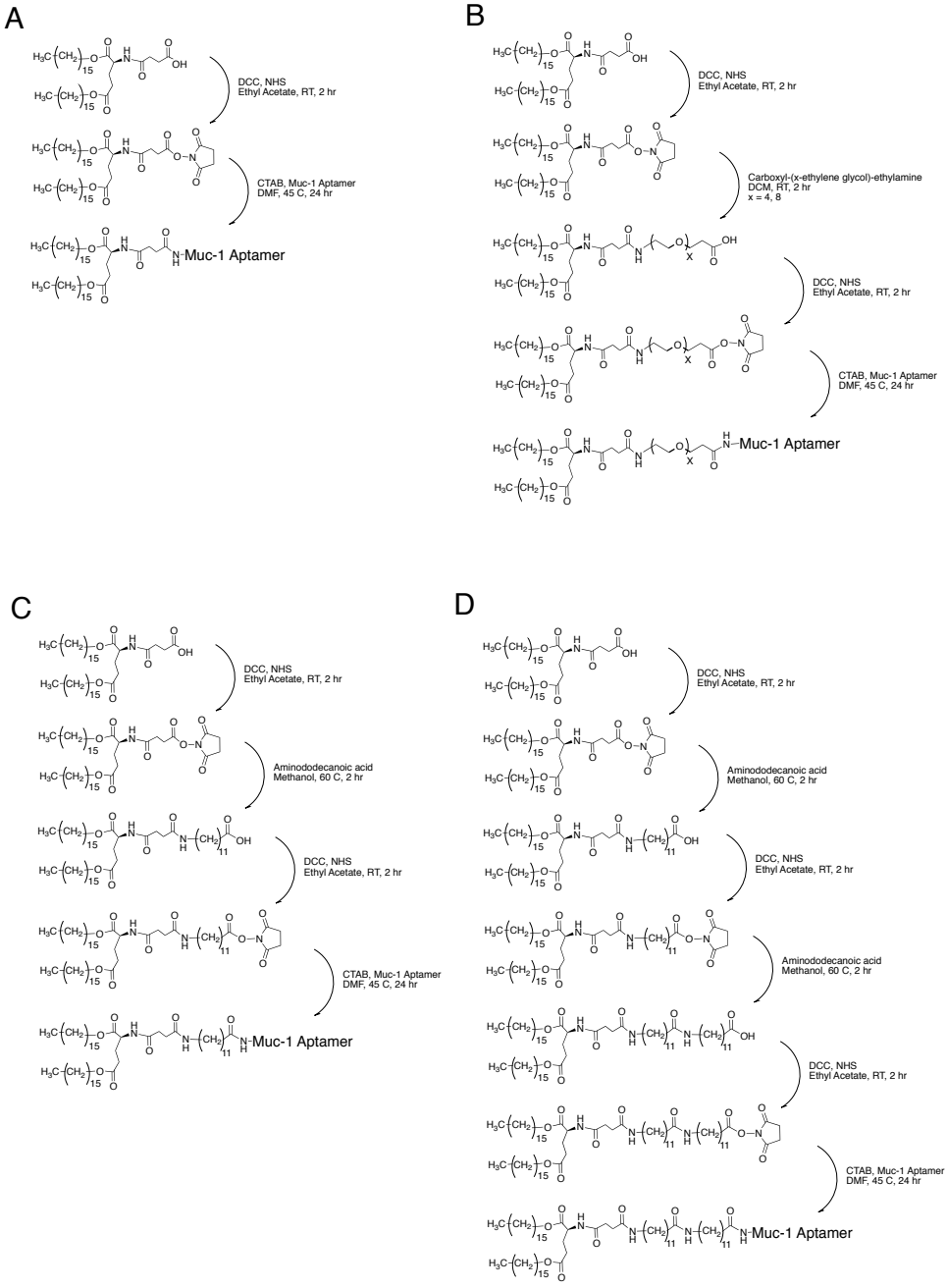

Figure 2.1: Synthesis schemes for Muc-1 aptamer-amphiphiles with A) NoSPR, B) hydrophilic PEG_4 and PEG_8, C) hydrophobic C_{12} spacer and D) hydrophobic C_{24} spacer.

To link the activated tails with the aptamer, 1.25x molar excess cetyl trimethylammonium bromide (CTAB) dissolved in water was added to Muc-1 aptamer. The NH_4^+ ammonium moiety of CTAB is electrostatically attracted to the PO_4^- of the aptamer backbone, forming a sheath of hydrocarbon chains that surround the hydrophilic DNA molecule, which renders the aptamer soluble in dimethylformamide (DMF). A 10x molar excess of activated tails were added to the CTAB-DNA complexes dissolved in DMF and the reaction was stirred at 50 °C for 24 h. After 24 h, the DMF was removed by evaporation and the aptamer-amphiphiles and any unreacted aptamers were purified by ethanol precipitation to remove unreacted tails and CTAB. Unreacted aptamer was separated from the aptamer-amphiphile using reverse-phase high performance liquid chromatography (RP-HPLC) after they were dissolved in water and filtered. HPLC information: Zorbax C18 300 Å SB column, 5-98 %B over 25 min, buffer A: H_2O+10 % methanol, 100 mM hexafluroisopropanol (HFIP), 14.4 mM triethylamine (TEA), buffer B: Methanol, 100 mM HFIP, 14.4 mM TEA. To confirm the success of the synthesis the molecular weights of the aptamer-amphiphiles were verified via liquid chromatography-mass spectroscopy (LC-MS) (Zorbax C18 300 Å SB column, 50-80 %B over 15 min, buffer A: H_2O+15 mM ammonium acetate, buffer B: Acetonitrile. Mass spectroscopy was acquired with an Agilent MSD ion trap).

2.3.3 Critical micelle concentration (CMC) evaluation

Concentrated solutions of each of the aptamer-amphiphiles were diluted with water to make amphiphile solutions ranging from 0.1-900 nM. 50 µL of these solutions were added to wells of a 96 well plate, followed by the addition of 1µL of a 0.05 mg/mL Nile

red dye dissolved in acetone. An orbital shaker operating at 200 rpm was used to mix the solutions for 3 h prior to reading the Nile red fluorescence of each well with a fluorescent plate reader (Ex: 540 nm, Em: 635 nm). Three experiments (n=3) for each amphiphile were performed in triplicate and averaged to produce a single fluorescence value for each.

2.3.4 Cryogenic transmission electron microscopy (Cryo-TEM)

4 μL of 400 or 500 μM amphiphile samples dissolved in water or KCl were deposited onto lacey Formvar/ carbon copper grids that were treated for 15 sec with glow discharge and vitrified in liquid ethane by Vitrobot (Vitrobot parameters: 5 sec blot time, -1 offset, 3 sec wait time, 3 sec relax time, 95 % humidity). Following vitrification, the grid was transferred to a Tecnai G2 Spirit TWIN 20-120 kV / LaB6 Transmission Electron Microscope. Images were captured using an Eagle 2k CCD camera with an accelerating voltage of 120 kV.

2.3.5 Small angle x-ray scattering (SAXS)

X-ray scattering experiments were conducted on the DND-CAT beamline at Argonne National Labs using a beam energy of 17 keV (λ=0.729 Å) and a sample to detector distance of 4.575 m, corresponding to a q-range of 0.0052 $Å^{-1}$ to 0.213 $Å^{-1}$. A low noise marCCD detector recorded the 2-D x-ray scattering data generated by 400 μM solutions of aptamer-amphiphiles sealed within quartz capillaries. Three exposures, each 4 sec in duration, were collected, averaged, and integrated over 120° to produce 1-D data of intensity versus q using FIT2D data reduction software. Scattering data were normalized to incident beam, exposure time, and transmission, and scaled to absolute units. Background scattering from a capillary containing only water was subtracted from the

amphiphile scattering data prior to analysis.

2.3.6 Circular dichroism (CD)

9-13 μM solutions of aptamer and aptamer-amphiphiles in water were heated to 95 °C, quickly cooled to room temperature and transferred to a 0.1 cm path length cuvette immediately prior to collecting their CD spectra using a Jasco J-815 spectrapolarimeter. Data were collected from 320-200 nm at a read speed of 50 nm/min in 1 nm steps. 3 accumulations per amphiphile solution were obtained, the background spectra from the water were subtracted, and the data averaged. Raw ellipticity data were converted to molar ellipticity (Θ) and smoothed with a Matlab filter.

2.4 Results and discussion

2.4.1 Amphiphile synthesis and characterization

In this work we created a set of ssDNA aptamer-amphiphiles with identical hydrophobic dialkyl tails and hydrophilic ssDNA aptamer headgroups but with different spacer molecules linking these groups together with the hypothesis that the type of spacer used would impact the macromolecular assembly. An aptamer that recognizes aberrantly expressed Muc-1 glycoprotein[106] was used as the ssDNA headgroup to demonstrate the possibility of creating ssDNA-amphiphiles that have an additional level of functionality beyond the intrinsic molecular code provided by the DNA bases of ssDNA. A simple solution-phase reaction (Figure 2.1) was developed to link the 25 nucleic acid Muc-1 aptamer (5'-amino C_6 modifier-AAGGGATGACAGGATACGCCAAGCT-3'; MW: 7,928 g/mol) directly to N-hydroxysuccinimide (NHS) activated $(C_{16})_2$-Glu-C_2 tails[30] ("NoSPR"), or to the tails via a PEG_4 spacer (MW: 265 g/mol), PEG_8 spacer (MW: 441 g/mol), C_{12} spacer (MW: 215 g/mol), or C_{24} (MW: 413 g/mol) spacer to create five different aptamer-

amphiphiles (Figure 2.2).

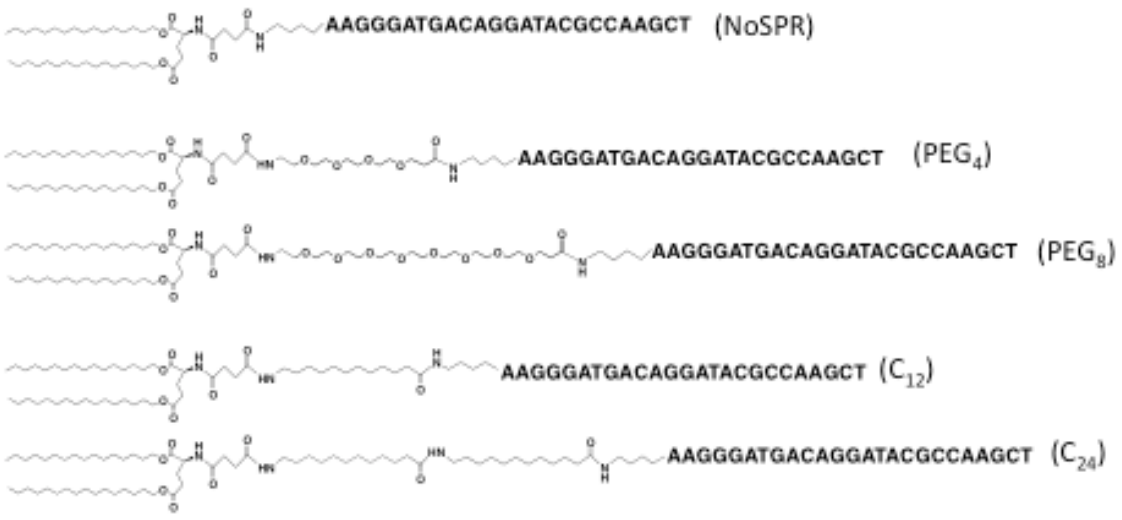

Figure 2.2: Chemical structures of the five Muc-1 aptamer-amphiphiles synthesized.

This simple solution-based synthesis offers an alternative to the popular solid-phase synthesis methods that use harsh cleavage and deprotection solutions, which are potentially damaging to DNA-amphiphiles. To overcome the disparate solubilities of the NHS activated $(C_{16})_2$-Glu-C_2 and $(C_{16})_2$-Glu-C_2-spacer tails and aptamer reactants, cetyl trimethylammonium bromide (CTAB) used to form a hydrophobic sheath of cetyl hydrocarbons around the aptamer via electrostatic attraction of the ammonium headgroups of CTAB to phosphates on the aptamer. This hydrocarbon cover allowed the aptamer to dissolve in dimethylformamide, a suitable solvent for the tails, but did not significantly hinder the aptamer-tail reaction. With this process >80% of the aptamer could be converted to amphiphile and the CTAB was easily separated from the aptamer-amphiphile once the reaction was complete via an ethanol precipitation and high performance liquid chromatography (HPLC) purification (see section 2.3.2 for details). Successful synthesis was confirmed with mass spectrometry (MS) after HPLC

purification (Figure 2.3).

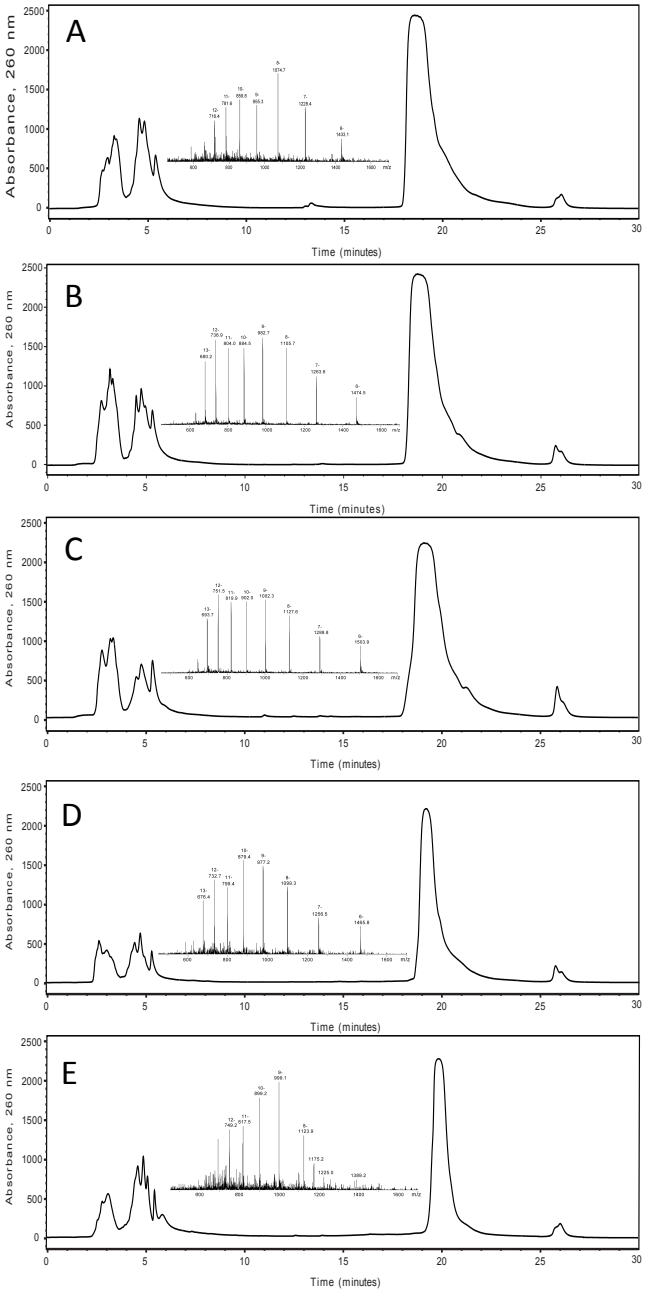

Figure 2.3: HPLC chromatogram of the A) NoSPR, B) PEG_4, C) PEG_8, D) C_{12}, E) C_{24}, Muc-1 amphiphiles. The peaks from 3-6 min are from the aptamer while the peak near 20 min is the aptamer-amphiphiles were determined by LC/MS (insets) and are in good agreement with the expected masses: A) expected mass: 8606.3; observed mass: 8606.9, B) expected mass: 8853.5; observed mass: 8853.4, C) expected mass: 9021.8; observed mass: 9029.1, D) expected mass: 8803.6; observed mass: 8803.3, E) expected mass: 9000.9; observed mass: 9000.9.

2.4.2 Determining critical micelle concentration

After synthesis and purification of the aptamer-amphiphiles, the lipophilic Nile red dye was used to confirm their ability to self-assemble when placed in an aqueous environment.[32] Self-assembly was observed at amphiphiles concentrations as low as ~100 nM (Figure 2.4).

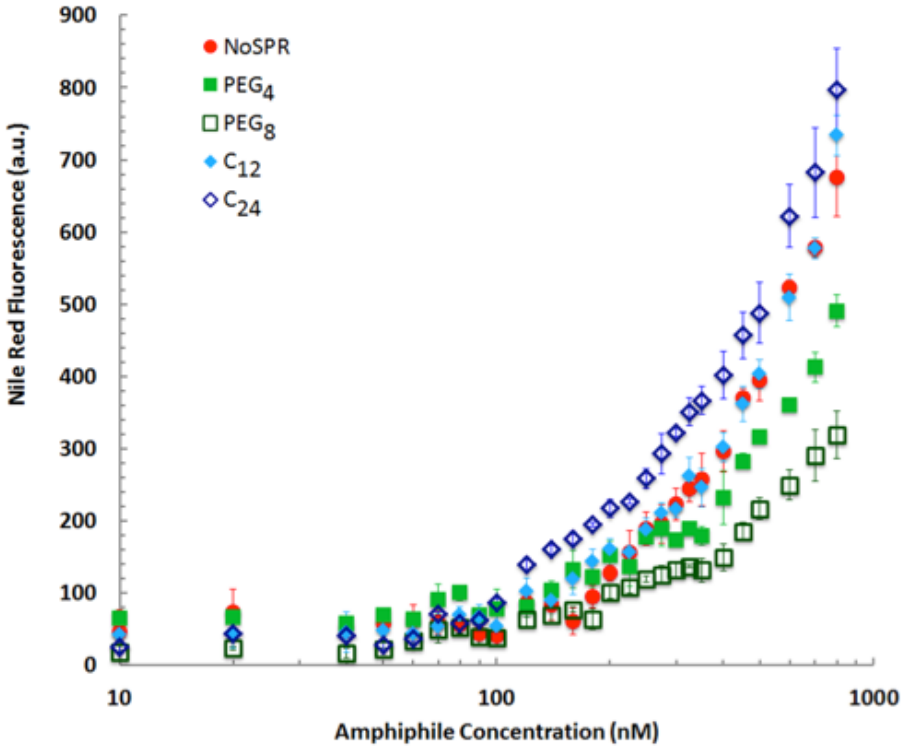

Figure 2.4: Fluorescence intensity of the Nile red dye solubilized in aptamer-amphiphile assemblies versus the aptamer-amphiphiles concentration.

2.4.3 Cryo-TEM of aptamer-amphiphiles

The size and shape of the self-assembled structures was then probed with cryo-TEM. Spherical micelles 10-15 nm in diameter were expected based upon recent examples of DNA-amphiphiles created by conjugating lipids to short sequences of ssDNA.[86,105] Cryo-

TEM imaging showed the NoSPR (Figure 2.5A), PEG_4 (Figure 2.5B), and PEG_8 (Figure 2.6A) spacer amphiphiles formed weakly ellipsoidal globular micelles.

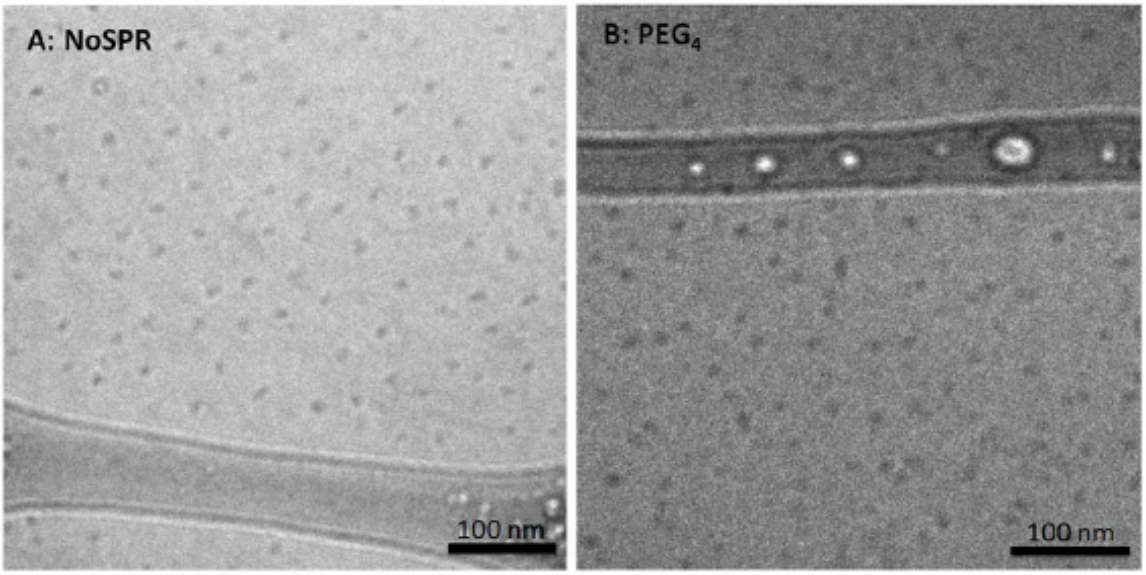

Figure 2.5: Cryo-TEM images of 400 μM Muc-1 aptamer-amphiphile solutions in H_2O. Globular micelles formed by A) NoSPR amphiphiles and B) PEG_4 spacer amphiphiles.

The different spacers did not seem to have a major effect on the size of the micelles formed. Micelles from all the amphiphiles had an average major axis length of 17 ± 3 nm, minor axis length of 13 ± 2 nm, and aspect ratio of 1.3. In addition to forming spherical micelles the C_{12} and C_{24} spacer amphiphiles also self-assembled into flat ribbon-like nanotape structures (Figure 2.6B,C). The observed nanotape structures had lengths ranging from 85-930 nm and widths varying from 25-80 nm. Despite their long lengths, the nanotape structures did not appear to deviate substantially from their longitudinal axis, suggesting they lack flexibility along this axis. The nanotapes are, however, flexible along their lateral axis and twist, a characteristic that is attributed to the chirality of the DNA headgroup.[107,108] Measuring the narrowest part of the twists allows

for the thickness of the nanotapes to be estimated (Figure 2.6D, white arrow),[108] and yields average thicknesses of 14 ± 1 nm for the C_{12} spacer amphiphiles and 14 ± 2 nm for the C_{24} spacer amphiphiles.

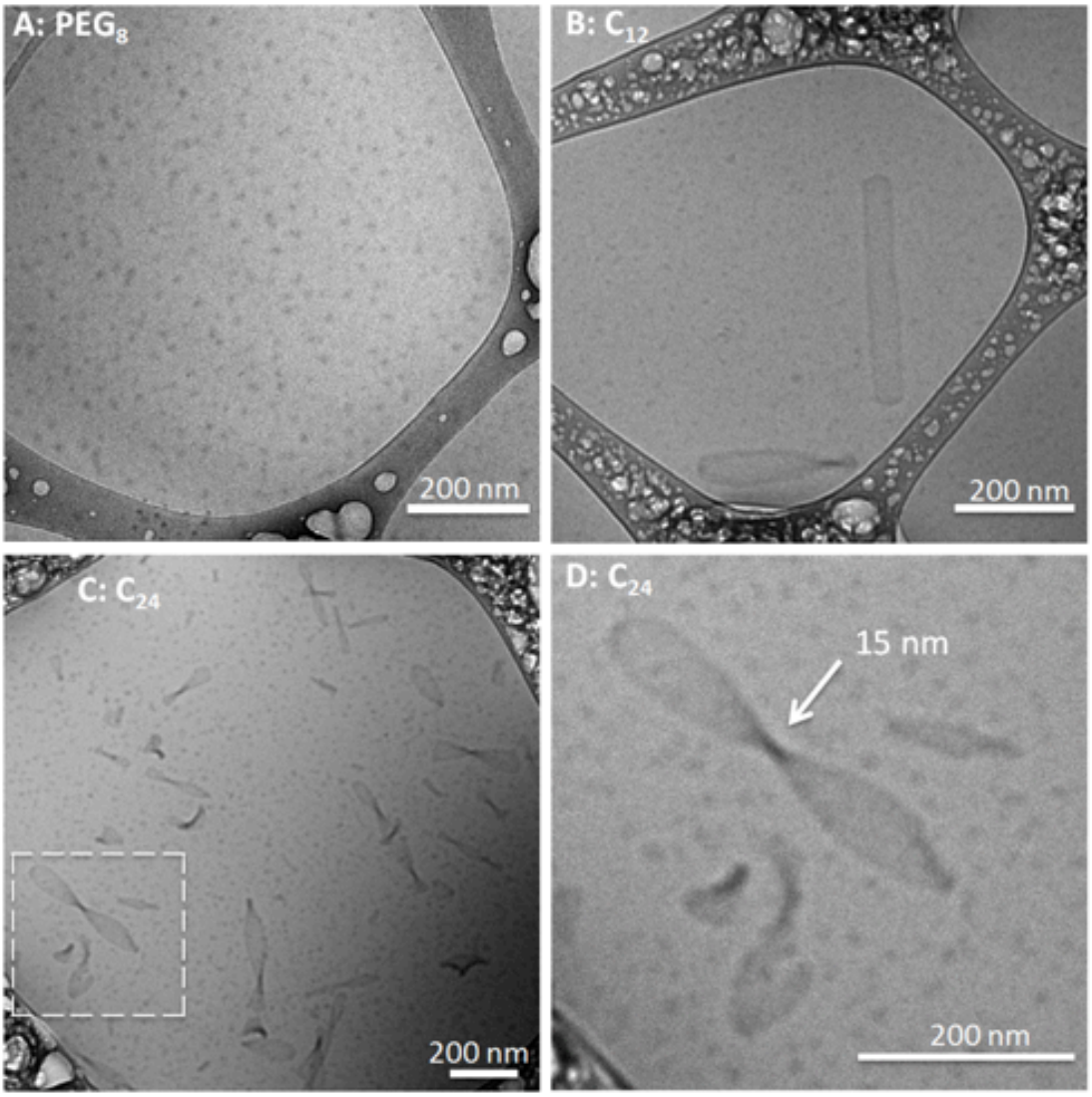

Figure 2.6: Cryo-TEM images of 400 μM Muc-1 aptamer-amphiphile solutions in H_2O. A) Globular micelles formed by PEG_8 amphiphiles. B) Nanotape structures as well as globular micelles are observed from the C_{12} spacer amphiphiles and C) C_{24} spacer amphiphiles. D) A magnified view of the dashed white box in C. The thickness of the nanotape structures is estimated by measuring the narrowest part of the nanotapes as they twist (arrow).

2.4.4 Small angle x-ray scattering by aptamer-amphiphiles

Data from small angle x-ray scattering (SAXS) experiments support the existence of multiple morphologies of the aggregates seen in the cryo-TEM images. Distinct local maxima and minima in one-dimensional scattering data are the result of sufficiently strong x-ray scattering caused by structures in the sample that share a spatial feature of a similar length.[109] In contrast, the lack of well-defined features in the scattering profile is an indication of polydispersity or heterogeneity in morphology.[109] One-dimensional x-ray scattering data from 400 μM amphiphile samples is shown in Figure 2.7.

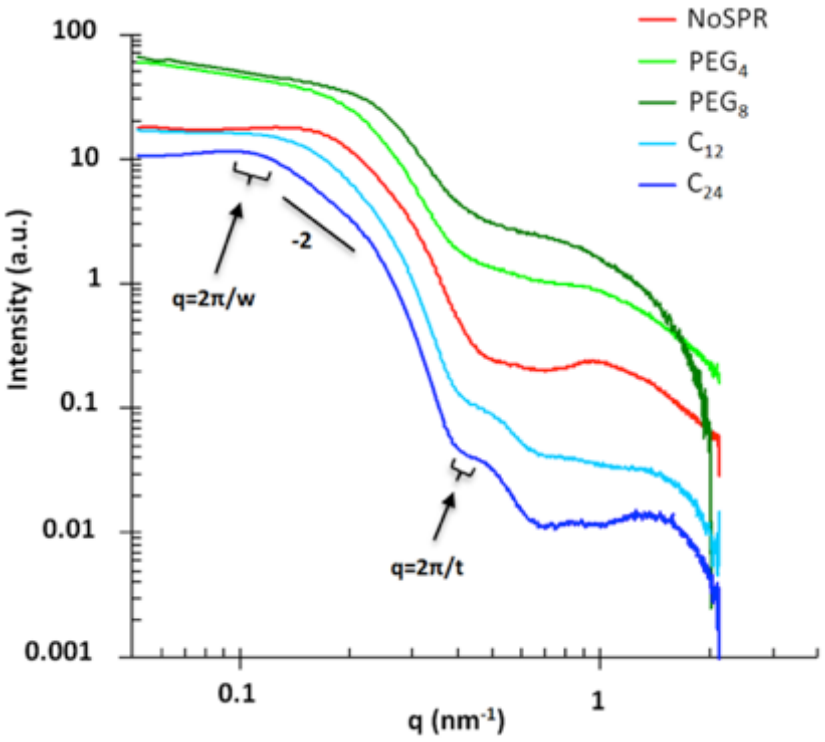

Figure 2.7: Small angle x-ray scattering (SAXS) from 400 μM aptamer-amphiphile samples in H_2O. The intensities are offset vertically for clarity.

The absence of minima corresponding to the globular micelles in the NoSPR, PEG_4 and PEG_8 spacer amphiphiles indicates polydispersity in size and shape, a result that is in

agreement with the cryo-TEM images. The scattering profiles of the C_{12} and C_{24} spacer amphiphiles both have minima between q = 0.4-0.45 nm^{-1} that are attributed to the nanotape structures formed by these amphiphiles. The observed minima between q = 0.4-0.45 nm^{-1} correspond to nanotape thicknesses "t" between 14-16 nm based upon the $q=2\pi/t$ relationship[109] for flat structures like the nanotapes and is in agreement with the 14 ± 2 nm thicknesses observed by cryo-TEM. Additionally, the low-q Guinier regime scattering data of the C_{12} and C_{24} spacer amphiphile samples displays q^{-2} dependence, which is indicative of scattering from flat particles. The transition from a slope of -2 to a slope of 0 in the scattering data occurs between 0.12-0.16 nm^{-1} and 0.10-0.13 nm^{-1} for the C_{12} and C_{24} spacer amphiphiles respectively. This location of this transition is related to the width 'w' of the nanotapes via $q = 2\pi/w$, which yields widths of 39-52 nm for nanotapes in the C_{12} spacer amphiphile samples and 48-63 nm for C_{24} spacer amphiphiles that are in good agreement with the observed widths from the cryo-TEM images (C_{12}: 49 ± 15 nm; C_{24}: 52 ± 13 nm).

2.4.5 Circular dichroism spectroscopy

Circular dichroism (CD) was used to determine the conformation of the aptamer headgroups in the self-assembled structures. Aptamers can adopt a variety of self-associative conformations including stem-loops formed by Watson-Crick base pairing (CD maximum ~277 nm, minimum ~245 nm) and G-quadruplex structures formed from planar stacking of G-quartet structures (maxima ~ 260 nm and 210 nm, minimum ~ 240 nm) when dissolved in pure H_2O or aqueous solutions.[110,111] As seen in Figure 2.8, unmodified Muc-1 aptamer has a CD maximum at 278 nm and a minimum at 244 nm, which is characteristic of stem-loop structure. Similar spectra are seen from aptamer-

amphiphiles with PEG_4 and PEG_8 spacers, which suggests that the assembly process does not significantly alter the secondary structure of the aptamer headgroups when the aptamers are conjugated to the hydrophobic tails via the hydrophilic PEG spacers. In contrast, the C_{12} and C_{24} spacer amphiphile spectra both have CD maxima at 265 nm and 207 nm. This closely matches the expected CD spectrum of parallel G-quadruplexes. Parallel G-quadruplexes can be formed from a single strand (intramolecular) or four different strands (intermolecular) of ssDNA. In both cases, at least two sets of the single-plane G-quartet structures must stack on top of one another, with the 5' ends of the nucleic acids oriented in the same direction. Inspection of the Muc-1 aptamer sequence reveals only 7 guanine residues, one short of the 8 needed to form an intramolecular G-quadruplex. This suggests that the G-quadruplex structures are formed from the association of four individual aptamer headgroups.

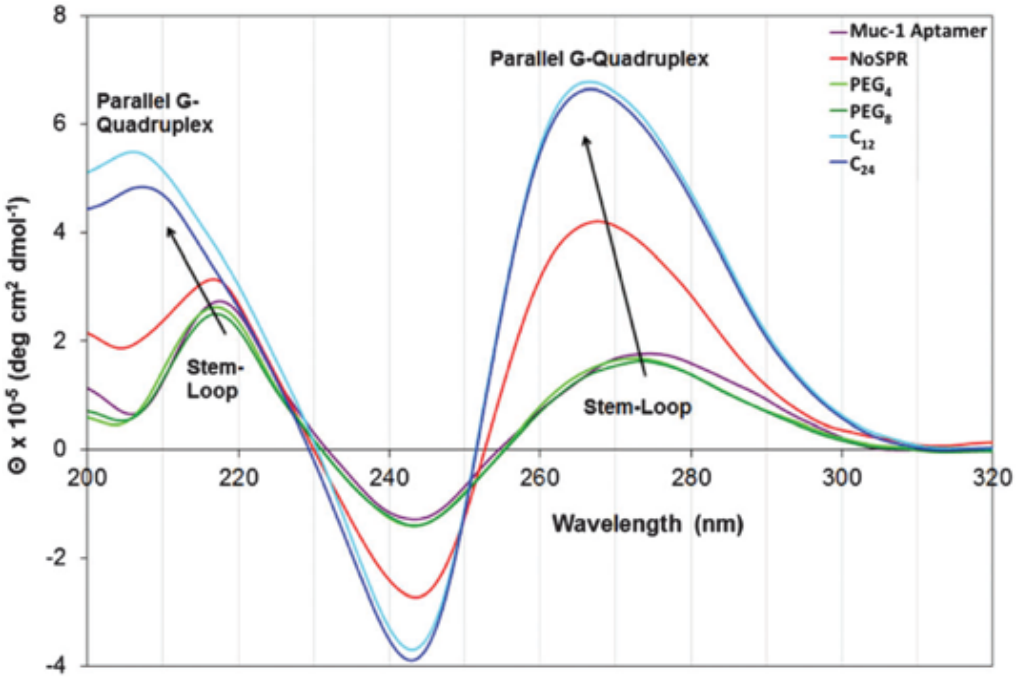

Figure 2.8: Circular dichroism of Muc-1 aptamer and Muc-1 aptamer-amphiphiles with different spacer in H_2O.

2.5 Discussion

Based on the cryo-TEM, SAXS, and CD data we hypothesize that the nanotapes are bilayer structures of C_{12} and C_{24} spacer amphiphiles with the hydrocarbon tails and spacers forming a hydrophobic core and the aptamer headgroups extending away from the hydrophobic interface (Figure 2.9).

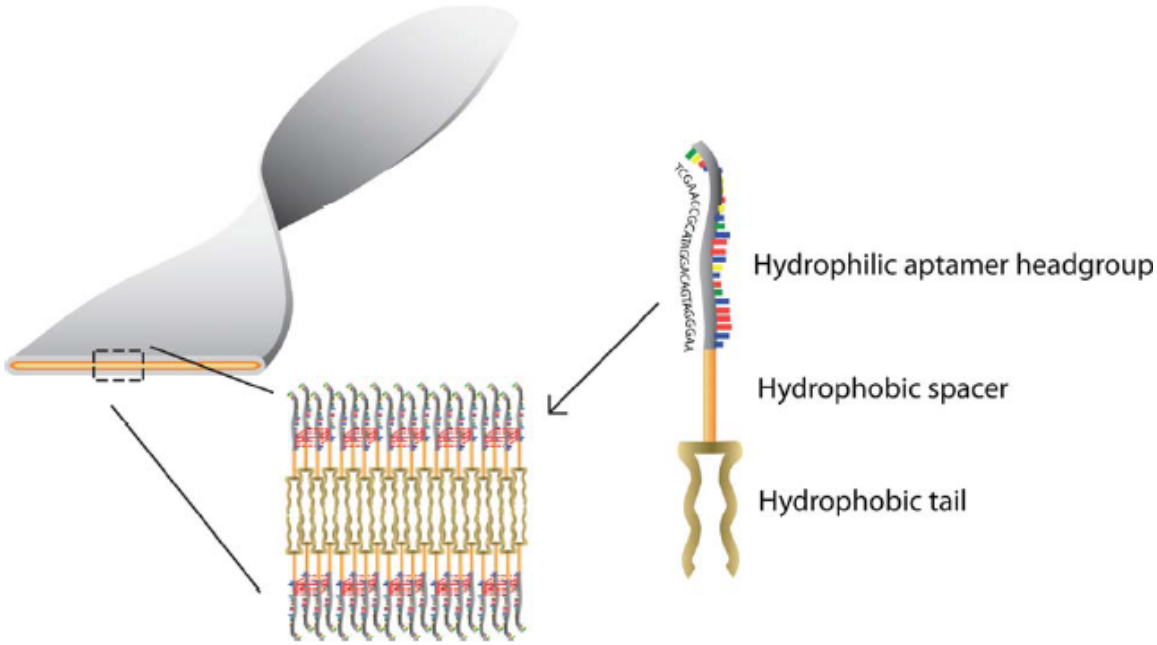

Figure 2.9: Graphical representation of the nanotapes structure formed from C12 and C24 spacer Muc-1 aptamer-amphiphiles. The red dotted lines show how we hypothesize that four aptamer headgroups may be forming G-quadruplexes.

The presence of the nanotapes cannot be predicted by the standard packing parameter analysis that is commonly used to describe the shapes of self-assembled molecules and is based on the relationships of the hydrophilic and hydrophobic amphiphile components. The packing parameter is defined as the (cross-sectional area of the tail)/(equilibrium area per molecule at the aggregate surface). The cross-sectional area

of each amphiphile, regardless of the spacer, is defined by the cross-sectional area of the C_{16} double tail while the equilibrium area occupied by each amphiphile at the aggregate surface is influenced by the steric and electrostatic repulsions present between the aptamer headgroups.[22] The packing parameter would therefore be identical for each of the amphiphiles and the formation of micelles would be expected for all aptamer-amphiphiles due to the large equilibrium area per molecule caused by the steric and electrostatic repulsions present between the aptamer headgroups. Additionally, it has been shown that when the length of the hydrophobic tail is increased there is an increase in the equilibrium area per molecule at the aggregate surface.[22] In this case the packing parameter would be even smaller for the C_{12} and C_{24} spacer amphiphiles and still predict the formation of micelles rather than the experimentally observed flat nanotape structures. We hypothesize that the attractive hydrophobic interactions between adjacent hydrophobic spacers force the aptamer headgroups to reside in close proximity to each other, reducing the area per aptamer at the interface and allowing the nanotape assemblies to form. As a result of this close packing the aptamer headgroups may extend from the interface of the assembled structures, which places the consecutive guanine residues of four separate aptamers in close proximity to one another and in position to form parallel G-quadruplex structures observed in the CD spectra of these samples. The Muc-1 aptamer-amphiphiles without hydrocarbon spacers lack the added attractive hydrophobic force necessary to overcome the steric and electrostatic repulsion of the aptamer headgroups and therefore do not readily form the nanotape structures even when salts are added to the solution to screen the negative charge of the aptamer headgroups and stabilize G-quadruplex formation (Figure 2.10 and 2.11).

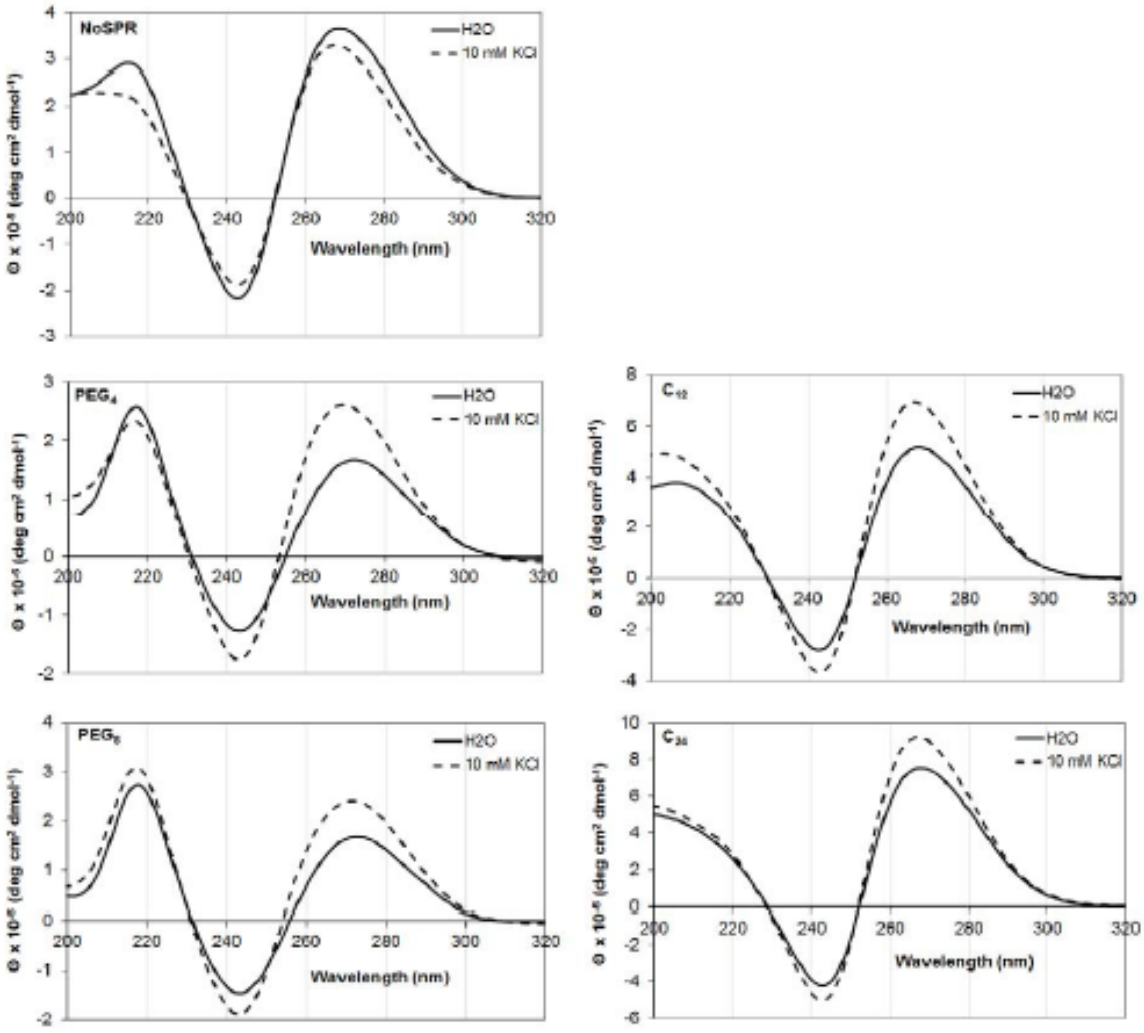

Figure 2.10: CD spectra of Muc-1 aptamer-amphiphiles with different spacers (NoSPR, PEG_4, PEG_8, C_{12}, and C_{24}) dissolved in H_2O or 10 mM KCl. The CD spectra suggest that the addition of salt to the solution does not change the structure of the amphiphiles' headgroups significantly.

Interestingly, coexistence of micelles and nanotapes was found to persist after 28 days of aging in water at room temperature (Figure 2.11).

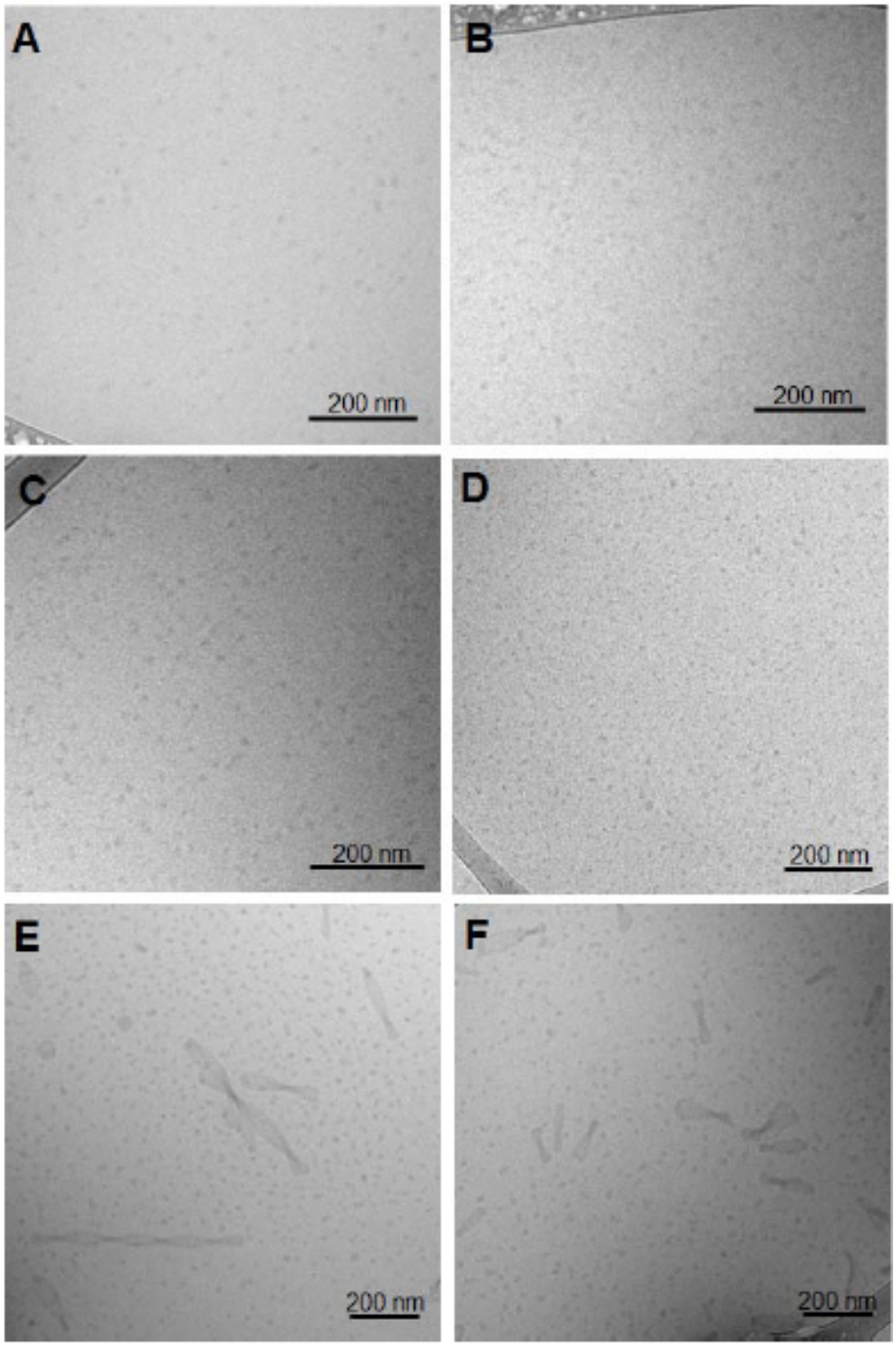

Figure 2.11: Cryo-TEM images of 500 μM Muc-1 aptamer-amphiphile solutions in H_2O (A, C, E) or 10 mM KCl (B, D, F). Samples in H_2O were kept at room temperature for 28 days prior to freezing and imaging. The 10 mM KCl samples were frozen and imaged immediately after the amphiphiles were dissolved. Globular micelles remain the only structures present in the NoSPR (A, B) and PEG_8 (C, D) samples while the C_{24} (E, F) amphiphiles assemble into both micelles and nanotapes for both solutions.

2.6 Conclusions

This work demonstrates that the choice of the spacer used to link the hydrophobic and hydrophilic blocks of an aptamer-amphiphile can dramatically influence their self-assembly, providing a new method to exert control over macromolecular organization. Nanotape structures formed by ssDNA-amphiphiles have not yet been described in the literature and are particularly interesting for applications in DNA nanotechnology like nanosensors, surface patterning, and targeted drug delivery. Additionally, the versatile solution-phase synthesis described here to create the amphiphiles offers an alternative to on-the-resin synthesis that requires potentially damaging deprotection and cleavage solutions, making it a widely accessible technique for nucleic acid chemistry.

3 DNA nanotubes and helical nanotapes via self-assembly of ssDNA-amphiphiles*

3.1 Synopsis

DNA nanotubes were created using molecular self-assembly of single-stranded DNA (ssDNA)-amphiphiles composed of a hydrophobic dialkyl tail and polycarbon spacer and a hydrophilic ssDNA headgroup. The nanotube structures were formed by bilayers of amphiphiles, with the hydrophobic components forming an inner layer that was shielded from the aqueous solvent by an outer layer of ssDNA. The nanotubes appeared to form via an assembly process that included transitions from twisted nanotapes to helical nanotapes to nanotubes. Amphiphiles that contained different ssDNA headgroups were created to explore the effect of the length and secondary structure of the ssDNA headgroup on the self-assembly behavior of the amphiphiles in the presence and absence of the polycarbon spacer. It was found that nanotubes could be formed using a variety of headgroup lengths and sequences. The ability to create nanotubes via ssDNA-amphiphile self-assembly offers an alternative to the other purely DNA-based approaches like DNA origami and DNA tile assembly for constructing these structures and may be useful for applications in drug delivery, biosensing, and electronics.

3.2 Introduction

The field of DNA nanotechnology has transformed DNA from a biological material that stores genetic information into a construction material that can be used to build 3-

dimensional scaffolds, structures, and devices with nanoscale features.[112,113] The ability to precisely control the organization of DNA relies on Watson-Crick base pairing, which acts as a molecular glue to hold strands of DNA together in a predictable manner. There are a variety of strategies that can be used to create DNA nanostructures, each that use a combination of different ssDNA sequences that when mixed together and subjected to specific annealing conditions (i.e., controlled cooling rates, specific ions, and pH) fold together to produce double stranded DNA segments that organize into highly uniform structures of the desired shape.[114–116] The predictability of base pairing offers an opportunity to rationally select these ssDNA sequences, often with the aid of software, that can combine together to form tetrahedrons, cages, barrels, and tube structures while maintaining ssDNA overhangs that act as addressable locations and allow the structures to be further functionalized with drugs, dyes, and metals for use as therapeutics, diagnostics, electronics and photonics, and in molecular and cellular biophysical studies.[113,116]

An alternative approach to form DNA nanostructures is to covalently link hydrophilic ssDNA sequences with hydrophobic tails (polymers or other hydrophobic moieties) to form amphiphilic molecules.[79,81] The amphiphilic nature of the conjugates induces their spontaneous assembly when added to an aqueous environment, with the hydrophobic tails preferring to sequester themselves into a hydrophobic domain while the ssDNA sequences extend into the aqueous solution. With this structural arrangement the ssDNA is not required to base pair in order to create the nanostructure and remains available for base pairing with complimentary ssDNA sequences. Additionally, this approach to forming DNA nanostructures does not require base pairing prediction

software and reduces the requirements for specific annealing conditions. However, this approach has not yet been used to create nanostructures with similar levels of complexity as those achieved by other approaches like DNA origami and DNA tile assembly.[116] To date, the majority of structures created by ssDNA-amphiphile assembly have been spherical and cylindrical micelles. [81,97]

In pursuit of enhancing the level of structural complexity achievable through self-assembly of ssDNA-amphiphiles we recently tested how an additional building block, a spacer molecule used to link a ssDNA aptamer headgroup and hydrophobic lipid-like tail, could affect ssDNA-amphiphile assembly.[117] It was found that globular micelles were formed when a 25 nucleotide aptamer was directly conjugated to a C_{16} dialkyl tail or conjugated to the tail via hydrophilic PEG_4 or PEG_8 spacers, but that flat and twisted nanotapes comprised of bilayers of amphiphiles were formed when hydrophobic C_{12} and C_{24} spacers were used.[117] The nanotape morphology achieved by including a hydrophobic spacer in the design of the amphiphile was not predicted by the standard packing parameter analysis, leading to the hypothesis that polycarbon spacers, through attractive hydrophobic interactions, may force the aptamer headgroups into close proximity of each other, thus reducing the interfacial headgroup area and allowing the nanotapes to form.[117] We have also recently shown that amphiphiles created with a 40 nucleotide ssDNA aptamer headgroup containing a large number of guanine nucleotides capable of forming intermolecular parallel G-quadruplexes with neighboring aptamer headgroups self-assembled into nanotapes in the absence of a polycarbon spacer.[118] This finding suggested that the intermolecular interactions that produced the G-quadruplex structure may have reduced the effective headgroup area of the ssDNA in a

manner analogous to the polycarbon spacer and encouraged the assembly of bilayer nanotapes.[118]

These previous findings suggested that variations in the ssDNA headgroups could influence the self-assembly behavior of ssDNA-amphiphiles. To investigate this possibility, ssDNA headgroups with random nucleotide sequences of variable length (10, 25, and 40 nucleotides) were conjugated to hydrophobic tails via the C_{12} spacer that was previously found to be important for forming twisted nanotape structures.[117] ssDNA headgroups that lacked guanine nucleobases were selected to eliminate the possibility of G-quadruplex interactions within the ssDNA headgroups. Additional headgroups that contained guanine-rich sequences at the 5' region of the headgroup were also created and directly conjugated to the hydrophobic tails to determine the possibility of using a guanine-rich sequence as a replacement for the C_{12} spacer. Finally, amphiphiles that contained both a guanine-rich headgroup and the C_{12} spacer were created to study the combined effect of these two variables.

It was found that amphiphiles containing the C_{12} spacers and the random guanine-free ssDNA headgroups of each length not only self-assembled into globular micelles and twisted nanotapes, as seen previously, but also helical nanotapes and nanotubes, nanostructures that have never before been created using ssDNA-amphiphiles. Amphiphiles created with these same headgroups but without the C_{12} spacer were unable to form the twisted or helical nanotapes or nanotubes, demonstrating the importance of the hydrocarbon spacer for forming these larger, more complex structures. Headgroups with oligo-guanine (G_5) sequences designed to replace the C_{12} spacer and

recapture the capability to form the nanotape and nanotube structures only succeeded in producing these larger structures when the headgroup was 40 nucleotides in length. It was also found that in the absence of the C_{12} spacer, 25 and 40 nucleotide headgroups that contained a $(GGGT)_3$ sequence, created to form intermolecular G-quadruplex interactions, could produce the twisted nanotape structures but not the helical nanotape and nanotube structures. Finally, when the C_{12} spacer was combined with the G_5-containing headgroups 25 and 40 nucleotides in length all of the nanostructures seen in the initial set of samples that contained the C_{12} spacer and guanine-free headgroups were again produced, while the amphiphiles with the G_5-modified headgroups 10 nucleotides in length only produced short nanotubes.

3.3 Materials and methods

3.3.1 Materials

Toluene, chloroform, acetone, methanol, and triethylamine (TEA) were purchased from Fischer Chemical (Hanover Park, IL). ssDNA was purchased from Integrated DNA Technologies (Coralville, IA), cetyl trimethylammonium bromide from Acros Organics (Morris Plains, NJ), and hexafluroisopropanol (HFIP) from Oakwood Products Inc. (West Columbia, SC). Lacey Formvar/carbon 200 mesh copper grids were purchased from Ted Pella Inc. (Redding, CA). Atomic force microscopy contact mode rectangular Si cantilevers with an Al-coated backside (NSC36/Al BS) were acquired from MikroMasch (Lady's Island, SC). Ruby mica sheets, V2 quality, were purchased from S&J Trading Inc. **(**Glen Oaks, NY). All other chemicals and materials were purchased from Sigma-Aldrich (St Louis, MO).

3.3.2 ssDNA-amphiphile synthesis

The ssDNA sequences with an amino-C_6 linker attached to their 5' end were conjugated directly to the N-hydroxysuccinimide (NHS) activated $(C_{16})_2$-Glu-C_2 tails[30] (NoSPR), or to the tails via a C_{12} spacer using a solution-phase synthesis as described previously[117] to create ssDNA-amphiphiles. Unreacted ssDNA was separated from ssDNA-amphiphiles using reverse-phase high performance liquid chromatography (HPLC). HPLC information: Zorbax C_8 300 Å SB column, 5-90% B over 25 min, buffer A: H_2O + 10% methanol, 100 mM HFIP, 14.4 mM TEA, buffer B: methanol, 100 mM HFIP, 14.4 mM TEA. To confirm the success of the synthesis the molecular weights of the purified amphiphiles were identified by liquid chromatography-mass spectroscopy (LC-MS) (Zorbax C_3 300 Å SB column, 50-80% B over 15 min, buffer A: H_2O + 15 mM ammonium acetate, buffer B: acetonitrile). Mass spectroscopy data were acquired with an Agilent MSD ion trap.

3.3.3 Cryogenic transmission electron microscopy (cryo-TEM)

4.5 µL of 500 µM amphiphile solutions were deposited onto lacey Formvar/carbon copper grids that had been treated with glow discharge for 60 sec and vitrified in liquid ethane by Vitrobot (Vitrobot parameters: 4 sec blot time, 0 offset, 3 sec wait time, 3 sec relax time, ambient humidity). The grids were kept under liquid nitrogen until they were transferred to a Tecnai G2 Spirit TWIN 20-120 kV/LaB6 TEM operated with an acceleration voltage of 120 keV. Images were captured using an Eagle 2k CCD camera.

3.3.4 Fluorescent microscopy

Nile red was added to ssDNA-amphiphile solutions at a ratio of 3 µL Nile red solution (0.1 mg/mL in methanol) to 50 µL of 20 µM amphiphile solutions to stain the hydrophobic

areas of the self-assembled structures. 3 μL of the amphiphile solutions were deposited onto clean glass slides and covered with clean glass coverslips. Fluorescent images were obtained using an EVOS FL microscope (Life Technologies, Grand Island, NY) with a Texas Red light cube (Ex: 585 nm, Em: 624 nm).

3.3.5 Circular dichroism

500 μM solutions of ssDNA-amphiphiles were diluted to 20 μM with Milli-Q water and transferred to a 0.1 cm path length cuvette. CD spectra from 320-200 nm were collected using a Jasco J-815 spectrapolarimeter using a read speed of 50 nm/min in 1 nm steps. 3 accumulations per amphiphile solution were recorded with the background spectrum from the water automatically subtracted. The accumulations were averaged and the raw ellipticity values were converted to molar ellipticity

3.3.6 Atomic Force Microscopy (AFM)

20 μL of 10 mM $MgCl_2$ solution was added to a freshly cleaved mica surface for 10 sec and then removed to enhance the adhesion of the ssDNA-amphiphiles to the mica substrate. 5 μL of a 500 nM solution of ssDNA-amphiphile was deposited onto the mica surface and left for 5 min to allow time for the amphiphiles to adhere to the surface. The surface was subsequently washed twice with 20 μL of Milli-Q water and allowed to dry in air prior to imaging. AFM imaging was performed with a Nanoscope V Multimode 8 SPM (Bruker, Santa Barbara, CA) in contact mode in air using rectangular Si cantilevers with a typical probe tip radius of 8 nm.

3.4 Results

3.4.1 ssDNA-amphiphile synthesis

An initial ssDNA headgroup 40 nucleotides in length was created using only adenine (A), cytosine (C), and thymine (T) nucleobases selected at random. This guanine-free (NoG) 40 nucleotide headgroup was then used to create headgroups with 10 and 25 nucleotides that conserved the nucleotide order at the 5' end of the headgroup (Figure 3.1A).

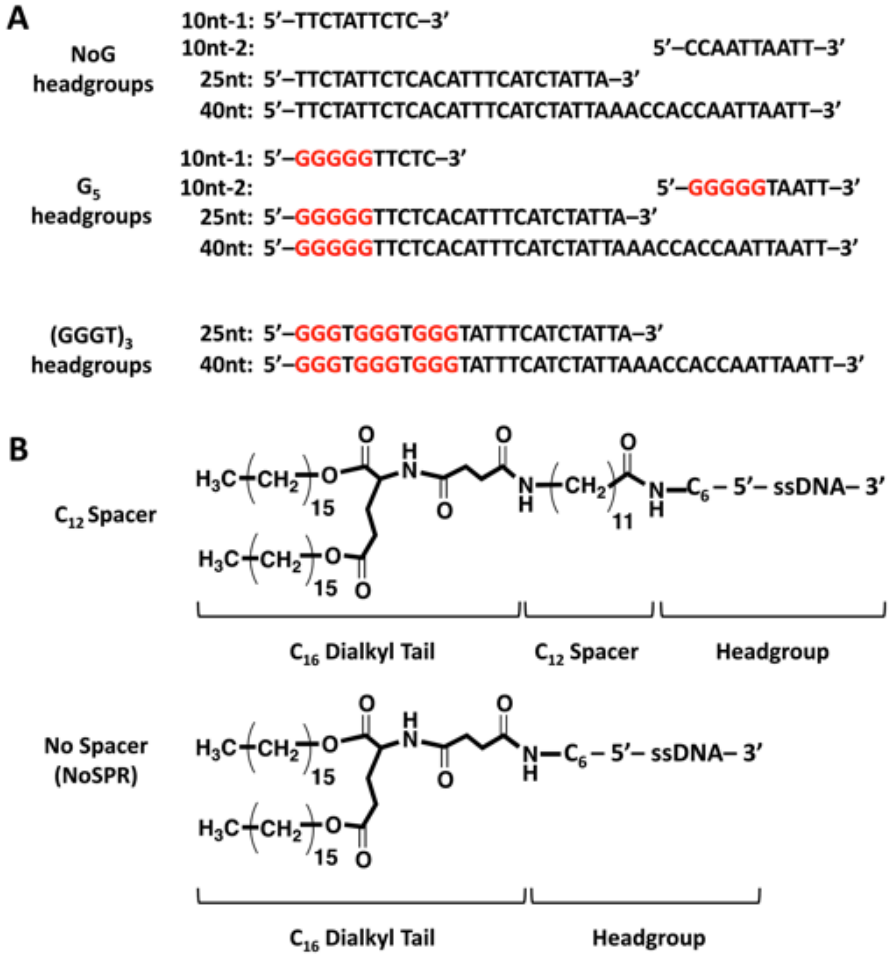

Figure 3.1: A) Sequences of the 10 nucleotide (nt), 25 nucleotide, and 40 nucleotide guanine-free (NoG) and guanine-modified headgroups (having either a G_5 or a $(GGGT)_3$ sequence) used to create the ssDNA-amphiphiles. B) Chemical structures of ssDNA-amphiphiles with a C_{16} dialkyl tail, a C_{12} spacer or without a spacer (NoSPR), and a ssDNA headgroup containing a C_6 linker and having different sequences as shown in A.

A second version of the 10 nucleotide sequence was created that conserved the 3' end of the headgroup, which provided a headgroup with the same length but a different random nucleotide sequence. Nucleotides containing the guanine nucleobase were used to replace some nucleotides at the 5' end of the headgroups, either as a single string of five guanines (G_5) or as a repeat of $(GGGT)_3$ (Figure 3.1A) to produce headgroups that had potential to form intermolecular G-quadruplex interactions. The 5' ends of the ssDNA headgroups were conjugated to dialkyl tails via C_{12} spacer molecules or directly to the tails without the use of a spacer (Figure 3.1B). Successful conjugation was confirmed by LC-MS (Table 3.1).

Table 3.1: Liquid chromatography-mass spectroscopy data of the 10, 25, and 40 nucleotide (nt) ssDNA-amphiphiles created with or without a C_{12} spacer and various headgroups, as shown in Figure 3.1.

		No Spacer		C_{12} Spacer	
		Expected Mass (M-H)	Oberved Mass (M-H)	Expected Mass (M-H)	Oberved Mass (M-H)
NoG headgroups	10nt-1	3,801.1	3,799.6	3,998.5	3,997.1
	10nt-2	3,834.2	3,832.6	4,031.6	4,030.0
	25nt	8,364.1	8,361.7	8,561.5	8,559.4
	40nt	12,930.1	12,927.2	13,127.5	13,127.5
G_5 headgroups	10nt-1	3,932.2	3,930.9	4,129.6	4,128.3
	10nt-2	3,980.2	3,979.4	4,177.6	4,176.3
	25nt	8,495.2	8,493.0	8,692.6	8,690.0
	40nt	13,061.1	13,058.5	13,258.5	13,255.3
$(GGGT)_3$ headgroups	25nt	8,631.2	8,630.9		
	40nt	13,197.2	13,196.9		

3.4.2 Self-assembly of ssDNA-amphiphiles with NoG headgroups and with or without a C_{12} spacer

Amphiphiles with NoG headgroups attached to the hydrophobic tails via C_{12} spacers were dissolved in Milli-Q water to form 500 μM solutions and were immediately (within 30 min) deposited onto cryo-TEM grids, vitrified in liquid ethane, and imaged to visualize the morphology of the self-assembled structures formed by the amphiphiles. A variety of structures were present in each of the amphiphile solutions with either a 10,

25 or 40 nucleotide NoG headgroup and a C_{12} spacer: globular micelles, twisted nanotapes, helical nanotapes, and nanotubes (Figure 3.2, Figure 3.3).

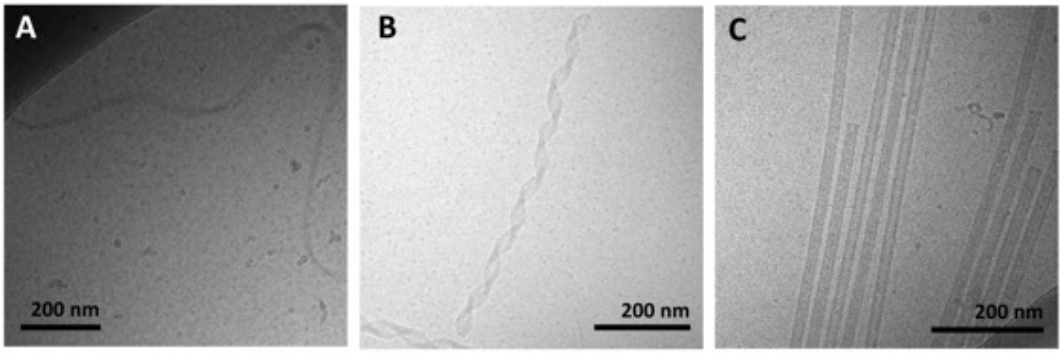

Figure 3.2: Cryo-TEM images of ssDNA-amphiphiles forming A) a twisted nanotape, B) helical nanotapes and C) nanotubes. All amphiphiles contained the C_{12} spacer and either the A) 25nt NoG, B) 10nt-2 NoG or C)10nt-1 NoG headgroups.

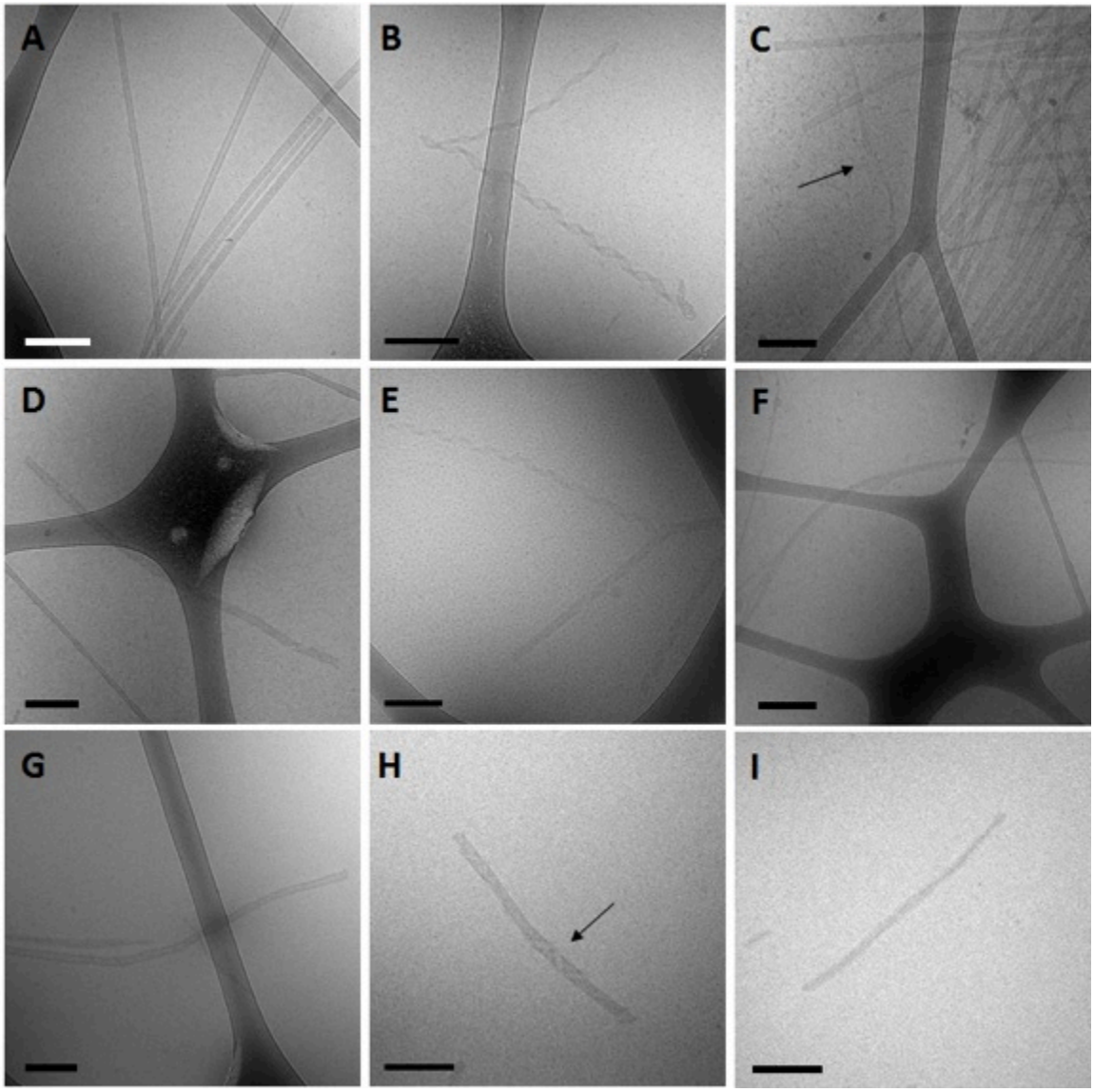

Figure 3.3: Cryo-TEM images of nanotubes (A, D, G), helical nanotapes (B, E, H), and twisted nanotapes (C, F, I) formed by ssDNA-amphiphiles with guanine-free (NoG) headgroups and C_{12} spacers. Top row: (A, C) 10nt-1 headgroup, (B) 10nt-2 headgroup. Middle row (D, E, F): 25nt headgroup. Bottom row (G, H, I): 40nt headgroup. The black arrow in C shows the twisted nanotape structure, and in H a helical section of the nanostructure. All scale bars are 200 nm.

Of particular interest were the nanotube structures, which have never before been formed via self-assembly of ssDNA-amphiphiles. Analysis of an image of a nanotube created from amphiphiles with a 25 nucleotide NoG headgroup and a C_{12} spacer

obtained at 0° and 45° stage-tilt (Figure 3.4A,B) showed that the diameter of the nanotube was unchanged when viewed from different angles, demonstrating its cylindrical shape. Line-scan analysis of the nanotube structure (Figure 3.4C) revealed a pattern of contrast consistent with that of a hollow tube, 34 nm in diameter with 10 nm thick walls, confirming the cylindrical structure observed in the sample is a nanotube.

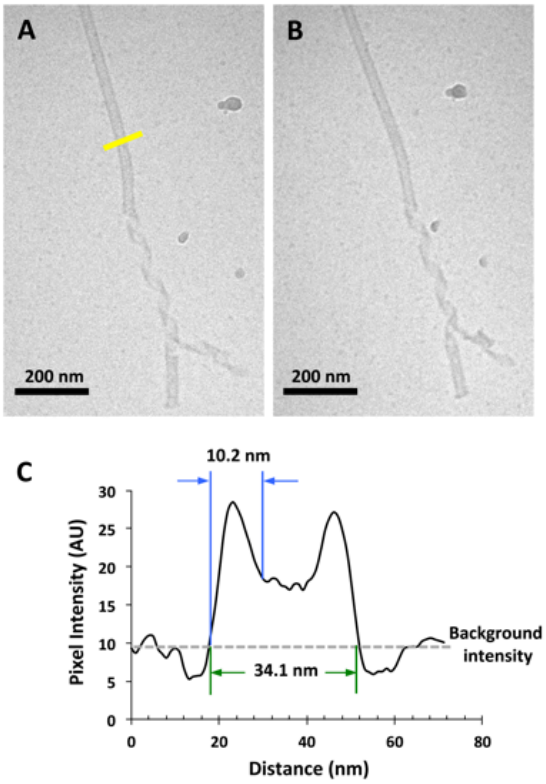

Figure 3.4: Cryo-TEM and line-scan analysis of ssDNA-amphiphiles with a 25 nucleotide NoG headgroup and a C_{12} spacer. Images of the same nanotube and helical nanotape section A) before and after B) a 45° stage tilt. The diameter of the nanotube segment at 0° and 45° tilt is 34 nm. C) Line-scan analysis of a segment of the untilted cryo-TEM image (yellow line in A) shows the characteristic shape of a hollow cylinder, 34 nm in diameter with 10 nm thick walls, confirming the cylindrical structure observed in the sample is a nanotube.

The cylindrical nanotube structures observed in the samples with headgroups containing 10 nucleotides had an overall average diameter of 30 ± 4 nm, while samples with the 25

and 40 nucleotide headgroups produced structures with average diameters of 32 ± 3 nm and 31 ± 1 nm, respectively. While the overall average diameters of the nanotubes produced by amphiphiles of different headgroup lengths were similar, the diameters of the nanotubes varied between different nanotubes in the same sample, and in some cases there was also variation along the length of a single nanotube. The lengths of the nanotubes formed by amphiphiles containing the 10, 25, and 40 nucleotide headgroups were variable, with each sample producing nanotubes 100s to 1,000s of nm in length and no apparent difference in the typical length between amphiphiles with different headgroups. High aspect ratio structures with lengths greater than 10 μm were observed in fluorescent images of amphiphile samples (Figure 3.5), providing further evidence that nanotubes and nanotapes assemble under ambient conditions.

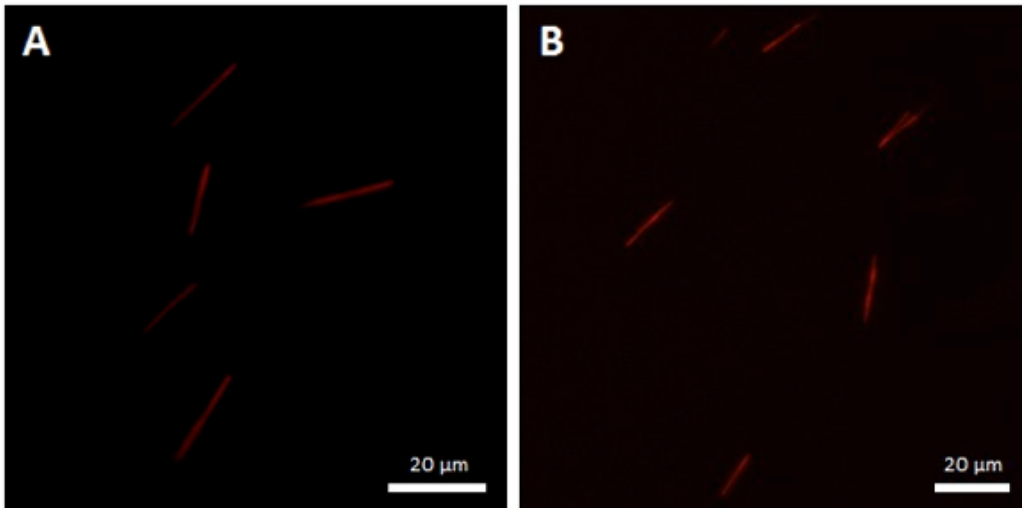

Figure 3.5: Fluorescent images of high aspect ratio structures formed by amphiphiles with the C_{12} spacer and guanine-free (NoG) headgroups A) 10 nucleotides (10nt-1) or B) 40 nucleotides in length. Amphiphile samples were stained with the hydrophobic Nile red dye prior to imaging.

However, the resolution and magnification of the fluorescent imaging is not sufficient to

definitively determine if the structures observed in the fluorescent images are single structures or aggregates and the sizes observed may not accurately represent the lengths and widths of the individual nanostructures.

Twisted and helical nanotapes were also observed in all the samples, but in lower numbers than the nanotubes. The majority of the twisted nanotapes in each of the different amphiphile samples did not twist in a periodic manner and had widths ranging from 20 to 50 nm. However, in a few instances the twisted nanotapes were observed to twist in a periodic manner they had an average pitch length of 132 ± 6 nm and an average width of 24 ± 2 nm. The helical nanotapes observed in each of the different amphiphile samples displayed clear periodicity with an average pitch length of 129 ± 7 nm, similar to that observed in the twisted nanotape structures. However, the average width of the helical nanotapes was 38 ± 4 nm, substantially larger than that of the regularly twisted nanotapes. Also present in all of the samples were globular micelles, some of which were spherical and some were weakly ellipsoidal. Micelles formed by each of the amphiphile samples had diameters (or ellipsoid axes lengths) of 9-20 nm with no measurable difference in average size between the amphiphiles with different length headgroups.

The same NoG headgroups were also conjugated directly to hydrophobic tails without the use of the C_{12} spacer (NoSPR) and imaged with cryo-TEM. These amphiphiles also formed micelles but were not observed to form any of the larger, more complex, bilayer nanotape and nanotube structures (Table 3.2). The inability for amphiphiles with NoG headgroups and lacking the C_{12} spacer to form more complex bilayer structures was not

surprising as it has been previously shown that amphiphiles with headgroups of similar lengths that lack G-quadruplex interactions only assemble into globular micelles.[105,117,118]

Table 3.2: A summary of the structure observed with cryo-TEM in each of the ssDNA-amphiphiles samples shown in Figure 3.1.

Sample	Twisted nanotape	Helical nanotape	Nanotube
10nt NoG C_{12}	Yes	Yes	Yes
25nt NoG C_{12}	Yes	Yes	Yes
40nt NoG C_{12}	Yes	Yes	Yes
10nt G_5 C_{12}	No	No	Yes[a]
25nt G_5 C_{12}	Yes	Yes	Yes
40nt G_5 C_{12}	Yes	Yes	Yes
10nt NoG NoSPR	No	No	No
25nt NoG NoSPR	No	No	No
40nt NoG NoSPR	No	No	No
10nt G_5 NoSPR	No	No	No
25nt G_5 NoSPR	No	No	No
40nt G_5 NoSPR	Yes[b]	Yes[b]	Yes[b]
25nt $(GGGT)_3$ NoSPR	Yes[b]	No	No
40nt $(GGGT)_3$ NoSPR	Yes[b]	No	No

[a] Nanotubes were substantially shorter in this sample than in all others.
[b] Structures were observed infrequently

3.4.3 Self-assembly of ssDNA-amphiphiles with guanine-modified headgroups and without a C_{12} spacer

To test if the presence of guanines positioned immediately adjacent to the site of conjugation to the hydrophobic tail could produce nanotape and nanotube structures in the absence of the C_{12} spacer a third set of amphiphiles was created that included the G_5 modification in the 10, 25, and 40 nucleotide ssDNA headgroups, with the headgroups directly linked to the hydrophobic tails (as shown in Figure 3.1). It was hypothesized that the inclusion of the five guanines would produce intermolecular

parallel G-quadruplex interactions between the headgroups that would bring the headgroups together and minimize the headgroup area in a similar manner as the C_{12} spacer, thus allowing the nanotapes to form. These amphiphile samples were dissolved in Milli-Q water at 500 μM, vitrified and imaged with cryo-TEM to determine their self-assembly behavior. The only structures observed in the amphiphile samples with 10 (Figure 3.6A) and 25 nucleotide headgroups were spherical and weakly ellipsoidal micelles (Table 3.2) that were of similar sizes as observed in the amphiphile samples with the NoG headgroups.

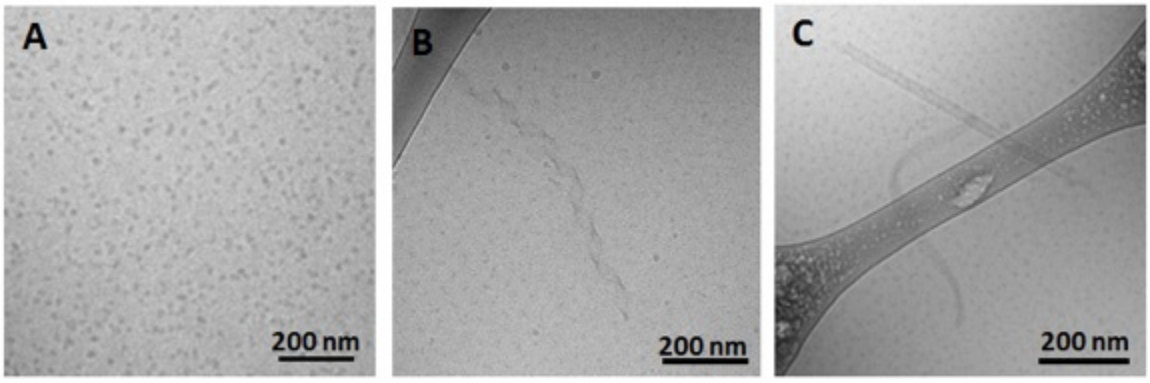

Figure 3.6: Cryo-TEM images of A) micelles formed by ssDNA-amphiphiles with a 10 nucleotide (10nt-1) G_5-modified headgroup lacking the C_{12} spacer (NoSPR), B) a helical nanotape and C) a twisted nanotape and nanotube formed by ssDNA-amphiphiles with the 40nt G_5-modified headgroup and without the C_{12} spacer (NoSPR).

Micelles of similar shape and size were also the most prevalent structure observed in the amphiphile samples with the 40 nucleotide G_5-modified headgroup, but twisted and helical nanotapes and nanotubes (Figure 3.6B,C, Table 3.2), that were similar to those produced by the NoG headgroups with the C_{12} spacer, were also observed infrequently.

CD was performed on the 40 nucleotide G_5-modified amphiphiles to probe for the

presence of G-quadruplex formations within the headgroups of these amphiphiles (Figure 3.7).

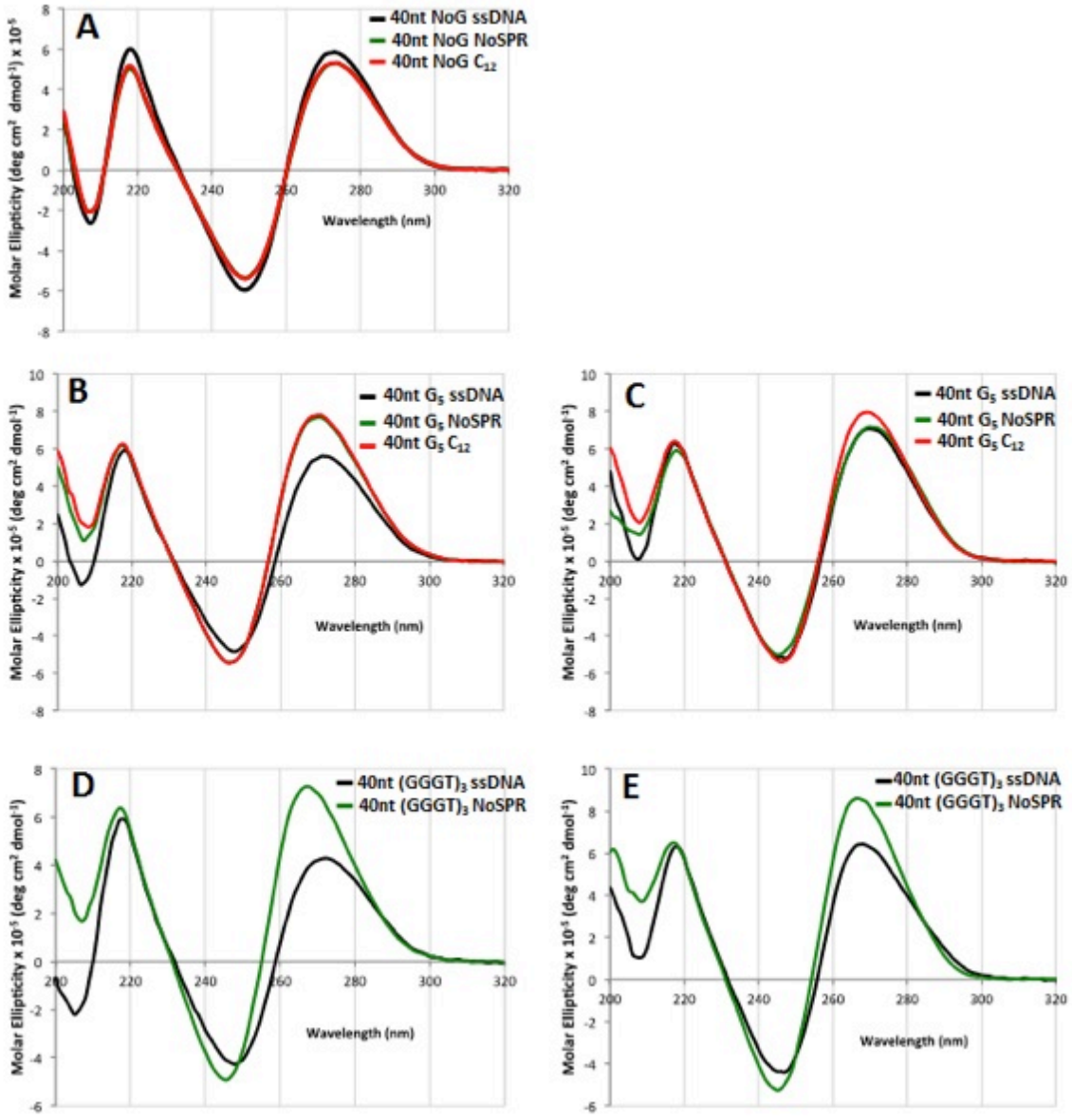

Figure 3.7: CD spectra in Milli-Q water (A, B, D) or 20 mM KCl (C, E) of 20 μM solutions of free ssDNA with 40nt NoG, G_5-, or $(GGGT)_3$-modified sequences and their amphiphiles with (C_{12}) and without (NoSPR) the C_{12} spacer.

Parallel G-quadruplex structures are tertiary DNA structures formed by the stacking of

G-quartet structures, with each G-quartet formed by four guanine nucleotides arranged in a planar, square geometry held together by Hoogsteen hydrogen bonding. These unique structures are stabilized by small cations that fit between the G-quartets but can also be formed in pure water[110] and produce a characteristic CD spectrum with a strong positive peak between 258-265 nm.[111,119] With only five guanines a single headgroup could not form a G-quadruplex with itself but it could form an intermolecular parallel G-quadruplex by interacting with three adjacent headgroups.[120] However, contrary to the hypothesis, the CD spectrum of the 40 nucleotide G_5-modified amphiphiles had a maximum at 270 nm in water, characteristic of a stem-loop, and only 1 nm different than the free ssDNA sequence (maximum at 271 nm) suggesting that there were no significant G-quadruplex interactions occurring between the amphiphiles' headgroups following self-assembly (Figure 3.7B, Table 3.3). Both the 40 nucleotide G_5-modified amphiphile and ssDNA sequence had a maximum at 269 nm upon addition of 20 mM KCl (Figure 3.7C, Table 3.3), that is outside the wavelength range typically attributed to a G-quadruplex (258-265 nm) or stem-loop (270-285 nm)[121] secondary structure.

In order to enhance the probability that the ssDNA headgroups would form parallel G-quadruplexes and provide additional knowledge about the effect of G-quadruplex interactions on the self-assembly of ssDNA-amphiphiles, two additional headgroups were created from the random guanine-free 25 and 40 nucleotide headgroups. These headgroups had the first 12 nucleotides of the original sequences replaced with the sequence $(GGGT)_3$, as shown in Figure 3.1, which is capable of inducing intermolecular G-quadruplexes.[118] The CD spectra in Milli-Q water of the 25 and 40 nucleotide $(GGGT)_3$-modified ssDNA sequences measured prior to conjugation to the hydrophobic

tails showed a maximum at 273 nm and 272 nm respectively, for each length, which can be attributed to the standard Watson-Crick base-pairing produced in stem-loop secondary structures that typically have a maximum between 270 and 285 nm.[121,122]

Table 3.3: Summary of cryo-TEM (Figures 3.3, 3.6, 3.9, 3.10) and circular dichroism (CD) observations (Figure 3.7) from amphiphiles containing 40 nucleotide (nt) headgroups in Milli-Q water or 20 mM KCl. The location of the long wavelength maximum in each CD spectrum was used to assign headgroup structure. Maxima occurring between 258-265 nm were assigned as G-quadruplex, between 270-285 nm were assigned as stem-loop, and between 266-269 nm were assigned as unclear.

Sample	High aspect ratio structures	CD maximum (nm) in H_2O/KCl	Headroup assignment
40nt NoG ssDNA	-	273	Stem-loop
40nt NoG NoSPR	No	273	Stem-loop
40nt NoG C_{12}	Yes	274	Stem-loop
40nt G_5 ssDNA	-	271/269	Stem-loop/Unclear
40nt G_5 NoSPR	No	270/269	Stem-loop/Unclear
40nt G_5 C_{12}	Yes	270/269	Stem-loop/Unclear
40nt $(GGGT)_3$ ssDNA	-	272/267	Stem-loop/Unclear
40nt $(GGGT)_3$ NoSPR	Yes	267/267	Unclear/Unclear

Addition of 20 mM KCl shifted the signal closer to that of a G-quadruplex sequence (258-265 nm), to 266 nm for the 25 nucleotide and 267 nm for the 40 nucleotide $(GGGT)_3$-modified ssDNA sequences. Following conjugation to the hydrophobic tails and subsequent self-assembly in Milli-Q water the 25 nucleotide long sequence produced a CD spectrum characteristic of G-quadruplex secondary structure, whereas the 40 nucleotide sequence had a maximum at 267 nm, in between the wavelength range for the G-quadruplex and stem-loop structures. Addition of KCl had no effect on the location

of the long wavelength maximum in the spectra of the amphiphiles. The CD spectra of the 40 and 25 nucleotide $(GGGT)_3$-modified ssDNA sequences and amphiphiles in Milli-Q water and KCl are shown in Figure 3.7 and Figure 3.8 and results are summarized in Table 3.3 and Table 3.4, respectively.

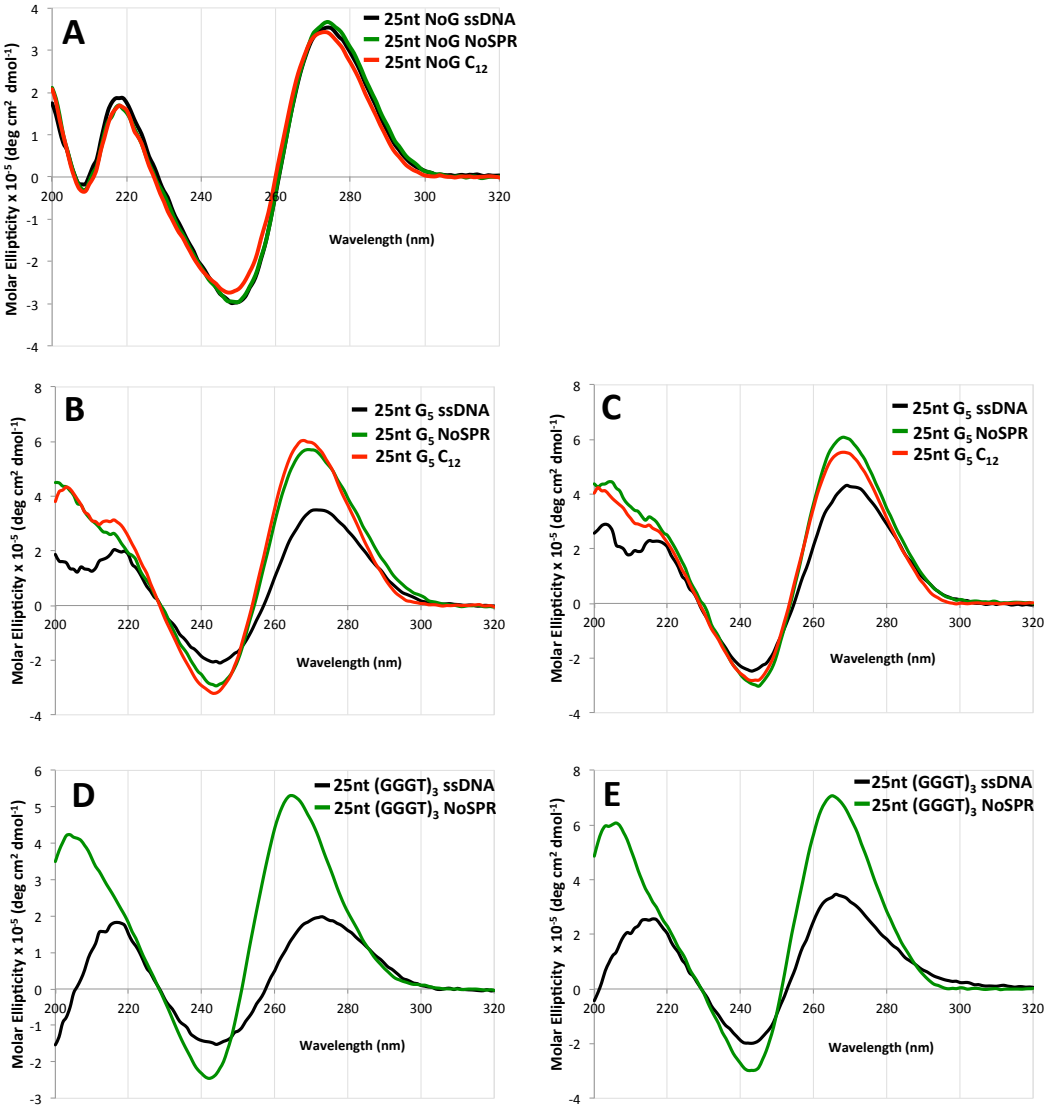

Figure 3.8: CD spectra in Milli-Q water (A, B, D) or 20 mM KCl (C, E) of 20 μM solutions of free ssDNA with 25nt NoG, G_5-, or $(GGGT)_3$-modified sequences and their amphiphiles with (C_{12}) or without (NoSPR) the C_{12} spacer.

Table 3.4: Summary of cryo-TEM (Figure 3.3, 3.4, 3.9, 3.10) and circular dichroism (CD) observations (Figure 3.8) from amphiphiles containing 25 nucleotide (nt) headgroups in Milli-Q water or 20 mM KCl. The location of the long wavelength maximum in each CD spectrum was used to assign headgroup structure. Maxima occurring between 258-265 nm were assigned as G-quadruplex, between 270-285 nm were assigned as stem-loop, and between 266-269 nm were assigned as unclear.

Sample	High aspect ratio structures	CD maximum (nm) in H_2O/KCl	Headroup assignment
25nt NoG ssDNA	-	274	Stem-loop
25nt NoG NoSPR	No	274	Stem-loop
25nt NoG C_{12}	Yes	273	Stem-loop
25nt G_5 ssDNA	-	272/269	Stem-loop/Unclear
25nt G_5 NoSPR	No	269/268	Unclear/Unclear
25nt G_5 C_{12}	Yes	268/269	Unclear/Unclear
25nt $(GGGT)_3$ ssDNA	-	273/266	Stem-loop/Unclear
25nt $(GGGT)_3$ NoSPR	Yes	265/265	G-quad/G-quad

Cryo-TEM imaging of these two samples showed that both amphiphiles with the 25 and 40 nucleotide $(GGGT)_3$-modified headgroups formed twisted nanotapes as well as micelles (Figure 3.9), although the nanotapes were observed very rarely and did not twist with a consistent periodicity. Thus, for the case of the 25 nucleotide headgroup, where the presence of the $(GGGT)_3$ sequence was able to clearly induce the formation of G-quadruplexes between the headgroups of the amphiphiles, bilayer twisted nanotape structures were observed in the absence of the C_{12} spacer but helical nanotapes or nanotubes were not (Table 3.2).

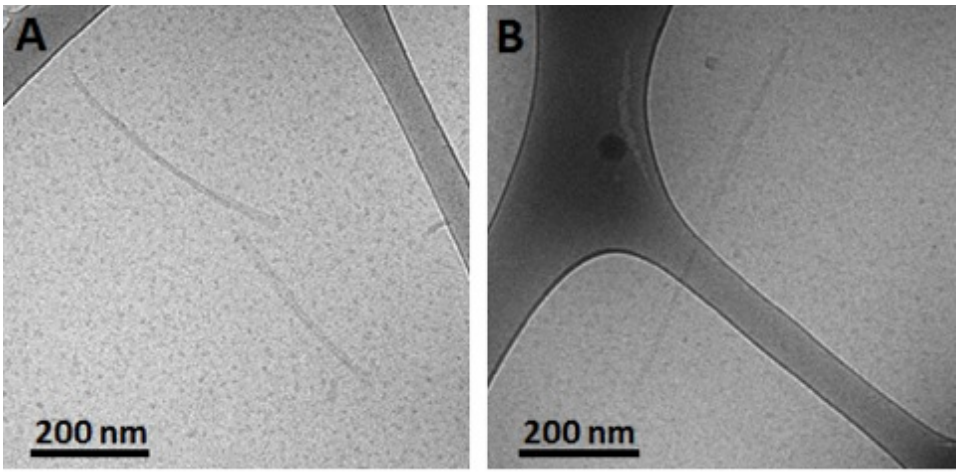

Figure 3.9: Cryo-TEM images of twisted nanotapes formed by ssDNA-amphiphiles with the A) 25nt $(GGGT)_3$-modified headgroup or B) 40nt $(GGGT)_3$-modified headgroup and without the C_{12} spacer (NoSPR).

3.4.4 Self-assembly of ssDNA-amphiphiles with G_5-modified headgroups and a C_{12} spacer

As a final test of the influence of the guanine-modification of the headgroups, amphiphiles that contained both the G_5-modified headgroups and the C_{12} spacers were created and their assembly compared to that of the amphiphiles with the C_{12} spacer and NoG headgroups. There were no apparent differences in the assembly behavior of amphiphiles with the C_{12} spacer containing the G_5-modified (Figure 3.10) and the NoG headgroups (Figure 3.3) with 25 and 40 nucleotides, as each formed twisted and helical nanotapes and nanotubes. However, there was a dramatic difference in the nanotubes formed by the amphiphiles with headgroups containing only 10 nucleotides. Both amphiphile samples produced nanotubes with similar average diameters (NoG: 29.0 ± 3.6 nm; G_5: 32.5 ± 1.3 nm), but amphiphiles with the NoG headgroup produced nanotubes that were microns in length while amphiphiles formed with the G_5 headgroup produced nanotubes that were nearly two orders of magnitude shorter and varied between 60 and 350 nm (Figure 3.11).

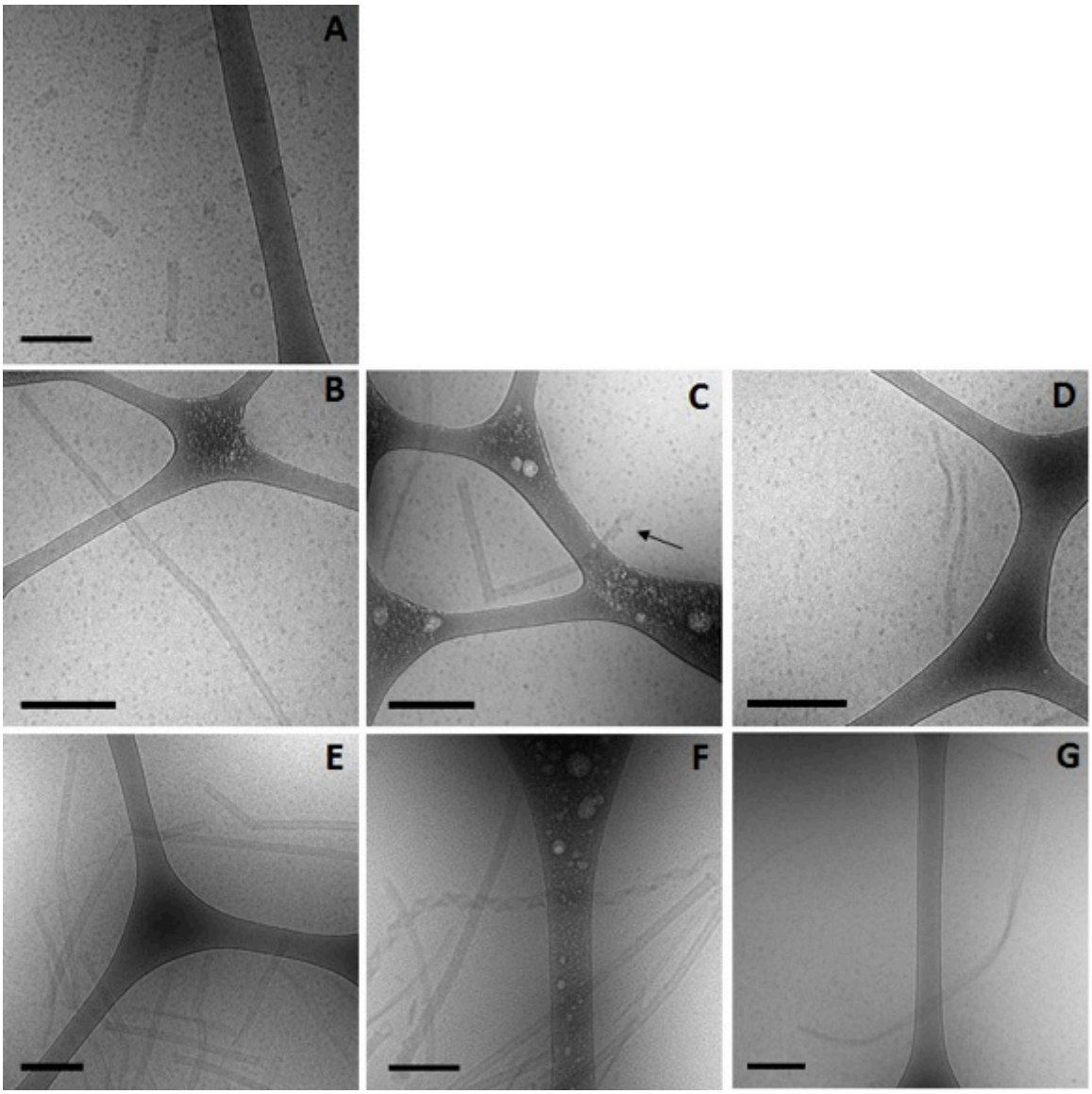

Figure 3.10: Cryo-TEM images of nanotubes (A, B, E), helical nanotapes (C, F), and twisted nanotapes (D, G) formed by ssDNA-amphiphiles with G_5-modified headgroups and C_{12} spacers. Top row (A): 10nt-1 headgroup. Middle row (B, C, D): 25nt headgroup. Bottom row (E, F, G): 40nt headgroup. The black arrow in C shows the helical section of the nanostructure. All scale bars are 200 nm.

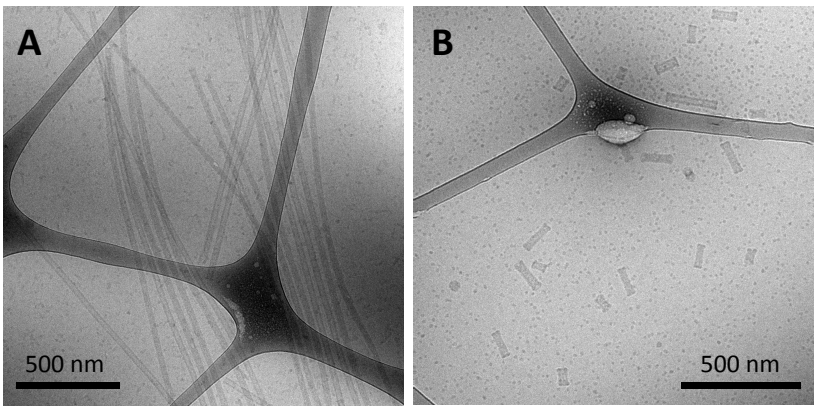

Figure 3.11: Cryo-TEM images of ssDNA nanotubes formed from the self-assembly of amphiphiles with a C_{12} spacer and A) 10nt-1 NoG or B) 10nt-1 G_5 headgroups.

Additional images of the short nanotubes produced by the amphiphiles with the G_5-modified headgroup and C_{12} spacer are provided in Figure 3.12. These images contain end-on views of the short nanotubes, allowing the hollow morphology of these structures to be observed.

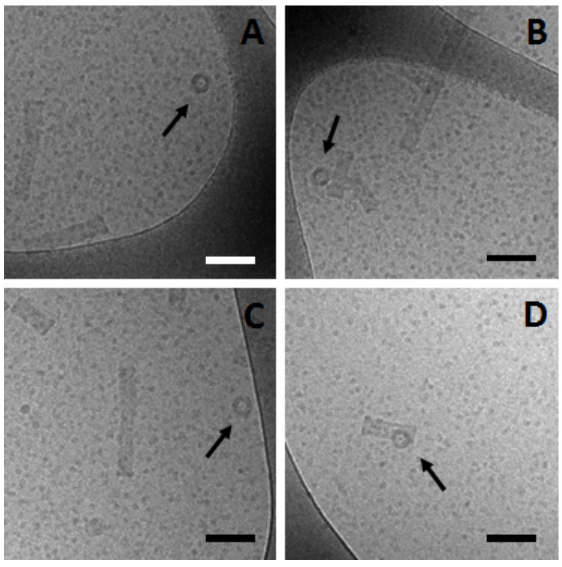

Figure 3.12: Cryo-TEM images of short nanotubes (A-D) formed by the amphiphiles with the 10nt-1 G_5-modified headgroup, and the C_{12} spacer. The black arrows point to nanotubes that are viewed end-on, demonstrating the hollow nature of these structures. All scale bars are 100 nm.

AFM imaging of amphiphiles with the 25 nucleotide G_5-modified headgroup and C_{12} spacer captured two sets of two nanotubes (Figure 3.13). The nanotubes were microns in length and each appeared to be around 65 nm in diameter based on the line-scan analysis of the friction image. The larger diameters and decreased heights of the nanotubes observed in the AFM images compared to cryo-TEM images is likely due to the flattening of the nanotubes during dehydration. It is possible that the parallel organization of the nanotubes was the result of the drying process that occurred during the sample preparation but it is also possible that the long nanotubes naturally align as observed in a number of cryo-TEM images including Figure 3.2C and 3.11A.

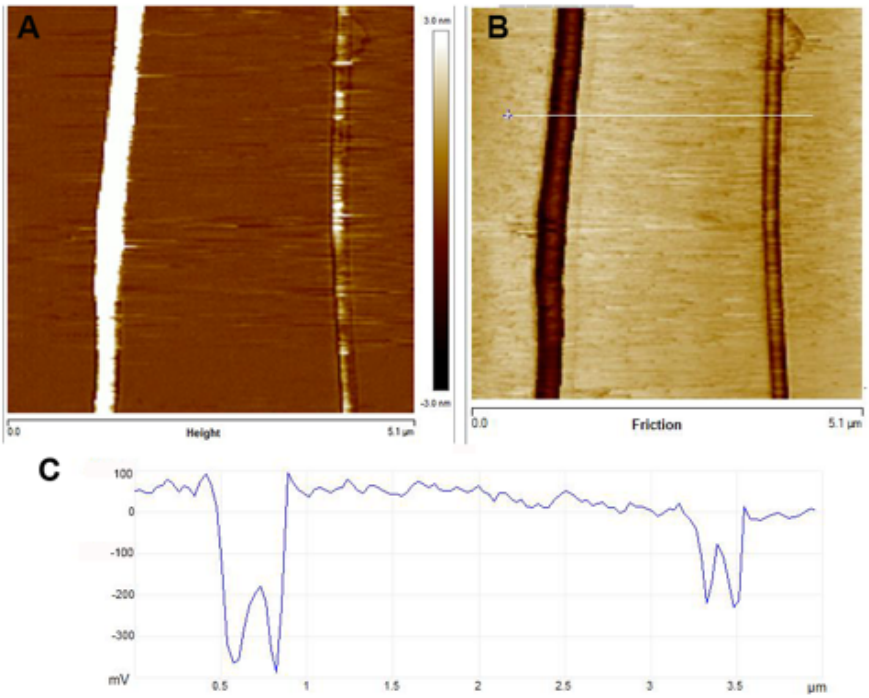

Figure 3.13: AFM images and line-scan analysis of nanotubes formed by amphiphiles containing the 25 nucleotide G_5-modified headgroup and the C_{12} spacer. A) Height image. B) Friction image. C) Line-scan analysis of the white line shown in B. Friction imaging can map relative differences in surface frictional characteristics, thus allowing the identification of surface features that may not be clear in height imaging. Friction imaging and line-scan analysis on the friction image shows the presence of four nanotubes.

CD was performed on each of the G_5-modified ssDNA sequences and their amphiphiles with C_{12} spacers to determine the effect of the G_5 sequence on the secondary structure of the ssDNA headgroup. The CD spectra of the amphiphiles with the C_{12} spacer and G_5-modified headgroups with 25 and 40 nucleotides had maxima at 268 and 270 nm respectively in water, which suggested that the headgroups of these amphiphiles formed either stem-loop structures or that the designation of the headgroup structure was unclear. For comparison, the CD spectra of the amphiphiles with a C_{12} spacer containing the NoG 25 and 40 nucleotide headgroups had maxima at 273 and 274 nm, indicative of a stem-loop structure. The spectra of the amphiphiles with the C_{12} spacer and the G_5-modified 10 nucleotide headgroups (10nt-1 and 10nt-2) had maxima at 264 nm, characteristic of a parallel G-quadruplex structure, while the CD spectra of amphiphiles with a C_{12} spacer and the 10 nucleotide NoG headgroups were consistent with that of stem-loop structures (Figure 3.14, Figure 3.15, Table 3.5). This suggested that of the amphiphiles formed with the C_{12} spacer and a G_5-modified headgroup only the amphiphiles with the shorter 10 nucleotide headgroups clearly produced G-quadruplex secondary structures.

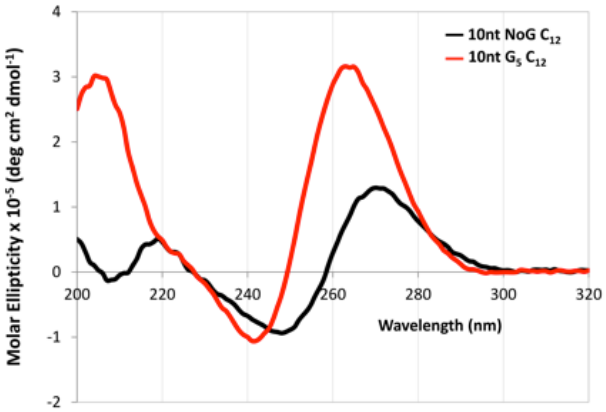

Figure 3.14: CD spectra in Milli-Q water of 20 μM ssDNA-amphiphiles with a C_{12} spacer and 10 nucleotide (10nt-1) NoG for G_5-modified headgroups.

CD spectra of ssDNA and ssDNA-amphiphiles with guanine-modified headgroups were also collected in 20 mM KCl to test if the addition of the K^+ cation would produce a substantial effect on the structure of the headgroups. Data show that the addition of KCl only produced minor changes in the CD spectra of the amphiphiles, suggesting that the presence of the G-quadruplex stabilizing K^+ cation did not substantially influence the secondary structures adopted by headgroups of the amphiphiles towards the formation of G-quadruplexes.

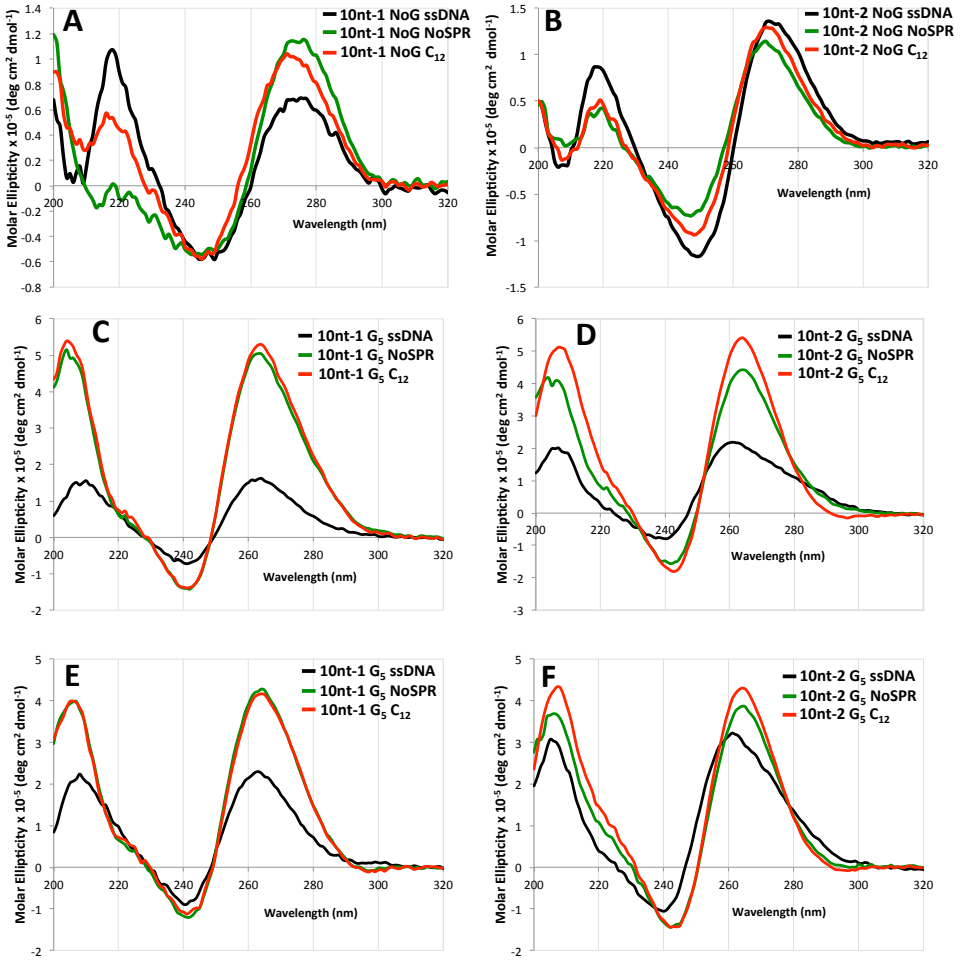

Figure 3.15: CD spectra in Milli-Q water (A-D) or 20 mM KCl (E, F) of 20 µM solutions of free ssDNA with 10nt NoG or G_5-modified headgroups and their amphiphiles with (C_{12}) and without (NoSPR) the C_{12} spacer.

Table 3.5: Summary of cryo-TEM (Figure 3.3, 3.6, 3.10, 3.11) and circular dichroism (CD) observations (Figure 3.15) from amphiphiles containing 10 nucleotide (nt) headgroups in Milli-Q water or 20 mM KCl. The location of the long wavelength maximum in each CD spectrum was used to assign headgroup structure. Maxima occurring between 258-265 nm were assigned as G-quadruplex, between 270-285 nm were assigned as stem-loop, and between 266-269 nm were assigned as unclear.

Sample	High aspect ratio structures	CD maximum (nm) in H_2O/KCl	Headroup assignment
10nt-1 NoG ssDNA	-	275	Stem-loop
10nt-1 NoG NoSPR	No	276	Stem-loop
10nt-1 NoG C_{12}	Yes	271	Stem-loop
10nt-2 NoG ssDNA	-	271	Stem-loop
10nt-2 NoG NoSPR	No	270	Stem-loop
10nt-2 NoG C_{12}	Yes	270	Stem-loop
10nt-1 G_5 ssDNA	-	264/263	G-quad/G-quad
10nt-1 G_5 NoSPR	No	263/264	G-quad/G-quad
10nt-1 G_5 C_{12}	Yes	264/264	G-quad/G-quad
10nt-2 G_5 ssDNA	-	261/261	G-quad/G-quad
10nt-2 G_5 NoSPR	No	264/264	G-quad/G-quad
10nt-2 G_5 C_{12}	Yes	264/264	G-quad/G-quad

3.4.5 Transitions between twisted nanotapes, helical nanotapes and nanotubes

Cryo-TEM images of the ssDNA-amphiphile nanostructures not only showed twisted nanotapes, helical nanotapes and nanotubes, but also captured the transition from twisted to helical nanotape as well as from helical nanotape to nanotube (Figure 3.4, Figure 3.16). These images provided direct evidence that the ssDNA-amphiphile nanostructures underwent transitions between these structures, likely in a similar manner as observed in other types of amphiphilic molecules as discussed in detail below.

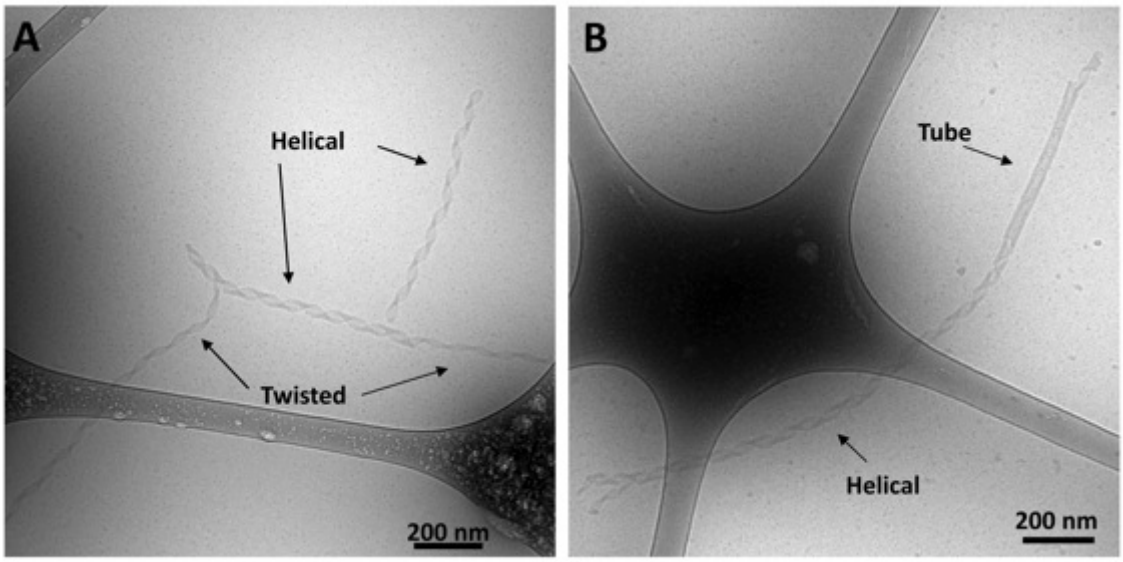

Figure 3.16: Cryo-TEM images of ssDNA-amphiphiles formed by the 10nt-2 NoG headgroup and C_{12} spacer undergoing transitions from A) twisted nanotapes to helical nanotapes and B) a helical nanotape to a nanotube.

Analysis of cryo-TEM images that captured the transition from twisted nanotapes into helical nanotapes showed that the twisted nanotape segments had widths that were substantially smaller than the helical nanotape segments (24 ± 2 versus 38 ± 4 nm) but pitch lengths that were similar (132 ± 6 nm for the twisted nanotapes and 129 ± 7 nm for the helical nanotapes).

To better understand the assembly mechanism of the ssDNA-amphiphiles a sample containing the 25 nucleotide G_5-modified headgroup and C_{12} spacer was heated to 90 °C for 10 min to induce the structures to disassemble. Prior to thermal disruption this sample contained globular micelles, nanotapes and nanotubes (Figure 3.17A).

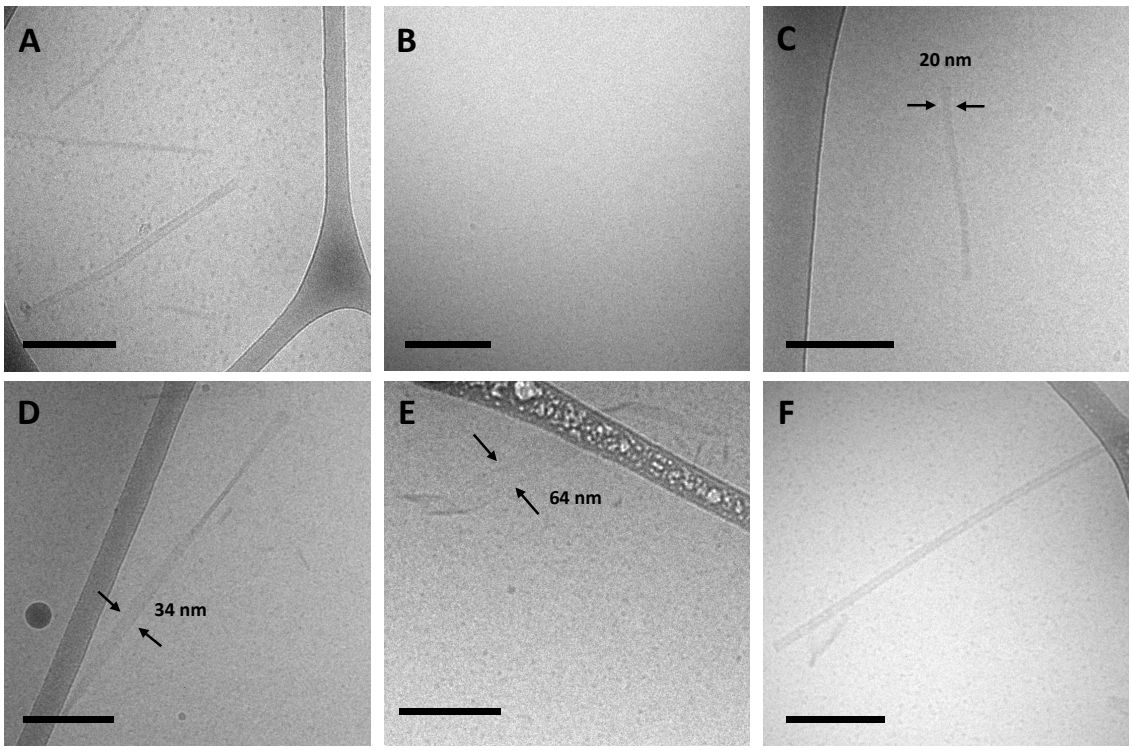

Figure 3.17: Cryo-TEM images of 25 nucleotide G_5-modified amphiphiles containing the C_{12} spacer at various times in the thermal disruption timeline. A) Prior to heating. B) From a solution heated at 90 °C for 10 min. C) After 2 days at room temperature. D) and E) After 9 days at room temperature. F) After 21 days at room temperature. All scale bars are 200 nm.

An aliquot of the sample was taken after 10 min of heating, while the solution was still at 90 °C, and was immediately vitrified and imaged to confirm the absence of any self-assembled structures following the heating regimen (Figure 3.17B). The sample was cooled to room temperature and another aliquot vitrified upon reaching room temperature. The remaining sample was kept at room temperature for 3 weeks and aliquots of the sample were vitrified and imaged after 2 days, 9 days, and 21 days. Globular micelles were observed upon cooling to room temperature, and after 2 days of aging at room temperature short and thin nanostructures along with the globular micelles were observed to exist in the sample (Figure 3.17C). These thin nanostructures had

widths of ~20 nm and their nanotape morphology was confirmed with stage tilting (Figure 3.18). After 9 days of aging, nanotapes that were longer, wider, and twisted (Figure 3.17D) or helical (Figure 3.17E) were observed. This suggested that the thin nanotapes broaden and begin twisting and transitioning to helical nanotapes over this timeframe. After 21 days, nanotubes were observed in the sample, suggesting the nanotubes reformed between 9 and 21 days after thermal disruption.

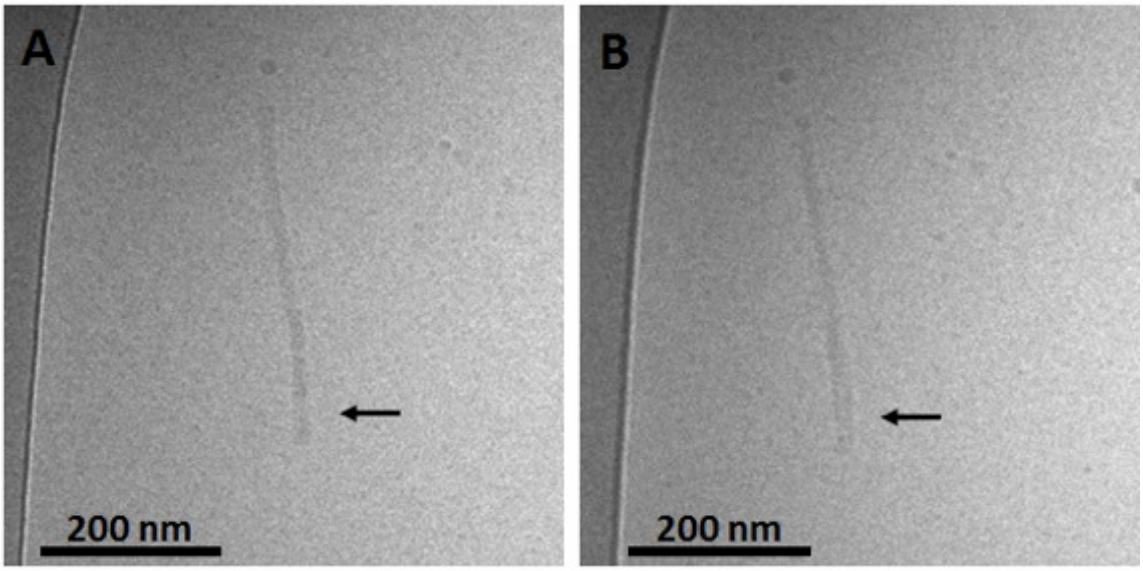

Figure 3.18: Cryo-TEM images of 25 nucleotide G_5-modified amphiphiles containing the C_{12} spacer after 2 days of aging at room temperature following thermal disruption. A) 0° stage tilt. B) 45° stage tilt. The visual change in width of the nanostructure following the stage tilt, most easily observed at the location indicated by the black arrows, demonstrates that the nanostructure is a bilayer nanotape rather than a cylindrical micelle.

3.5 Discussion

In this work three building blocks were used to create ssDNA-amphiphiles: a hydrophobic tail, a hydrophilic ssDNA headgroup, and a spacer molecule that links the tail and the headgroup. Our previous work identified the hydrophobic force produced by

the dialkyl tails as a major driving force for the assembly of a ssDNA aptamer-amphiphile and that the inclusion of a hydrophobic spacer is important for the assembly of the ssDNA-amphiphiles into flat or twisted nanotapes.[117] This work explored the influence of the headgroup length and sequence on the self-assembly behavior of ssDNA-amphiphiles created with the same dialkyl C_{16} tail and C_{12} spacer to expand our understanding of the role of the ssDNA headgroup in the self-assembly of ssDNA-amphiphiles. Our current data demonstrated that ssDNA-amphiphiles with C_{12} spacers and NoG headgroups of 10, 25, or 40 nucleotides not only produced the twisted nanotapes previously seen, but also helical nanotapes and nanotubes. Each of these structures is formed from bilayers of amphiphiles with the hydrophobic tails organized into an interior core and the ssDNA headgroups forming an exterior shell (Figure 3.19, Figure 3.20).

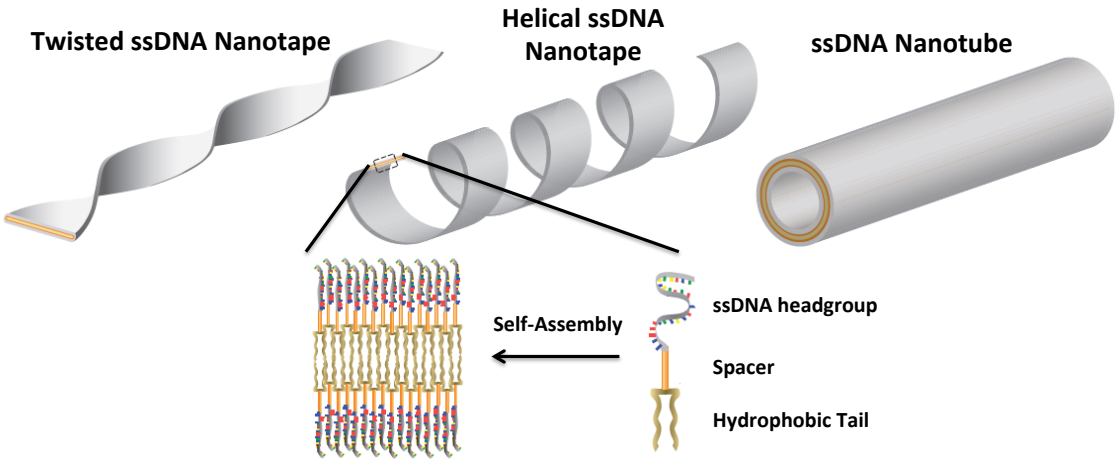

Figure 3.19: An artistic rendering of the self-assembly of ssDNA-amphiphiles into an ordered bilayer structure and the twisted and helical nanotapes and nanotubes that they form. The amphiphile contains three building blocks: a hydrophobic tail, a spacer, and a hydrophilic headgroup (the secondary structure of the headgroup is not shown).

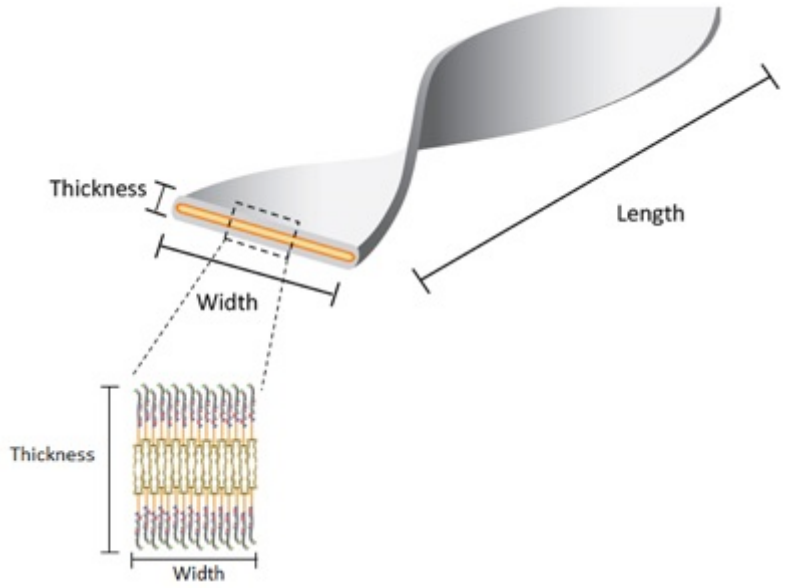

Figure 3.20: An artistic rendering of the self-assembly of ssDNA-amphiphiles into a bilayer nanotape structure. The thickness, width, and length dimensions of the nanotape are identified for clarity.

Similar nanotape and nanotube structures were observed in solutions of different amphiphilic molecules including glycolipids, peptide-amphiphiles, and bolaamphiphiles.[55,57,123] In each case the nanotape and nanotube structures were created from bilayers of amphiphiles, with the hydrophobic moieties sequestered into an inner layer and surrounded with the hydrophilic headgroups to form the exterior of the nanostructure. The chirality of the individual amphiphile requires that the amphiphiles organize with their neighboring molecules at non-zero angles, generating a preferred orientation of each amphiphile tail and headgroup within the self-assembled bilayer, which induces twisting.[124] The ssDNA-amphiphiles we have created are rich in chirality, with chiral centers in the hydrophobic tails as well as the nucleotides of the ssDNA headgroups. As such, it is likely that the chirality of the individual ssDNA-amphiphile is responsible for producing the twisting that was observed in the ssDNA-amphiphile

nanotapes.

The ability for self-assembled structures to transition from a twisted nanotape morphology to a helical nanotape morphology has been captured and described in a number of publications.[55,56,124–127] For example, a peptide-amphiphile that contained three phenylalanine residues that were capable of intermolecular π-π stacking was observed to form short twisted bilayer nanotapes 30 sec after dissolution in water.[55] These short structures grew into long twisted nanotapes within ten min, coexisted with helical tapes after two weeks and transitioned entirely to helical tapes after four weeks. Similarly, single amino acid amphiphiles dissolved in water were found to form twisted nanotapes after 24 h, a mixture of twisted and helical nanotapes after one week, which were almost entirely helical after four weeks, and finally transitioned into nanotubes between one and four months.[56]

These and other reports propose that the transition from a twisted to helical nanotape morphology requires a change in membrane curvature from Gaussian (saddle-like) to cylindrical, an event that is often attributed to a rearrangement of the individual amphiphiles into a molecular organization that is more ordered or crystalline.[55,57,61,62] The forces that are often identified as causing the order or crystallinity are hydrogen-bonding and π-π stacking between individual amphiphiles although electrostatic and hydrophobic forces are also likely important.[55,56] The C_{12} spacer has previously been found to play an important role in producing the bilayer nanotapes, possibly by forcing the aptamer headgroups into close proximity of each other, thus reducing their interfacial headgroup area, which allows the nanotapes to form.[117,118] The C_{12} spacer may also be helping to

ensure that the amphiphiles can organize into crystalline or well-ordered bilayers by extending the large ssDNA headgroups away from the interface and relieving some of the electrostatic or steric constraints that could impede close and ordered packing of the amphiphiles. This may be especially important in the case of the NoG headgroups that do not appear to form significant interactions with each other.

Hydrogen bonding can occur between guanine nucleobases and produce the G-quartet structures that can stack into G-quadruplexes, which led us to test whether guanine-rich headgroups that can form parallel G-quadruplexes could be used in place of the C_{12} spacer to produce nanotapes and nanotubes. Amphiphiles with the $(GGGT)_3$-modified headgroups of 25 and 40 nucleotides in length and without the C_{12} spacer (NoSPR) were found to assemble into twisted nanotapes but did not appear to progress into helical nanotapes or nanotubes while amphiphiles with a NoG sequence and without a spacer formed only micelles. This result is in agreement with our previous study that found that amphiphiles with a different 40 nucleotide headgroup containing the $(GGGT)_3$ sequence and directly conjugated to the hydrophobic tail (NoSPR) also formed twisted nanotapes but were not observed to form helical nanotapes or nanotubes.[118] Additionally, we have also observed previously that amphiphiles formed with C_{12} hydrophobic spacers and a Muc-1 aptamer headgroup (25 nucleotides long) that adopted parallel G-quadruplex secondary structure only assembled into globular micelles and twisted nanotapes.[117] Thus, the findings of this and our previous studies suggest that long headgroups (with 25 or 40 nucleotides) with additional hydrogen bonding interactions present in G-quadruplex structures may encourage the formation of the bilayer nanotape structures in the absence of a hydrophobic C_{12} spacer, but may not

allow for the change in membrane curvature required for twisted nanotapes to transition into helical nanotapes and nanotubes.

The literature offers insight into the transition from twisted to helical nanotapes and from helical nanotapes to nanotubes. Recent theoretical and experimental work shows that the width of the nanotape is a critical parameter in determining the morphology of the nanotape.[56,126,128] Specifically, as the bilayer grows in width it becomes energetically favorable for the bilayer to transition from Gaussian to cylindrical curvature, thus producing the transition from a twisted to helical morphology. Theoretical studies also pointed out that shape selection in self-assembled chiral molecules may involve a geometrical frustration, and thus a competition between bending and stretching.[129,128] The transition from twisted to helical ribbons (or nanotapes) to nanotubes has been described by two competing theories: a “closing-pitch model” and a “growing width model”.[130] The closing-pitch model assumes that a helical nanotape maintains its width while the pitch shortens until the edges of the nanotape meet to form a nanotube, while the growing width model assumes the pitch remains constant and the nanotape widens until a closed nanotube is formed. An alternate possibility is that some of the twisted and helical nanotapes are at equilibrium and never transition into nanotubes as observed previously in other amphiphilic systems.[131]

Analysis of cryo-TEM images that captured the transition from twisted nanotapes into helical nanotapes, like those shown in Figure 3.16, showed that the twisted nanotape segments had widths that were substantially smaller than the helical nanotape segments. This suggests that the transition from twisted to helical nanotape occurs as

the width of the nanotape increases and that the “growing width” model rather than the “shortening pitch” model better describes the mechanism of transitioning from twisted to helical nanotapes as well as nanotube formation. However, based on the presence of twisted and helical nanotapes in an amphiphile solution aged for 6 months (Figure 3.21), it is possible that not all nanotapes will progress into nanotubes. This can be either because there are no more micelles to contribute to the growth mechanism (as seen in Figure 3.21) or because some nanostructures may get locked into a twisted or helical nanotape morphology, an outcome that has recently been theorized[24] and has been observed experimentally.[32]

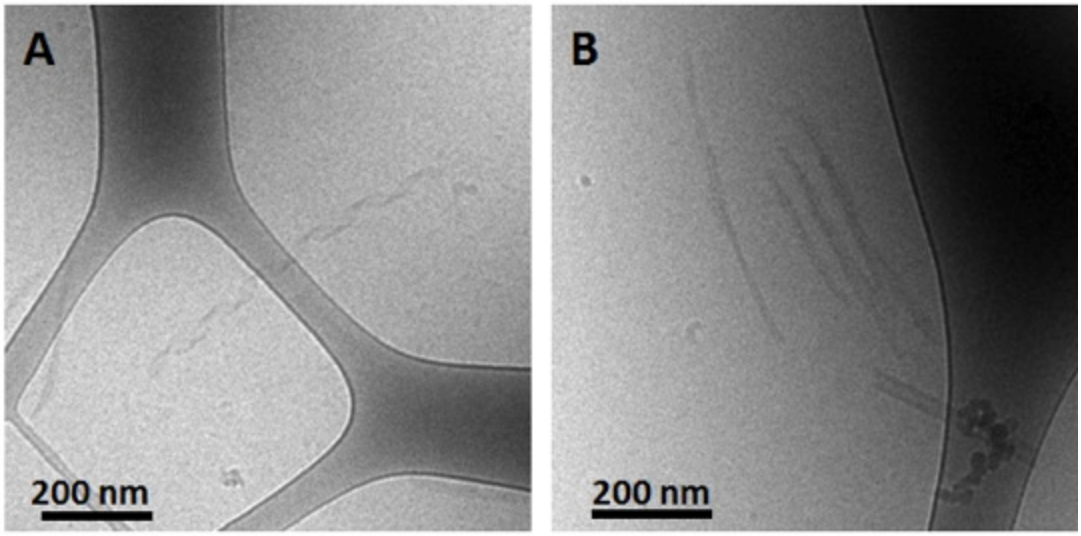

Figure 3.21: Cryo-TEM images of ssDNA-amphiphiles containing a 25 nucleotide NoG headgroup and the C_{12} spacer after 6 months of aging at room temperature.

Further support for the “growing width” mechanism is provided by the observed progression from thin nanotapes to nanotubes following thermal disruption of the nanostructures. The heating process was found to cause all self-assembled structures to disassemble, allowing the reassembly process to be monitored over time. Immediately

after cooling to room temperature only globular micelles were observed. After 2 days of aging, globular micelles and thin nanotapes were present. After 9 days, wider, longer nanotapes that were twisted, as well as much wider helical nanotapes were observed. And finally, after 21 days, nanotubes were observed (images were not collected between 9 and 21 days). The reassembly progression seen over time in the cryo-TEM images of Figure 3.17, along with the images shown in Figure 3.16, suggest that nanotapes transition into nanotubes due to the increasing width of the nanotapes.

Interestingly, the timescale of nanotape and nanotube assembly appeared to be substantially slower following the thermally induced disassembly than after the sample was initially synthesized, purified and dissolved in water. The heat treatment did not appear to cause appreciable degradation of the amphiphiles, as LC-MS of an amphiphile sample following the thermal disruption procedure showed that over 98% of the amphiphiles still had the expected molecular weight. Following thermal disruption and cooling to room temperature, samples were imaged at four time points: immediately after cooling, and at 2, 9 and 21 days after cooling. The twisted nanotapes were observed after 9 days of aging and the nanotubes after 21 days, a timescale similar to that observed in other amphiphilic systems.[55,56,132] However, nanotapes and nanotubes were observed within 30 min after the amphiphiles were dissolved in Milli-Q water following their synthesis and purification. At this time the cause of the dramatic difference in assembly dynamics between the ssDNA-amphiphiles and other amphiphilic molecules remains unclear. One possible cause though for the apparent rapid assembly of the ssDNA nanotubes following synthesis and purification of the ssDNA-amphiphiles is that the amphiphiles may began to assemble during the purification steps used to separate

the ssDNA-amphiphiles from the unreacted ssDNA, hydrophobic tails and other reaction inputs. During this purification process the newly formed ssDNA-amphiphiles, as well as other amphiphilic molecules, are exposed to an aqueous environment that contains salts, elevated temperatures, and mixtures of aqueous and organic solvents (including methanol and ethanol). These factors have all been implicated in the formation of tubular structures by self- assembling amphiphiles,[60,64,133,134] and may play a role in accelerating the assembly of the ssDNA-amphiphiles more than other amphiphiles.

3.6 Conclusions

This work demonstrates that ssDNA-amphiphiles containing a random nucleic acid headgroup can adopt a variety of self-assembled structures including twisted and helical bilayer nanotapes and nanotubes, structures that are substantially more complex than spherical and cylindrical micelles observed by others in the literature. The ability to create DNA nanotubes from ssDNA-amphiphiles is particularly exciting, as nanotubes have been utilized for targeted drug delivery of small molecules and siRNA, as templates for nanowires and as tracks for molecular motors. For many of these applications there is no need for the complex designs made possible by other DNA nanotechnology approaches that rely entirely on DNA base pairing. ssDNA-amphiphile assembly into nanotubes occurs rapidly via the association of the hydrophobic tails and does not require stringent annealing conditions as demonstrated by the nanotube formation min after amphiphile dissolution in water. Furthermore, DNA nanotubes were formed using a single ssDNA sequence, that varied in length and sequence, and the addition of a guanine-rich sequence in the headgroup was found to be capable of modifying the assembly, all of which demonstrate the versatility of the amphiphile-based self-assembly

strategy for forming DNA nanostructures.

4 Concluding remarks

Molecular self-assembly is an incredibly powerful but complex phenomenon that has been, and will continue to be, a significant topic of research with far-ranging applications in nanotechnology. DNA, with its intrinsic molecular code, is a material well suited to construct self-assembling structures and devices with nanometer precision. Indeed, the field of DNA nanotechnology includes many approaches to create intricate structures and devices entirely out of DNA. Well-known approaches include DNA origami and DNA tile assembly. This thesis describes an alternative and complimentary approach to form DNA structures. The approach utilizes ssDNA-amphiphiles that can self-assemble into spherical micelles, twisted and helical nanotapes, and nanotubes structures based on the amphiphilic nature of the molecules and not simply based on DNA-DNA base pairing. Specifically, we found that the type of spacer molecules used to connect hydrophilic DNA headgroups and hydrophobic tails as well as the length and composition of the DNA headgroups are important in defining the morphology of the self-assembled structures.

The impact of the spacer was studied by creating a set of five amphiphiles, each containing the same ssDNA headgroup and hydrophobic tail but different spacers linking these groups together. We found that amphiphiles containing hydrophilic PEG spacers and amphiphiles lacking a spacer assembled into spherical micelles while amphiphiles containing hydrophobic spacers assembled into twisted nanotapes as well as spherical micelles. The twisted nanotapes observed in this study were the first such structures produced by DNA-amphiphiles and clearly demonstrated that this class of amphiphiles

could adopt more complex structures than the micelles and vesicles previously observed by others. We next studied the effect of the amphiphile headgroup on the assembly of ssDNA-amphiphiles by creating another set of amphiphiles that contained the same hydrophobic tails, hydrophobic C_{12} spacers, and headgroups 10, 25 and 40 nucleotides in length. Amphiphiles created with random guanine-free ssDNA headgroups 10, 25, and 40 nucleotides in length were found to form helical nanotapes and nanotubes microns in length, along with the spherical micelles and twisted nanotapes observed in the first study. The reintroduction of five guanine nucleotides into the headgroups was found to impact the length of the nanotubes formed by amphiphiles with 10 nucleotide headgroups but not those with 25 and 40 nucleotides. Of particular interest moving forward is identifying methods to produce specific morphologies of nanostructures (e.g. short or long nanotubes) in high yields. While the theories of amphiphilic assembly discussed in section one of this thesis can help identify key parameters that may promote the creation of specific nanostructures, it is expected that the assembly of ssDNA-amphiphiles may not respond as predicted due to the complexity of the molecular components of ssDNA-amphiphiles.

Finally, as our understanding of the assembly increases we will be better equipped to utilize ssDNA-amphiphile assembly for science and engineering applications. In particular, there have been a number of interesting applications for nanotubes demonstrated in the DNA nanotechnology literature as well as the lipid and peptide nanotube literature. For instance, lipid nanotubes can be used as scaffolds capable of supporting metallization, which allows them to form electrically conducting nanowires that can be integrated into composite materials to manipulate electromagnetic properties

or used to facilitate circuit miniaturization.[135] Peptide nanotubes have been used as artificial ion channels, deposited onto carbon electrodes to produce supercapacitors, for antimicrobial therapeutics, and to create bioactive hydrogels.[136] And DNA nanotubes have been used as templates for nanofabrication,[137] as a light-harvesting antenna for energy transport,[138] as carriers for enhanced drug delivery,[139,140] and as an aligning agents for studying protein structure.[141]

The ability for ssDNA-amphiphiles to produce nanotube structures similar to those produced by other DNA nanotechnology approaches, such as DNA origami, but in a simple and robust manner could substantially increase the utility of DNA nanotubes for these applications and open the door for the development of new ones. In particular, the ability of ssDNA-amphiphile assembly to produce nanotubes quickly, without thermal annealing, without specific buffers, and from a single nucleotide sequence makes forming these structures more straightforward, which will be useful for translational research and industrial production. Additionally, ssDNA-amphiphile assembly does not require the DNA to form extensive base-pairing interactions in order to produce the nanotube structure. This may allow for DNA nanotubes formed via amphiphile self-assembly to have their surfaces decorated with guest molecules by introducing complementary ssDNA sequences tethered to these guest molecules into solutions of preassembled nanotubes. Finally, ssDNA-amphiphile assembly may be well suited for biomedical applications like the delivery of small molecule drugs or DNA-based therapeutics to specific areas of the body. This may be possible by creating specific nanostructures like micelles or nanotubes entirely out of mixtures of amphiphiles that each contain a bioactive ssDNA headgroup like an aptamer, antisense DNA, or immune

stimulating oligonucleotide. The flexibility in design of ssDNA-amphiphiles may allow the ssDNA headgroups to be readily changed with headgroups of different biological activity, which would make the self-assembling nanostructures easily adaptable for the rapid treatment of many diseases.

Bibliography

(1) Biswas, A.; Bayer, I. S.; Biris, A. S.; Wang, T.; Dervishi, E.; Faupel, F. *Adv. Colloid Interface Sci.* **2012**, *170*, 2–27.

(2) Bishop, K. J. M.; Wilmer, C. E.; Soh, S.; Grzybowski, B. A. *Small* **2009**, *5*, 1600–1630.

(3) Lu, W.; Lieber, C. M. *Nat. Mater.* **2007**, *6*, 841–850.

(4) Yu, H.-D.; Regulacio, M. D.; Ye, E.; Han, M.-Y. *Chem. Soc. Rev.* **2013**, *42*, 6006–6018.

(5) Balzani, V.; Credi, A.; Venturi, M. *Chemistry* **2002**, *8*, 5524–5532.

(6) Qin, S.; Kim, T.-H.; Wang, Z.; Li, A.-P. *Rev. Sci. Instrum.* **2012**, *83*, 063704.

(7) Lehn, J.-M. *Proc. Natl. Acad. Sci. U. S. A.* **2002**, *99*, 4763–4768.

(8) Hiemenz, P. C.; Rajagopalan, R. *Principles of colloid and surface chemistry*; 3rd ed.; CRC Press: Boca Raton, 1997.

(9) Tanford, C. *Science* **1978**, *200*, 1012–1018.

(10) Tanford, C. *The hydrophobic effect: formation of micelles and biological membranes*; 1st ed.; Wiley: New York, 1973; p. 200.

(11) Curtis, V. A. *J. Epidemiol. Community Health* **2007**, *61*, 660–664.

(12) Karsa, D. *Industrial applications of surfactants IV*; Karsa, D., Ed.; The Royal Society of Chemistry, 1999; pp. 23–39.

(13) Aida, T.; Meijer, E. W.; Stupp, S. I. *Science* **2012**, *335*, 813–817.

(14) Chandler, D. *Nature* **2005**, *437*, 640–647.

(15) Min, Y.; Akbulut, M.; Kristiansen, K.; Golan, Y.; Israelachvili, J. *Nat. Mater.* **2008**, *7*, 527–538.

(16) Hiemenz, P. C. *J. Chem. Educ.* **1972**, *49*, 164–170.

(17) Kalsin, A. M.; Fialkowski, M.; Paszewski, M.; Smoukov, S. K.; Bishop, K. J. M.; Grzybowski, B. A. *Science* **2006**, *312*, 420–424.

(18) Sukhorukov, G. B.; Antipov, A. A.; Voigt, A.; Donath, E.; Ḿhwald, H. *Macromol. Rapid Commun.* **2001**, *22*, 44–46.

(19) Israelachvili, J. N. *Intermolecular and Surface Forces*; 3rd ed.; Elsevier, 2011; p. 710.

(20) Steiner, T. *Angew. Chem. Int. Ed. Engl.* **2002**, *41*, 49–76.

(21) Israelachvili, J. N.; Mitchell, D. J.; Ninham, B. W. *J. Chem. Soc. Faraday Trans. 2* **1976**, *72*, 1525–1568.

(22) Nagarajan, R. *Langmuir* **2002**, *18*, 31–38.

(23) Zhang, J.; Li, X.; Li, X. *Prog. Polym. Sci.* **2012**, *37*, 1130–1176.

(24) Nagarajan, R.; Ruckenstein, E. *Langmuir* **1991**, 2934–2969.

(25) Nagarajan, R. *Colloids Surfaces B Biointerfaces* **1999**, *16*, 55–72.

(26) Geng, Y.; Ahmed, F.; Bhasin, N.; Discher, D. E. *J. Phys. Chem. B* **2005**, *109*, 3772–3779.

(27) Nagarajan, R. *Langmuir* **2002**, *18*, 31–38.

(28) Zhang, L.; Barlow, R. J.; Eisenberg, A. *Macromolecules* **1995**, *28*, 6055–6066.

(29) Craig, J. A.; Rexeisen, E. L.; Mardilovich, A.; Shroff, K.; Kokkoli, E. *Langmuir* **2008**, *24*, 10282–10292.

(30) Mardilovich, A.; Kokkoli, E. *Biomacromolecules* **2004**, *5*, 950–957.

(31) Adil, M.; Belur, L.; Pearce, T. R.; Levine, R. M.; Tisdale, A. W.; Sorenson, B. S.; McIvor, R. S.; Kokkoli, E. *Biomater. Sci.* **2013**, *1*, 393–401.

(32) Rexeisen, E. L.; Fan, W.; Pangburn, T. O.; Taribagil, R. R.; Bates, F. S.; Lodge, T. P.; Tsapatsis, M.; Kokkoli, E. *Langmuir* **2010**, *26*, 1953–1959.

(33) Shroff, K.; Pearce, T. R.; Kokkoli, E. *Langmuir* **2012**, *28*, 1858–1865.

(34) Mardilovich, A.; Craig, J. A.; McCammon, M. Q.; Garg, A.; Kokkoli, E. *Langmuir* **2006**, *22*, 3259–3264.

(35) Cui, H.; Webber, M. J.; Stupp, S. I. *Biopolymers* **2010**, *94*, 1–18.

(36) Loh, X. J.; del Barrio, J.; Lee, T.-C.; Scherman, O. A. *Chem. Commun.* **2014**, *50*, 3033–3035.

(37) Hentschel, J.; ten Cate, M. G. J.; Börner, H. G. *Macromolecules* **2007**, *40*, 9224–9232.

(38) Versluis, F.; Marsden, H. R.; Kros, A. *Chem. Soc. Rev.* **2010**, *39*, 3434–3444.

(39) Dehsorkhi, A.; Hamley, I. W.; Seitsonen, J.; Ruokolainen, J. *Langmuir* **2013**, *29*, 6665–6672.

(40) Koda, D.; Maruyama, T.; Minakuchi, N.; Nakashima, K.; Goto, M. *Chem. Commun.* **2010**, *46*, 979–981.

(41) Muraoka, T.; Koh, C.-Y.; Cui, H.; Stupp, S. I. *Angew. Chem. Int. Ed. Engl.* **2009**, *48*, 5946–5949.

(42) Gore, T.; Dori, Y.; Talmon, Y.; Tirrell, M.; Bianco-Peled, H. *Langmuir* **2001**, *17*, 5352–5360.

(43) Makovitzki, A.; Baram, J.; Shai, Y. *Biochemistry* **2008**, *47*, 10630–10636.

(44) Paramonov, S. E.; Jun, H.-W.; Hartgerink, J. D. *J. Am. Chem. Soc.* **2006**, *128*, 7291–7298.

(45) Dehsorkhi, A.; Castelletto, V.; Hamley, I. W.; Adamcik, J.; Mezzenga, R. *Soft Matter* **2013**, *9*, 6033.

(46) Trent, A.; Marullo, R.; Lin, B.; Black, M.; Tirrell, M. *Soft Matter* **2011**, *7*, 9572–9582.

(47) Fleming, S.; Ulijn, R. V. *Chem. Soc. Rev.* **2014**, *43*, 8150–8177.

(48) Shao, H.; Parquette, J. R. *Angew. Chem. Int. Ed. Engl.* **2009**, *48*, 2525–2528.

(49) Lim, Y.-B.; Lee, E.; Lee, M. *Angew. Chem. Int. Ed. Engl.* **2007**, *46*, 9011–9014.

(50) Missirlis, D.; Farine, M.; Kastantin, M.; Ananthanarayanan, B.; Neumann, T.; Tirrell, M. *Bioconjug. Chem.* **2010**, *21*, 465–475.

(51) Peters, D.; Kastantin, M.; Kotamraju, V. R.; Karmali, P. P.; Gujraty, K.; Tirrell, M.; Ruoslahti, E. *Proc. Natl. Acad. Sci. U. S. A.* **2009**, *106*, 9815–9819.

(52) Missirlis, D.; Chworos, A.; Fu, C. J.; Khant, H. A.; Krogstad, D. V; Tirrell, M. *Langmuir* **2011**, *27*, 6163–6170.

(53) Castelletto, V.; Hamley, I. W.; Perez, J.; Abezgauz, L.; Danino, D. *Chem. Commun.* **2010**, *46*, 9185–9187.

(54) Moyer, T. J.; Cui, H.; Stupp, S. I. *J. Phys. Chem. B* **2013**, *117*, 4604–4610.

(55) Pashuck, E. T.; Stupp, S. I. *J. Am. Chem. Soc.* **2010**, *132*, 8819–8821.

(56) Ziserman, L.; Lee, H.-Y.; Raghavan, S. R.; Mor, A.; Danino, D. *J. Am. Chem. Soc.* **2011**, *133*, 2511–2517.

(57) Shao, H.; Seifert, J.; Romano, N. C.; Gao, M.; Helmus, J. J.; Jaroniec, C. P.; Modarelli, D. A.; Parquette, J. R. *Angew. Chem. Int. Ed. Engl.* **2010**, *49*, 7688–7691.

(58) Lin, B. F.; Marullo, R. S.; Robb, M. J.; Krogstad, D. V; Antoni, P.; Hawker, C. J.; Campos, L. M.; Tirrell, M. V. *Nano Lett.* **2011**, *11*, 3946–3950.

(59) Svenson, S.; Messersmith, P. B. *Langmuir* **1999**, *15*, 4464–4471.

(60) Thomas, B. N.; Safinya, C. R.; Plano, R. J.; Clark, N. A. *Science* **1995**, *267*, 1635–1638.

(61) Spector, M. S.; Singh, A.; Messersmith, P. B.; Schnur, J. M. *Nano Lett.* **2001**, *1*, 375–378.

(62) Selinger, J. V.; Spector, M. S.; Schnur, J. M. *J. Phys. Chem. B* **2001**, *105*, 7157–7169.

(63) Madine, J.; Davies, H. A.; Shaw, C.; Hamley, I. W.; Middleton, D. A. *Chem. Commun.* **2012**, *48*, 2976–2978.

(64) Castelletto, V.; Hamley, I. W.; Harris, P. J. F.; Olsson, U.; Spencer, N. *J. Phys. Chem. B* **2009**, *113*, 9978–9987.

(65) Hamley, I. W.; Dehsorkhi, A.; Castelletto, V.; Furzeland, S.; Atkins, D.; Seitsonen, J.; Ruokolainen, J. *Soft Matter* **2013**, *9*, 9290–9293.

(66) Jung, J. H.; Do, Y.; Lee, Y.-A.; Shimizu, T. *Chemistry* **2005**, *11*, 5538–5544.

(67) Jung, J. H.; Lee, S. H.; Yoo, J. S.; Yoshida, K.; Shimizu, T.; Shinkai, S. *Chem. - A Eur. J.* **2003**, *9*, 5307–5313.

(68) Whitehead, K. A.; Langer, R.; Anderson, D. G. *Nat. Rev. Drug Discov.* **2009**, *8*, 129–138.

(69) Tamm, I.; Dörken, B.; Hartmann, G. *Lancet* **2001**, *358*, 489–497.

(70) Wilson, D. S.; Szostak, J. W. *Annu. Rev. Biochem.* **1999**, *68*, 611–647.

(71) McKee, M. L.; Milnes, P. J.; Bath, J.; Stulz, E.; O'Reilly, R. K.; Turberfield, A. J. *J. Am. Chem. Soc.* **2012**, *134*, 1446–1449.

(72) Xiao, Z.; Ji, C.; Shi, J.; Pridgen, E. M.; Frieder, J.; Wu, J.; Farokhzad, O. C. *Angew. Chem. Int. Ed. Engl.* **2012**, *51*, 11853–11857.

(73) Höbartner, C.; Silverman, S. K. *Biopolymers* **2007**, *87*, 279–292.

(74) Bath, J.; Turberfield, A. J. *Nat. Nanotechnol.* **2007**, *2*, 275–284.

(75) Banchelli, M.; Betti, F.; Berti, D.; Caminati, G.; Bombelli, F. B.; Brown, T.; Wilhelmsson, L. M.; Nordén, B.; Baglioni, P. *J. Phys. Chem. B* **2008**, *112*, 10942–10952.

(76) Chan, Y.-H. M.; van Lengerich, B.; Boxer, S. G. *Proc. Natl. Acad. Sci. U. S. A.* **2009**, *106*, 979–984.

(77) Gambinossi, F.; Banchelli, M.; Durand, A.; Berti, D.; Brown, T.; Caminati, G.; Baglioni, P. *J. Phys. Chem. B* **2010**, *114*, 7338–7347.

(78) Wu, Y.; Sefah, K.; Liu, H.; Wang, R.; Tan, W. *Proc. Natl. Acad. Sci. U. S. A.* **2010**, *107*, 5–10.

(79) Patwa, A.; Gissot, A.; Bestel, I.; Barthélémy, P. *Chem. Soc. Rev.* **2011**, *40*, 5844–5854.

(80) Moreau, L.; Barthélémy, P.; El Maataoui, M.; Grinstaff, M. W. *J. Am. Chem. Soc.* **2004**, *126*, 7533–7539.

(81) Kwak, M.; Herrmann, A. *Chem. Soc. Rev.* **2011**, *40*, 5745–5755.

(82) Grijalvo, S.; Ocampo, S. M.; Perales, J. C.; Eritja, R. *J. Org. Chem.* **2010**, *75*, 6806–6813.

(83) Van Lengerich, B.; Rawle, R. J.; Boxer, S. G. *Langmuir* **2010**, *26*, 8666–8672.

(84) Gosse, C.; Boutorine, A.; Aujard, I.; Chami, M.; Kononov, A.; Cogné-Laage, E.; Allemand, J.-F.; Li, J.; Jullien, L. *J. Phys. Chem. B* **2004**, *108*, 6485–6497.

(85) Thompson, M. P.; Chien, M.-P.; Ku, T.-H.; Rush, A. M.; Gianneschi, N. C. *Nano Lett.* **2010**, *10*, 2690–2693.

(86) Kwak, M.; Minten, I. J.; Anaya, D.-M.; Musser, A. J.; Brasch, M.; Nolte, R. J. M.; Müllen, K.; Cornelissen, J. J. L. M.; Herrmann, A. *J. Am. Chem. Soc.* **2010**, *132*, 7834–7835.

(87) Liu, H.; Kwong, B.; Irvine, D. J. *Angew. Chem. Int. Ed. Engl.* **2011**, *50*, 7052–7055.

(88) Dentinger, P. M.; Simmons, B. A.; Cruz, E.; Sprague, M. *Langmuir* **2006**, *22*, 2935–2937.

(89) Li, Z.; Zhang, Y.; Fullhart, P.; Mirkin, C. a. *Nano Lett.* **2004**, *4*, 1055–1058.

(90) Jeong, J. H.; Park, T. G. *Bioconjug. Chem.* **2001**, *12*, 917–923.

(91) Alemdaroglu, F. E.; Alemdaroglu, N. C.; Langguth, P.; Herrmann, A. *Adv. Mater.* **2008**, *20*, 899–902.

(92) Ding, K.; Alemdaroglu, F. E.; Börsch, M.; Berger, R.; Herrmann, A. *Angew. Chem. Int. Ed. Engl.* **2007**, *46*, 1172–1175.

(93) Teixeira, F.; Rigler, P.; Vebert-Nardin, C. *Chem. Commun.* **2007**, *1*, 1130–1132.

(94) Talom, R. M.; Fuks, G.; Kaps, L.; Oberdisse, J.; Cerclier, C.; Gaillard, C.; Mingotaud, C.; Gauffre, F. *Chemistry* **2011**, *17*, 13495–13501.

(95) Alemdaroglu, F. E.; Ding, K.; Berger, R.; Herrmann, A. *Angew. Chemie* **2006**, *45*, 4206–4210.

(96) Sivakova, S.; Rowan, S. J. *Chem. Soc. Rev.* **2005**, *34*, 9–21.

(97) Chien, M.-P.; Rush, A. M.; Thompson, M. P.; Gianneschi, N. C. *Angew. Chem. Int. Ed. Engl.* **2010**, *49*, 5076–5080.

(98) Guéron, M.; Leroy, J. *Curr. Opin. Struct. Biol.* **2000**, *10*, 326–331.

(99) Lane, A. N.; Chaires, J. B.; Gray, R. D.; Trent, J. O. *Nucleic Acids Res.* **2008**, *36*, 5482–5515.

(100) Kendrick, S.; Hurley, L. H. *Pure Appl. Chem.* **2010**, *82*, 1609–1621.

(101) Zhao, Z.; Wang, L.; Liu, Y.; Yang, Z.; He, Y.-M.; Li, Z.; Fan, Q.-H.; Liu, D. *Chem. Commun.* **2012**, *48*, 9753–9755.

(102) Liu, H.; Moynihan, K. D.; Zheng, Y.; Szeto, G. L.; Li, A. V; Huang, B.; Van Egeren, D. S.; Park, C.; Irvine, D. J. *Nature* **2014**.

(103) Zhang, S. *Nat. Biotechnol.* **2003**, *21*, 1171–1178.

(104) Kokkoli, E.; Mardilovich, A.; Wedekind, A.; Rexeisen, E. L.; Garg, A.; Craig, J. A. *Soft Matter* **2006**, *2*, 1015–1024.

(105) Liu, H.; Zhu, Z.; Kang, H.; Wu, Y.; Sefan, K.; Tan, W. *Chemistry* **2010**, *16*, 3791–3797.

(106) Ferreira, C. S. M.; Cheung, M. C.; Missailidis, S.; Bisland, S.; Gariépy, J. *Nucleic Acids Res.* **2009**, *37*, 866–876.

(107) Aggeli, A.; Nyrkova, I. A.; Bell, M.; Harding, R.; Carrick, L.; McLeish, T. C.; Semenov, A. N.; Boden, N. *Proc. Natl. Acad. Sci. U. S. A.* **2001**, *98*, 11857–11862.

(108) Cui, H.; Muraoka, T.; Cheetham, A. G.; Stupp, S. I. *Nano Lett.* **2009**, *9*, 945–951.

(109) *Neutrons, X-rays, and Light: Scattering Methods Applied to Soft Condensed Matter*; Zemb, Thomas; Lindner, P., Ed.; 1st ed.; Elsevier Science B.V.: Amsterdam, 2002; p. 541.

(110) Choi, E. W.; Nayak, L. V; Bates, P. J. *Nucleic Acids Res.* **2010**, *38*, 1623–1635.

(111) Kypr, J.; Kejnovská, I.; Renciuk, D.; Vorlícková, M. *Nucleic Acids Res.* **2009**, *37*, 1713–1725.

(112) Seeman, N. C. *Annu. Rev. Biochem.* **2010**, *79*, 65–87.

(113) Pinheiro, A. V; Han, D.; Shih, W. M.; Yan, H. *Nat. Nanotechnol.* **2011**, *6*, 763–772.

(114) Tørring, T.; Voigt, N. V; Nangreave, J.; Yan, H.; Gothelf, K. V. *Chem. Soc. Rev.* **2011**, *40*, 5636–5646.

(115) Lin, C.; Liu, Y.; Rinker, S.; Yan, H. *Chemphyschem* **2006**, *7*, 1641–1647.

(116) Aldaye, F. A.; Palmer, A. L.; Sleiman, H. F. *Science* **2008**, *321*, 1795–1799.

(117) Pearce, T. R.; Waybrant, B.; Kokkoli, E. *Chem. Commun.* **2014**, *50*, 210–212.

(118) Waybrant, B.; Pearce, T. R.; Kokkoli, E. *Langmuir* **2014**, *30*, 7465–7474.

(119) Gray, D. M.; Wen, J.; Gray, C. W.; Repges, R.; Repges, C.; Raabe, G.; Fleischhauer, J. *Chirality* **2008**, *20*, 431–440.

(120) Rajendran, A.; Endo, M.; Hidaka, K.; Tran, P. L. T.; Mergny, J.-L.; Sugiyama, H. *Nucleic Acids Res.* **2013**, *41*, 8738–8747.

(121) Leung, C.; Chan, D. S.; Man, B. Y.; Wang, C.; Lam, W.; Cheng, Y.; Fong, W.; Hsiao, W. W.; Ma, D. *Anal. Chem.* **2011**, *83*, 463–466.

(122) Efthimiadou, E. K.; Sanakis, Y.; Katsarou, M.; Raptopoulou, C. P.; Karaliota, A.; Katsaros, N.; Psomas, G. *J. Inorg. Biochem.* **2006**, *100*, 1378–1388.

(123) Cuvier, A.-S.; Berton, J.; Stevens, C. V; Fadda, G. C.; Babonneau, F.; Van Bogaert, I. N. A.; Soetaert, W.; Pehau-Arnaudet, G.; Baccile, N. *Soft Matter* **2014**, *10*, 3950–3959.

(124) Sorrenti, A.; Illa, O.; Ortuño, R. M. *Chem. Soc. Rev.* **2013**, *42*, 8200–8219.

(125) Chen, Z.; Majidi, C.; Srolovitz, D. J.; Haataja, M. *Appl. Phys. Lett.* **2011**, *98*, 011906.

(126) Ziserman, L.; Mor, A.; Harries, D.; Danino, D. *Phys. Rev. Lett.* **2011**, *106*, 238105.

(127) Perino, A.; Schmutz, M.; Meunier, S.; Mésini, P. J.; Wagner, A. *Langmuir* **2011**, *27*, 12149–12155.

(128) Armon, S.; Aharoni, H.; Moshe, M.; Sharon, E. *Soft Matter* **2014**, *10*, 2733–2740.

(129) Ghafouri, R.; Bruinsma, R. *Phys. Rev. Lett.* **2005**, *94*, 138101.

(130) Shimizu, T.; Masuda, M.; Minamikawa, H. *Chem. Rev.* **2005**, *105*, 1401–1443.

(131) Oda, R.; Huc, I.; Schmutz, M.; Candau, S.; MacKintosh, F. *Nature* **1999**, *399*, 566–569.

(132) Adamcik, J.; Castelletto, V.; Bolisetty, S.; Hamley, I. W.; Mezzenga, R. *Angew. Chem. Int. Ed. Engl.* **2011**, *50*, 5495–5498.

(133) Castelletto, V.; Hamley, I. W.; Cenker, C.; Olsson, U. *J. Phys. Chem. B* **2010**, *114*, 8002–8008.

(134) Barclay, T. G.; Constantopoulos, K.; Zhang, W.; Fujiki, M.; Matisons, J. G. *Langmuir* **2012**, *28*, 14172–14179.

(135) Schnur, J. M. *Science* **1993**, *262*, 1669–1676.

(136) Hamley, I. W. *Angew. Chem. Int. Ed. Engl.* **2014**, *53*, 6866–6881.

(137) Zhang, G.; Surwade, S. P.; Zhou, F.; Liu, H. *Chem. Soc. Rev.* **2013**, *42*, 2488–2496.

(138) Dutta, P. K.; Varghese, R.; Nangreave, J.; Lin, S.; Yan, H.; Liu, Y. *J. Am. Chem. Soc.* **2011**, *133*, 11985–11993.

(139) Hamblin, G. D.; Carneiro, K. M. M.; Fakhoury, J. F.; Bujold, K. E.; Sleiman, H. F. *J. Am. Chem. Soc.* **2012**, *134*, 2888–2891.

(140) Douglas, S. M.; Bachelet, I.; Church, G. M. *Science* **2012**, *335*, 831–834.

(141) Berardi, M. J.; Shih, W. M.; Harrison, S. C.; Chou, J. J. *Nature* **2011**, *476*, 109–113.